Recombination …

FP I ZS 2024 XE 19. 12.

electron –ion recombination

atomic ions

molecular ions

ion –ion recombination

Recombination

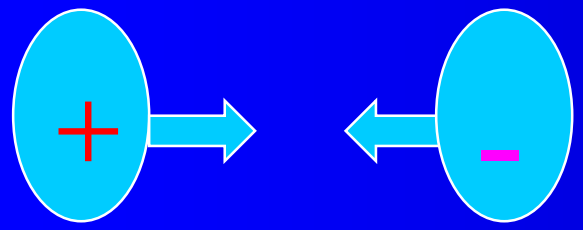

Radiative recombination

$Ar^+ + e^- \rightarrow Ar + h\nu$

Dissociative recombination

$AB^+ + e \rightarrow A + B$

$O_2^+ + e \rightarrow A + B$

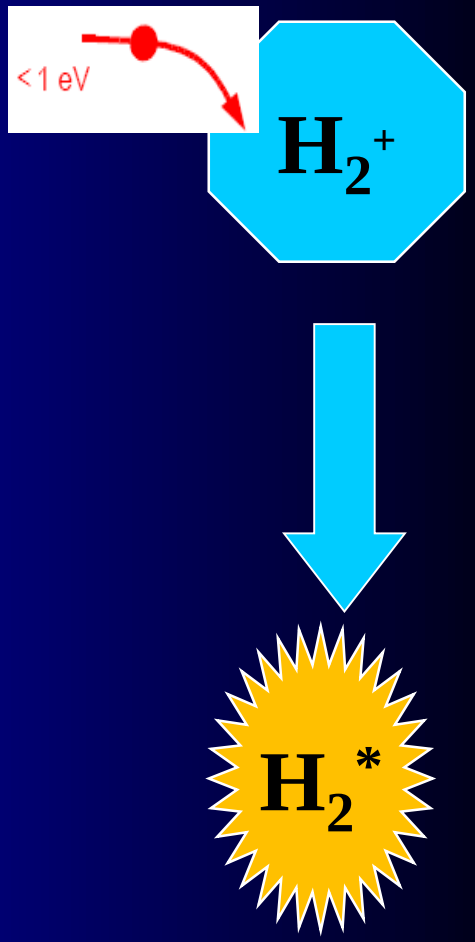
<1 eV
H_2^+
H_2^*

$e^- + AB^+$

Capture

AB* resonant state(s)

H_2^+

H_2^*

$e^- + AB^+$

Capture

Auto ionization

AB* resonant state(s)

predissociation

To get high recombination rate, we need

(a) efficient capture

(b) predissociation faster than auto-ionization

Electron –ion recombination

$H^+ + e^- \rightarrow$ products

$H_2^+ + e^- \rightarrow$ products

$H_3^+ + e^- \rightarrow$ products

$H_5^+ + e^- \rightarrow$ products

Processes: at low impact energies

Elastic scattering

$AB + e \longrightarrow AB + e$

Electronic excitation

$AB + e \longrightarrow AB^* + e$

Vibrational excitation

$AB(v''=0) + e \longrightarrow AB(v') + e$

Rotational excitation

$AB(N'') + e \longrightarrow AB(N') + e$

Dissociative attachment /

$AB + e \longrightarrow A^- + B$

$\longrightarrow A + B^-$

Impact dissociation

$AB + e \longrightarrow A + B + e$

All go via $(AB^-\ldots.)^{**}$.

Dissociative recombination

$AB^+ + e \longrightarrow A + B$

Go via $(AB\ldots.)^{**}$.

$H_2^+ + e^- \rightarrow H + H,$

Dissociative Recombination - DR

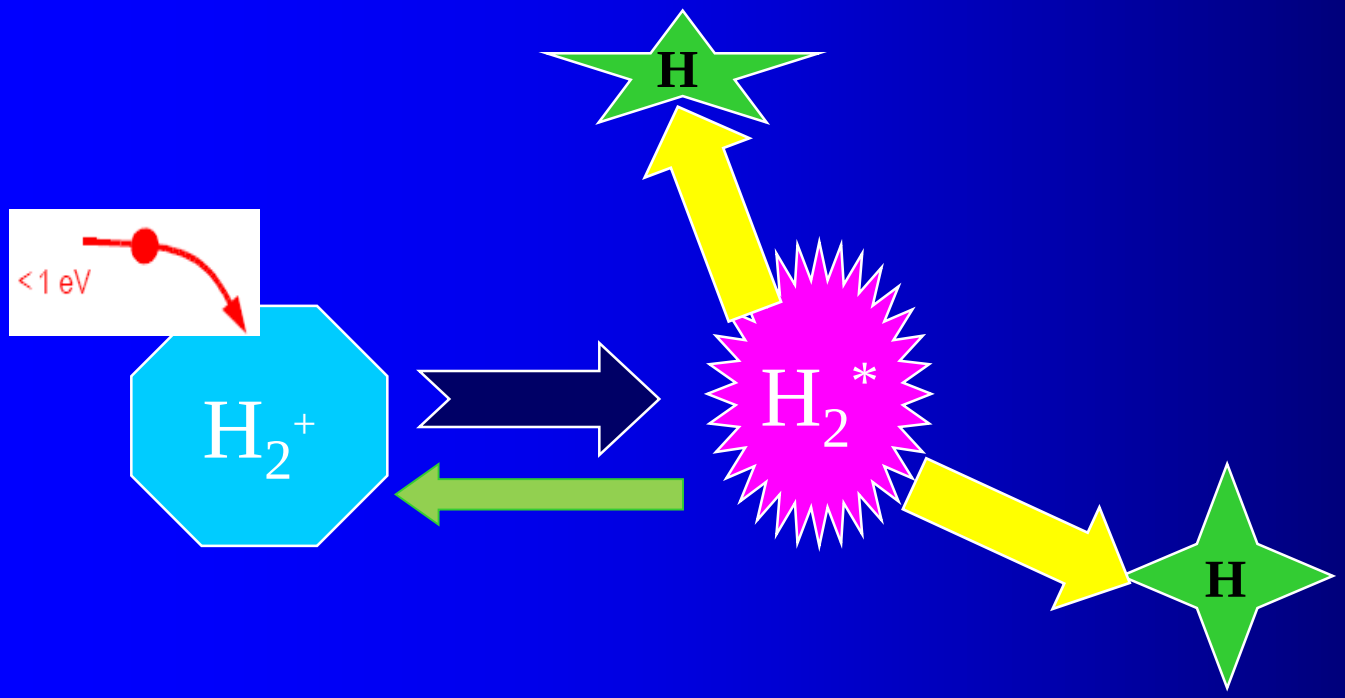

Electron collisions with $H_2^{+\ -}$ how to describe ????

$H_2^+ + e^- \rightarrow H + H,$

Dissociative Recombination - DR

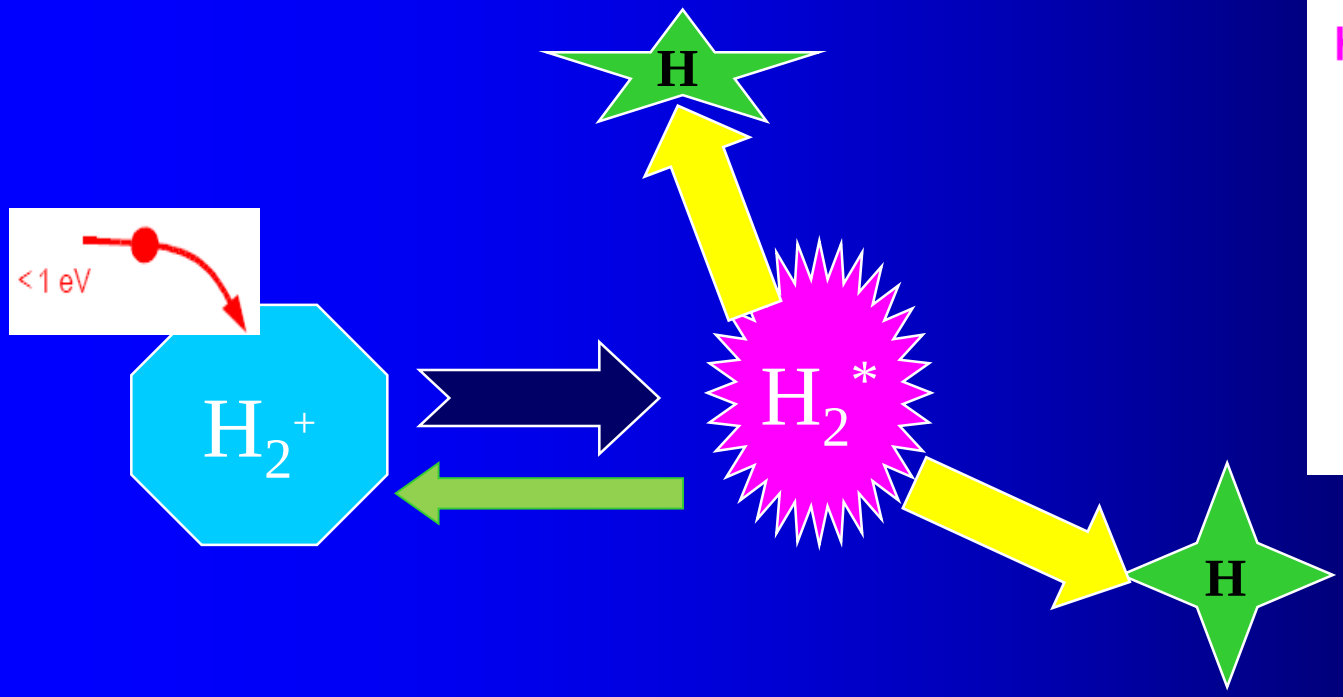

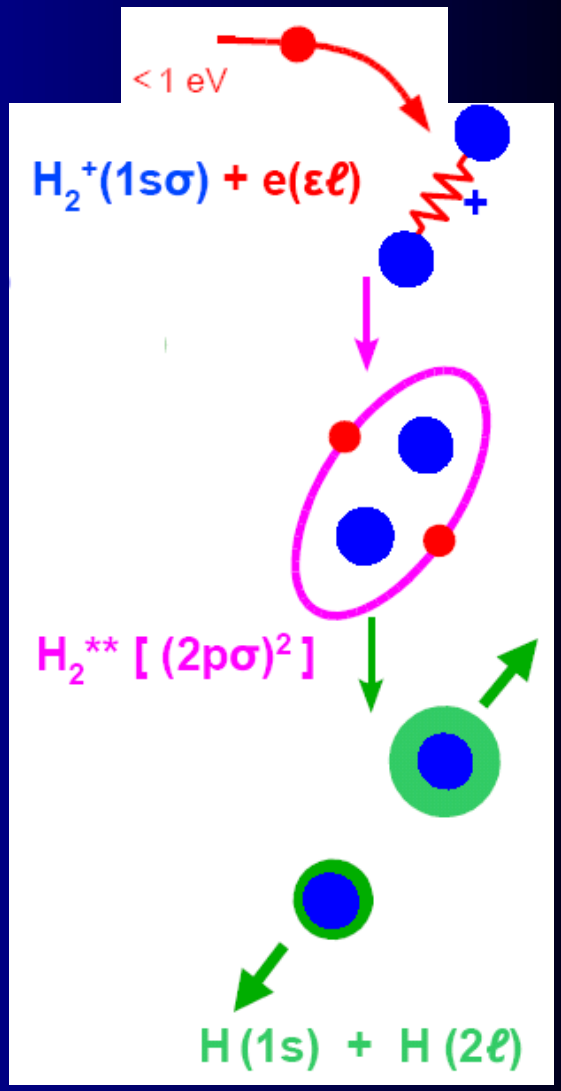

Electron collisions with H_2^{+} - how to describe ????

Direct DR process

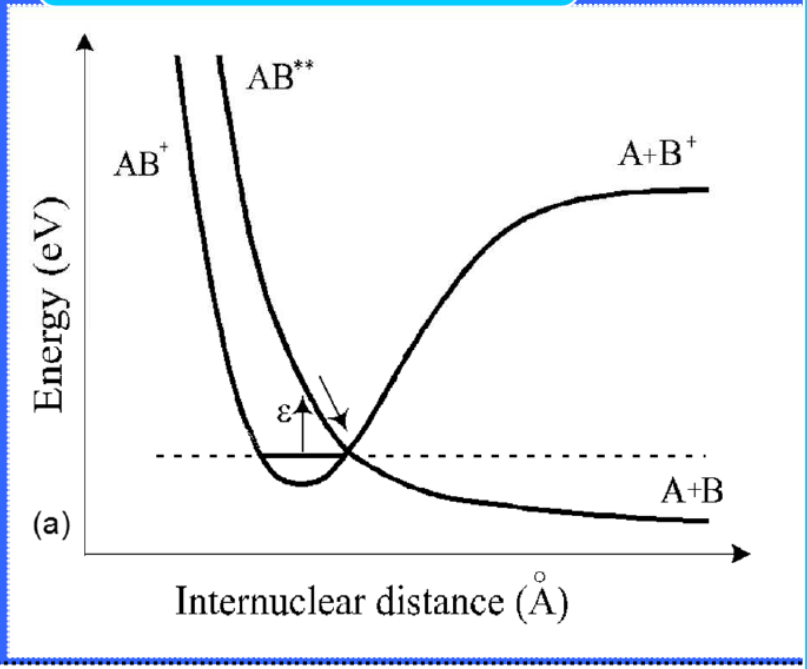

$$AB^{+} + e^{-} \underset{k_{auto}}{\overset{k_c}{\rightleftharpoons}} AB^{**} \xrightarrow{k_{stab}} A + B$$

$$\alpha_{dr} \approx T_e^{-0.5}$$

Ions: Ar_2^+, N_2^+, CH_4^+, $NH_4^+(NH_3)_2$ - $\alpha \sim 10^{-7} - 10^{-6}$ cm^3 s^{-1}

Theoretical calculation: H_2^+, HD^+, D_2^+- $\alpha = 2.3\times10^{-8}$, 2.2×10^{-8}, 4×10^{-9} cm^3 s^{-1}, respectively

Direct DR process

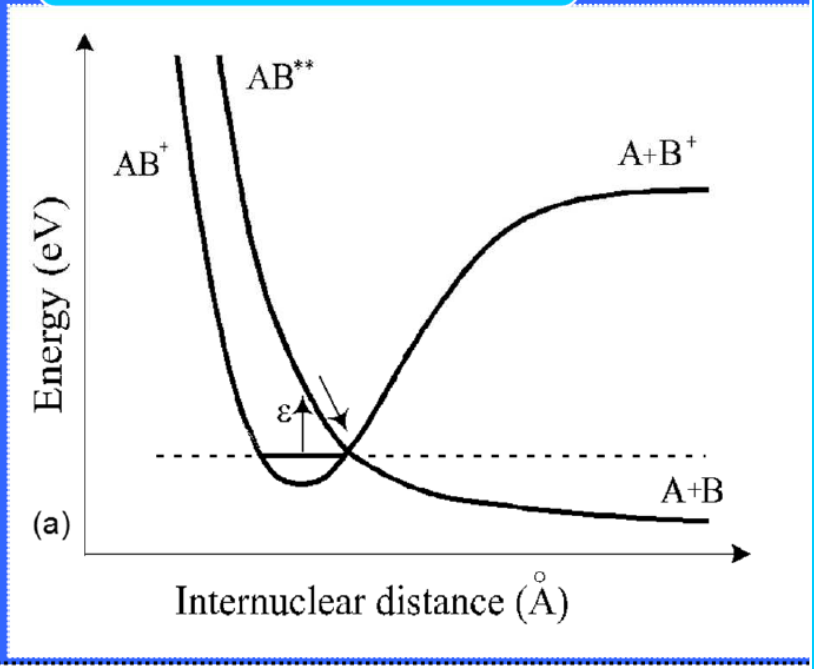

$$AB^+ + e^- \underset{k_{auto}}{\overset{k_c}{\rightleftharpoons}} AB^{**} \xrightarrow{k_{stab}} A + B$$

$$\alpha_{dr} \approx T_e^{-0.5}$$

Indirect DR process

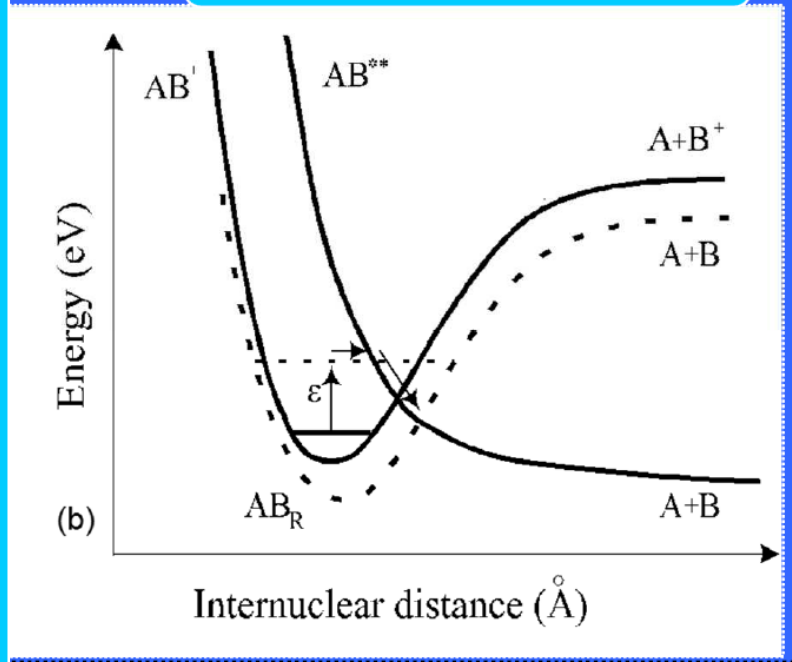

$$AB^+ + e^- \rightleftarrows AB_R^{**} \rightleftarrows AB^{**} \rightarrow A + B$$

$$\alpha_{idr} \approx T_e^{-1.5}$$

$$\alpha(T_e, T_v) \approx T_e^{-0.5}\, T_v^{-1}$$

Ions: Ar_2^+, N_2^+, CH_4^+, $NH_4^+(NH_3)_2$ - $\alpha \sim 10^{-7} - 10^{-6}$ cm^3 s^{-1}

Theoretical calculation: H_2^+, HD^+, D_2^+- $\alpha = 2.3\times10^{-8}$, 2.2×10^{-8}, 4×10^{-9} cm^3 s^{-1}, respectively

THEORETICAL FRAMEWORK

The states involved: exemple for He_2^+/He_2 system

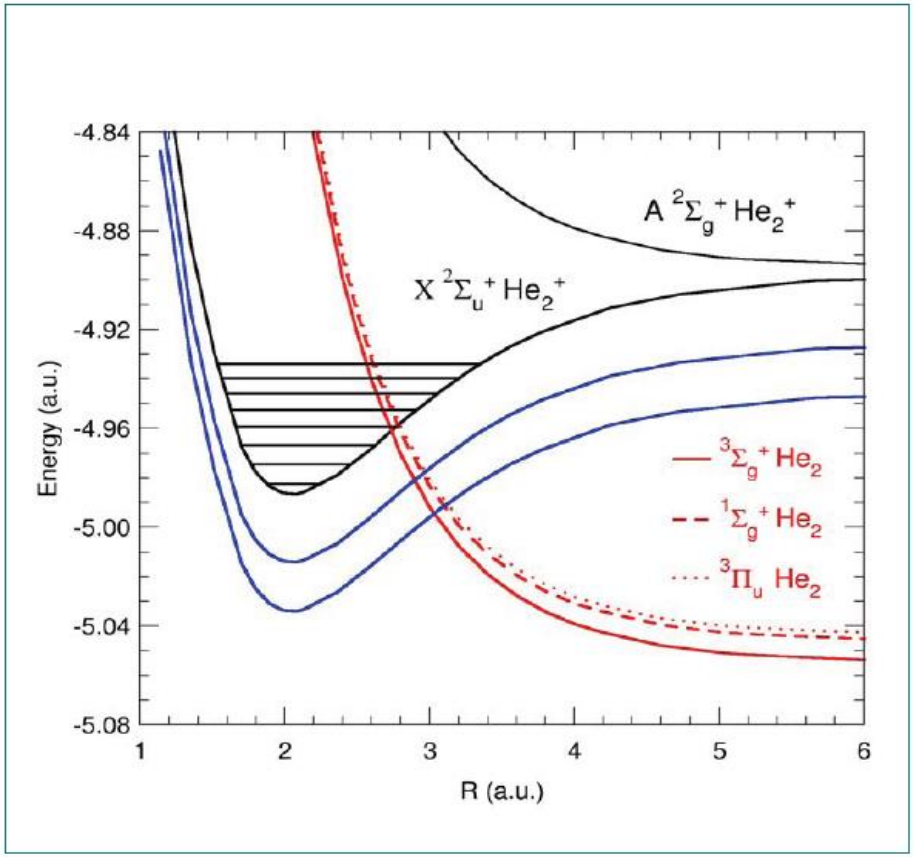

2004 DR6 Mosbach

I. Schneider, et al., DR2004 Mosbach

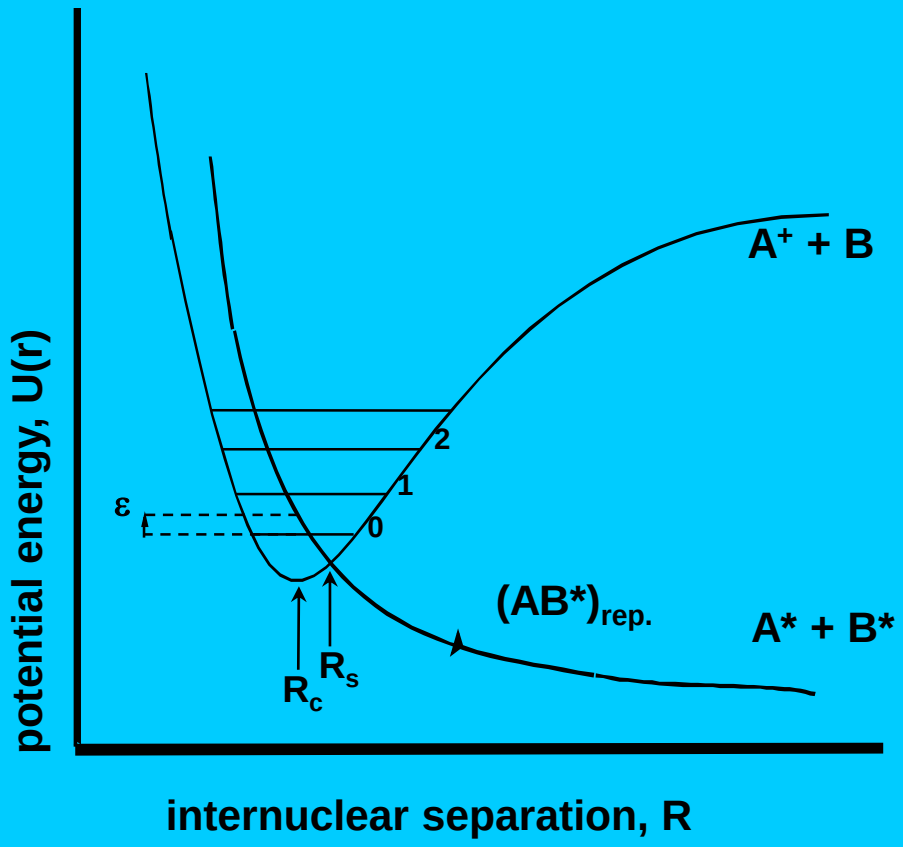

Direct mechanism

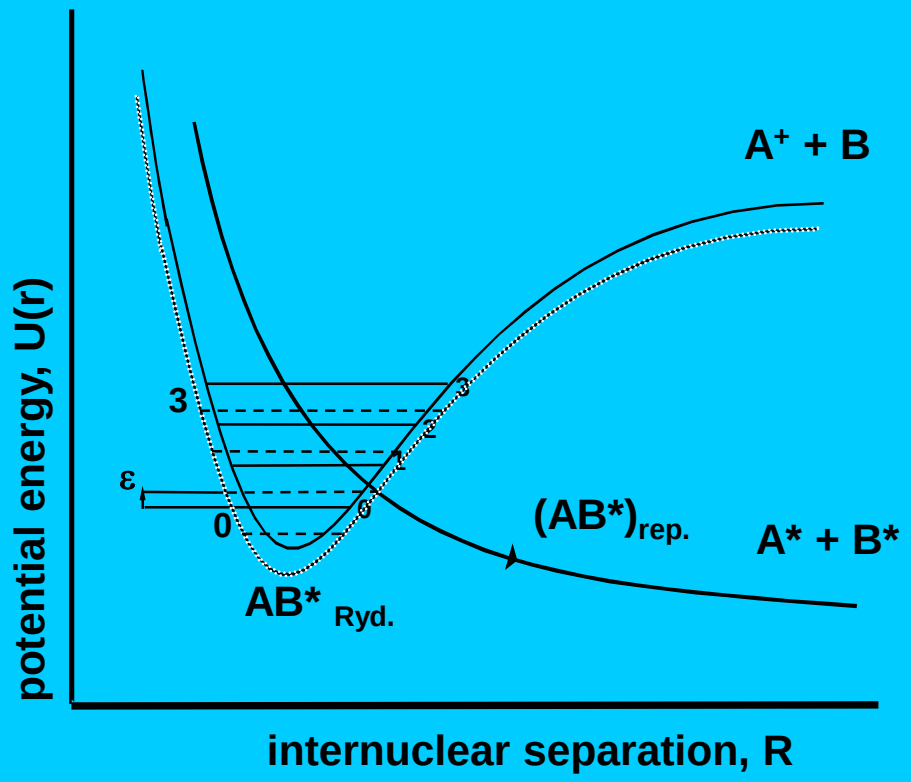

Indirect mechanism

Electron-cold molecular ion reaction: Dissociative Recombination

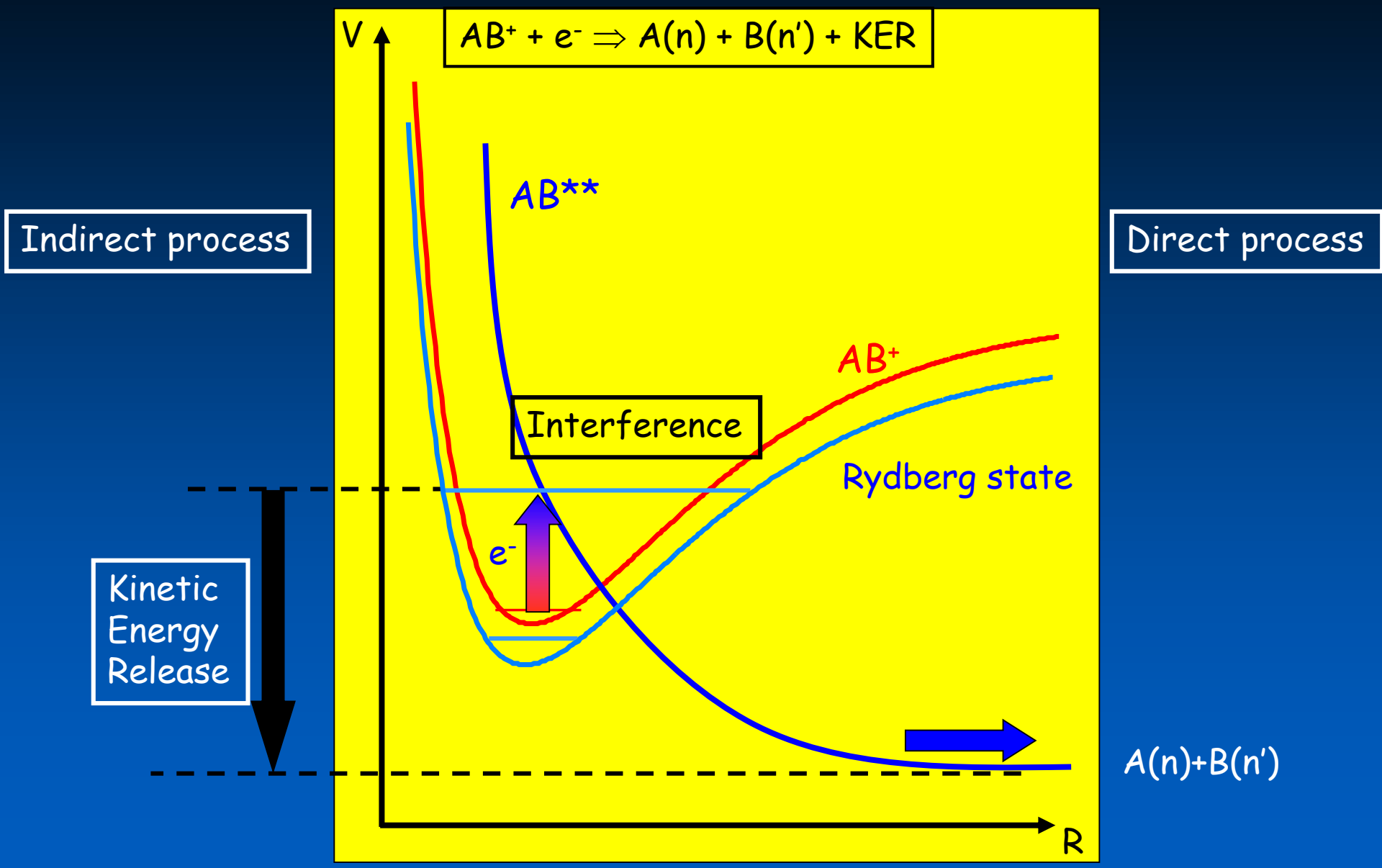

Recombination of H_3^+ : No ion-neutral crossing

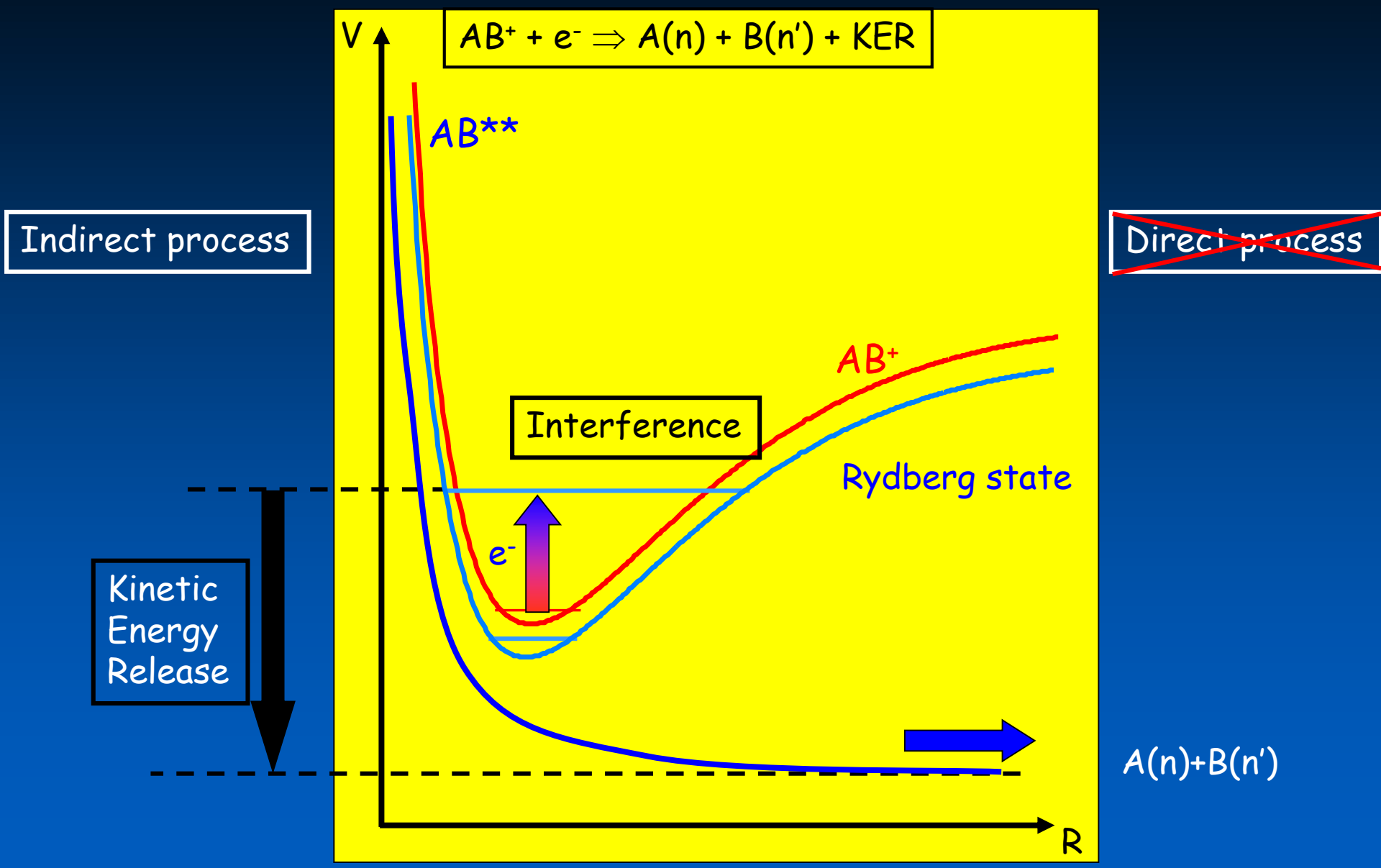

$H_3^+ + e^- \rightarrow H + H_2; 3H$

Single collision

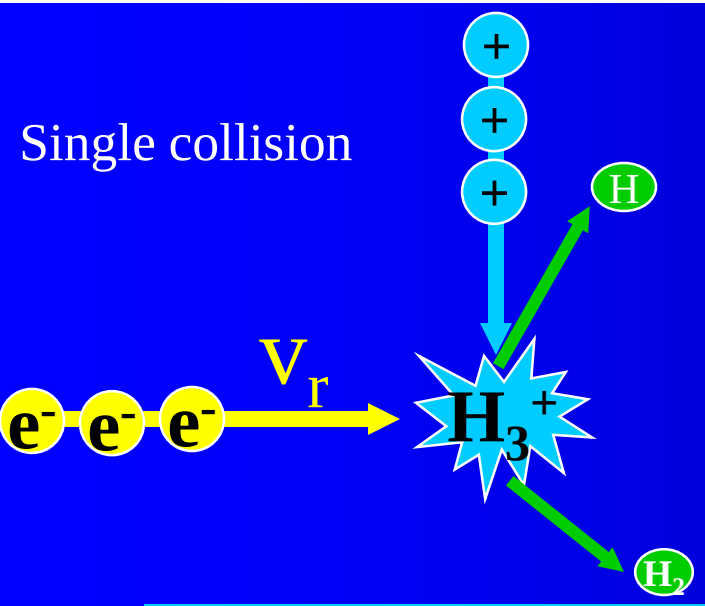

$\sigma(v_r)$ **recombination cross section**

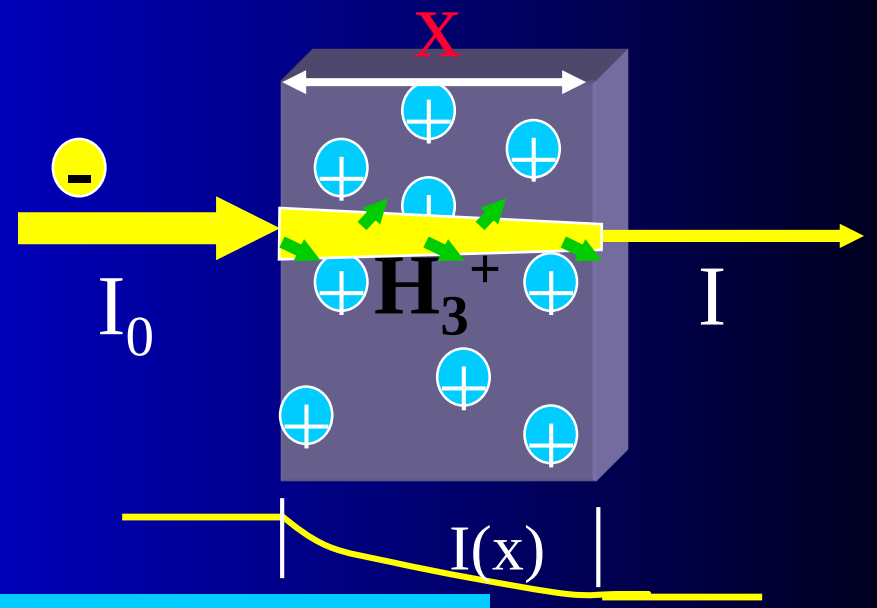

$$I=I_0\exp(-\sigma n_i x)$$

$$k(T)=\langle v\sigma\rangle$$

Multiple collision

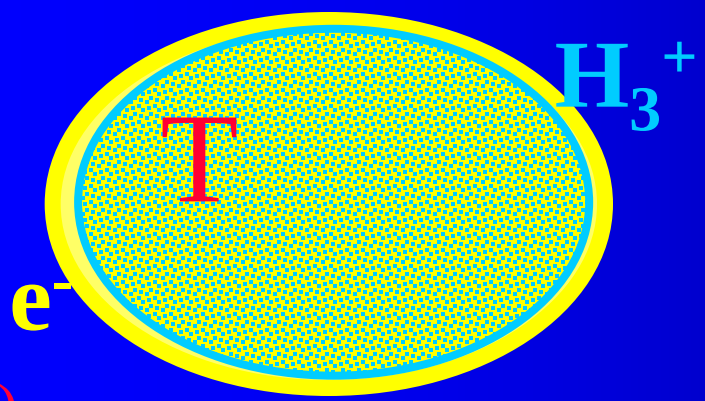

k(T)

recombination rate coefficient

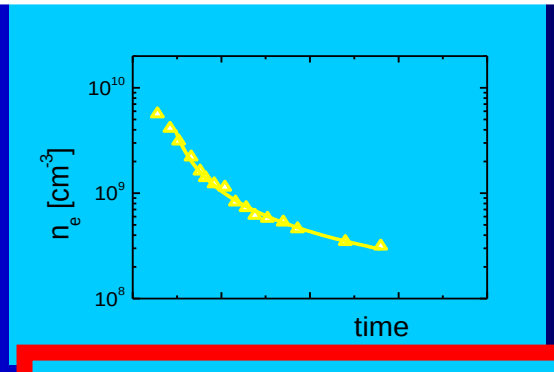

$$\alpha$$

$$dn_i/dt=-kn_in_e$$

$$dn_e/dt=-kn_e^2$$

Concept of recombination rate coefficient (plasma binary reactions)

at T

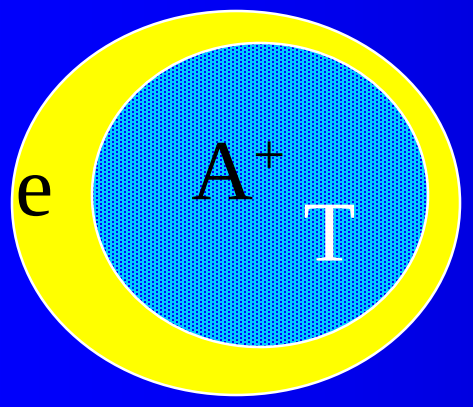

$e^- + A^+ \rightarrow$ products

$dN_A/dt = -\alpha n_e N_A$

RECOMBINATION RATE COEFFICIENT

$\alpha = \alpha(T)$

$\sigma = \sigma(v) = \sigma(\varepsilon)$

Collision rate coefficient, Recombination rate coefficient

$\alpha = \langle \sigma u_r \rangle$

Recombination processes in plasma

Binary Recombination

$$H^+ + e \rightarrow H + h\nu$$ RR

$$O_2^{\ +} + e \rightarrow O + O$$ DR

$$Fe^{7+} + e \rightarrow Fe^{6+}$$ DiR

$$\frac{dn_e}{dt} = \frac{d[O_2^{\ +}]}{dt} = -\alpha[O_2^{\ +}]n_e = -\alpha n_e^{\ 2}$$

Recombination processes in plasma

Binary Recombination

$$H^+ + e \rightarrow H + h\nu$$

RR

$$O_2^{\ +} + e \rightarrow O + O$$

DR

$$\frac{dn_e}{dt} = \frac{d[O_2^{\ +}]}{dt} = -\alpha[O_2^{\ +}]n_e = -\alpha n_e^{\ 2}$$

$$Fe^{7+} + e \rightarrow Fe^{6+}$$

DiR

Ternary electron assisted recombination

$$Ar^+ + e + e \rightarrow Ar + e$$

$$\frac{dn_e}{dt} = \frac{d[Ar^+]}{dt} = -K_e[Ar^+]n_e^{\ 2} = -\alpha_{eff}[Ar^+]n_e$$

Collisional Radiative Recombination CRR

$$\alpha_{eff} = K_e n_e$$

Ternary neutral assisted recombination

$$Ar^+ + e + He \rightarrow Ar + He$$

$$\frac{dn_e}{dt} = \frac{d[Ar^+]}{dt} = -K_M[Ar^+]n_e[He] = -\alpha_{eff}[Ar^+]n_e$$

$$\alpha_{eff} = K_M[He]$$

$$O_2^+ + e \rightarrow O + O$$

Five exothermic channels are available for vibrational ground state O_2^+ ions in zero relative energy collisions with electrons. They are summarized as follows with the associated kinetic energy releases:

$$O_2^+(X^2\Pi_g, v=0) + e^- \rightarrow O(^3P) + O(^3P) + 6.65 \text{ eV} \quad (1a)$$

$$\rightarrow O(^3P) + O(^1D) + 4.99 \text{ eV} \quad (1b)$$

$$\rightarrow O(^1D) + O(^1D) + 3.02 \text{ eV} \quad (1c)$$

$$\rightarrow O(^3P) + O(^1S) + 2.77 \text{ eV} \quad (1d)$$

$$\rightarrow O(^1D) + O(^1S) + 0.80 \text{ eV}. \quad (1e)$$

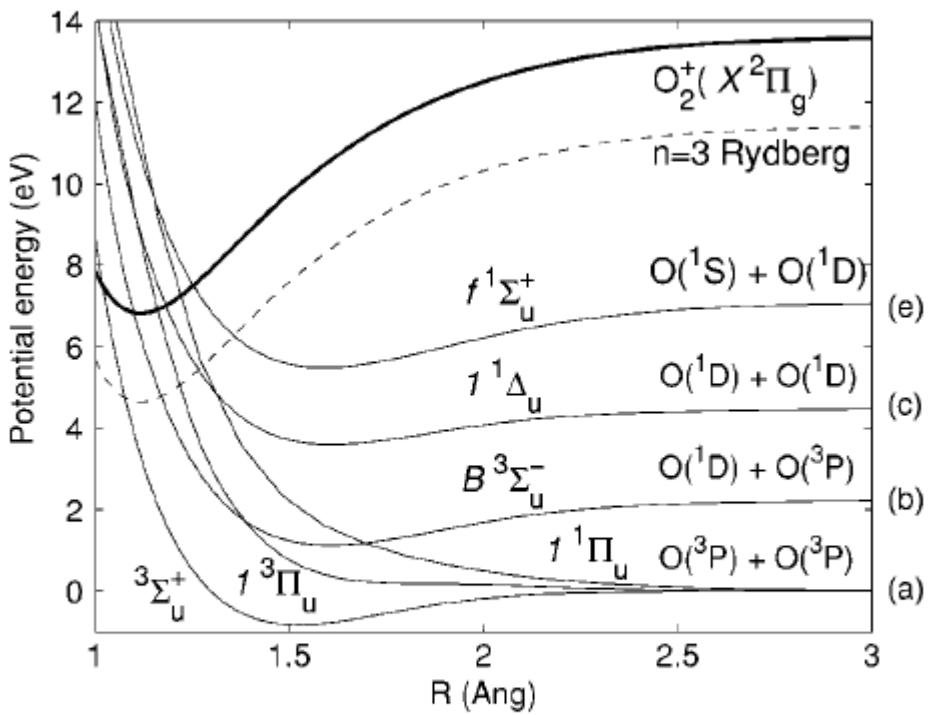

FIG. 1. Schematic of the diabatic potential curves relevant for the DR of O_2^+. The dissociation limits connected with each valence capture state are given on the right. The labels (a)–(c), and (e) refer to Eqs. (1a)–(1c) and (1e), respectively.

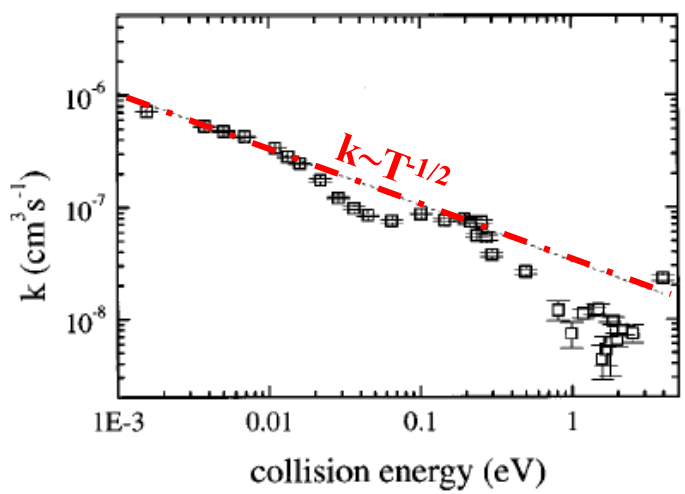

FIG. 2. DR rate coefficient k as a function of electron collision energy from 1 meV to 5 eV. Statistical errors are shown at the 1σ level. The dotted line shows the threshold $E^{-1/2}$ behavior. Both the rate coefficient and the energy are shown on a logarithmic scale.

Electron - Ion Recombination

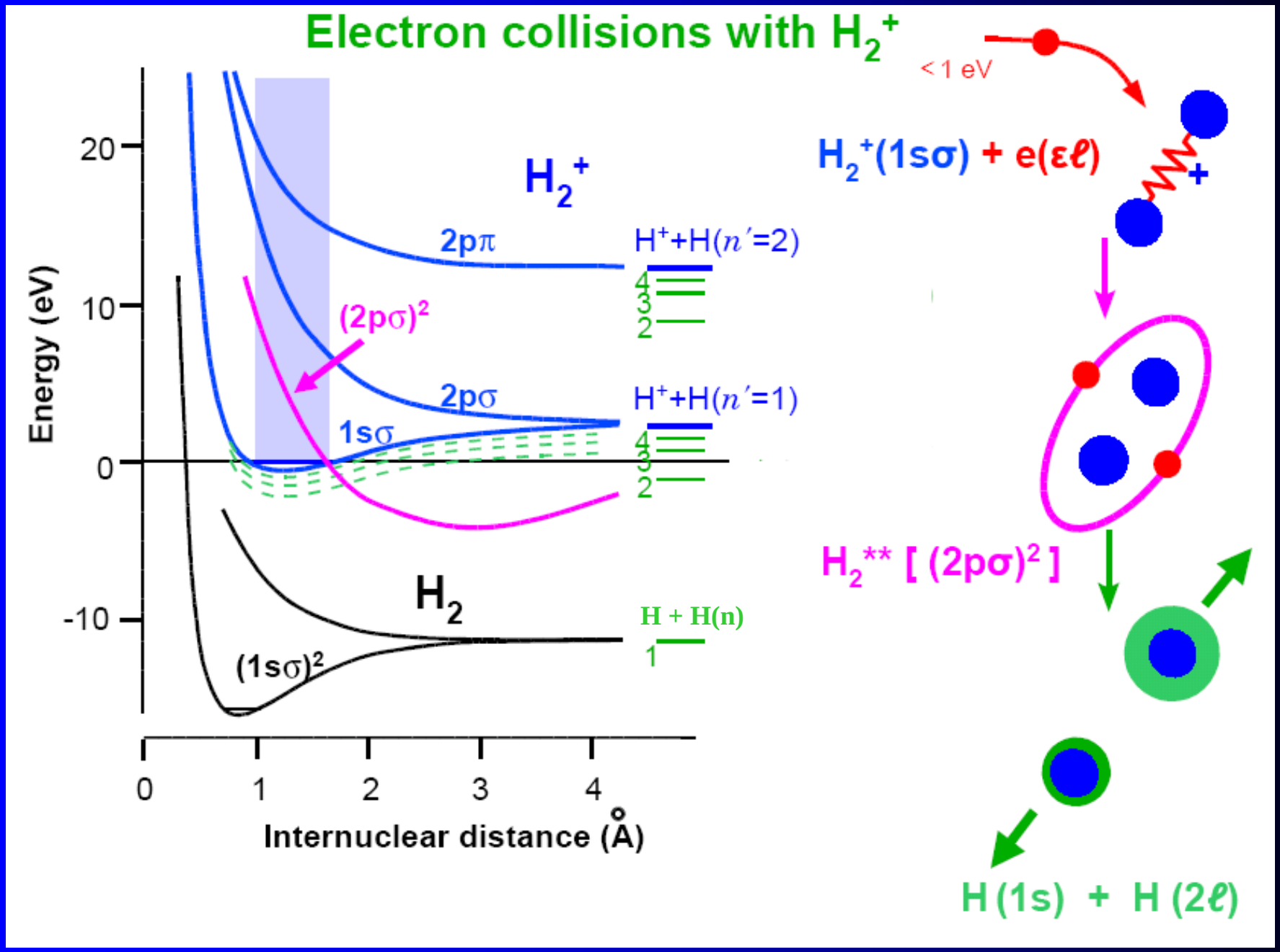

Resonances

Resonances

Autoionizing and pre-dissociating Rydberg states

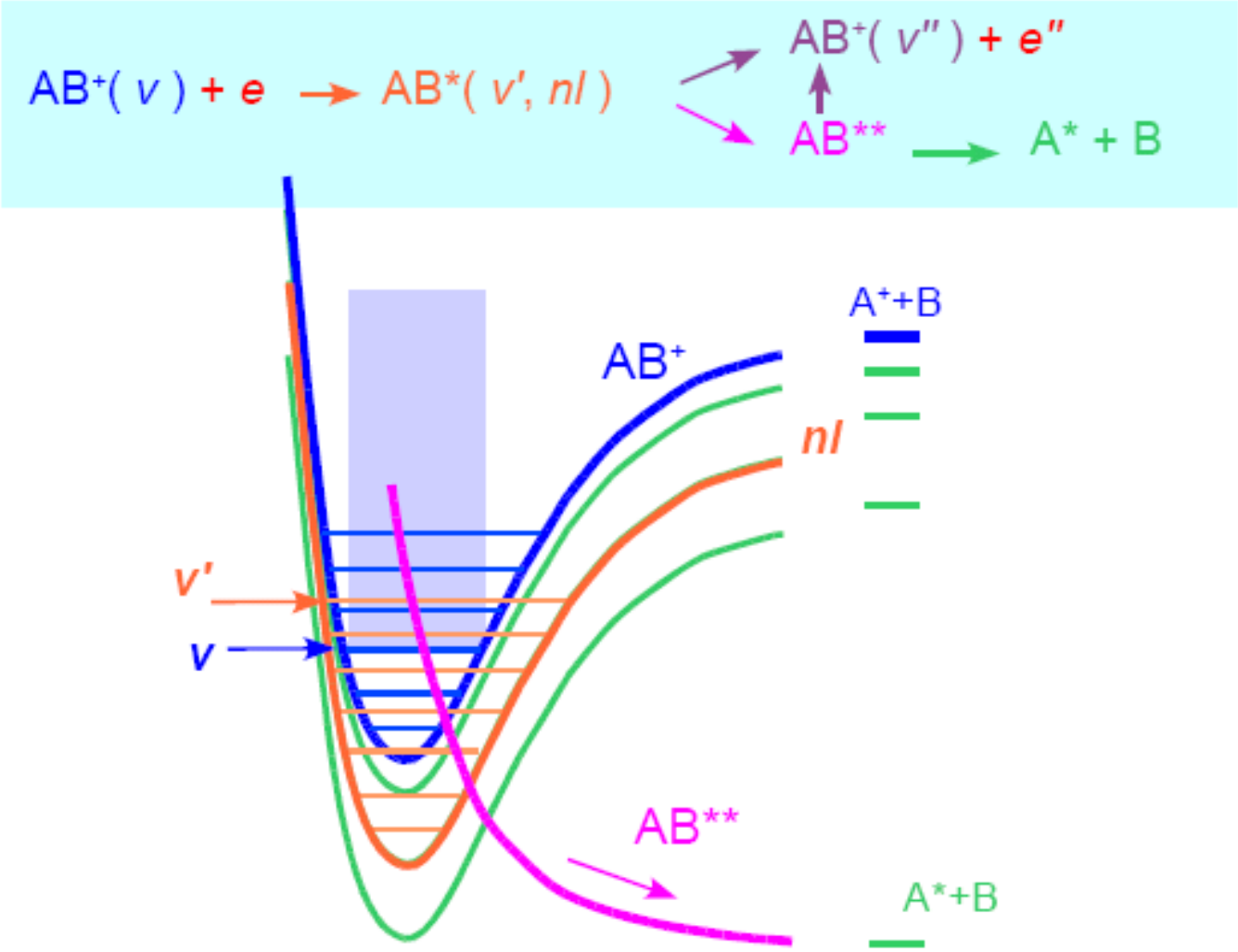

Dissociative recombination

Resonances

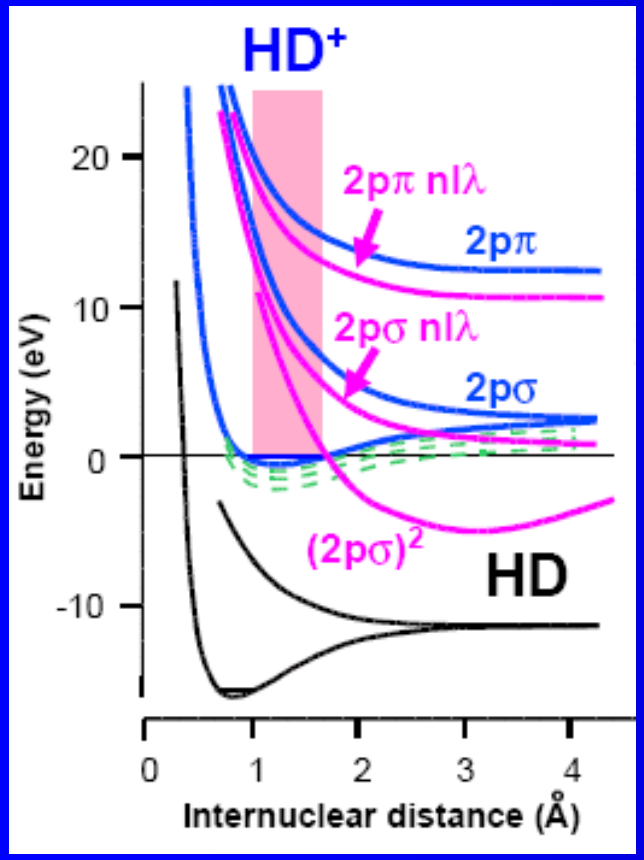

Dissociative recombination

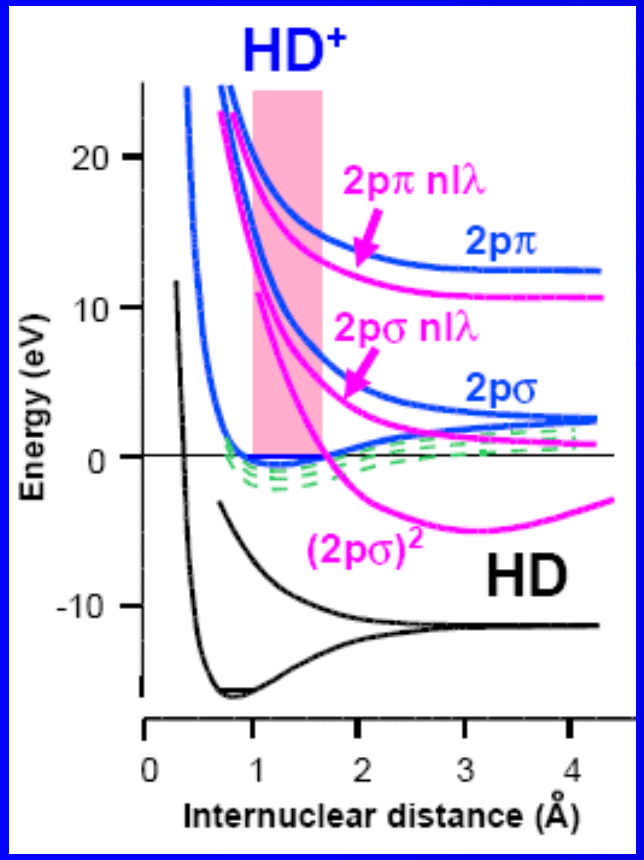

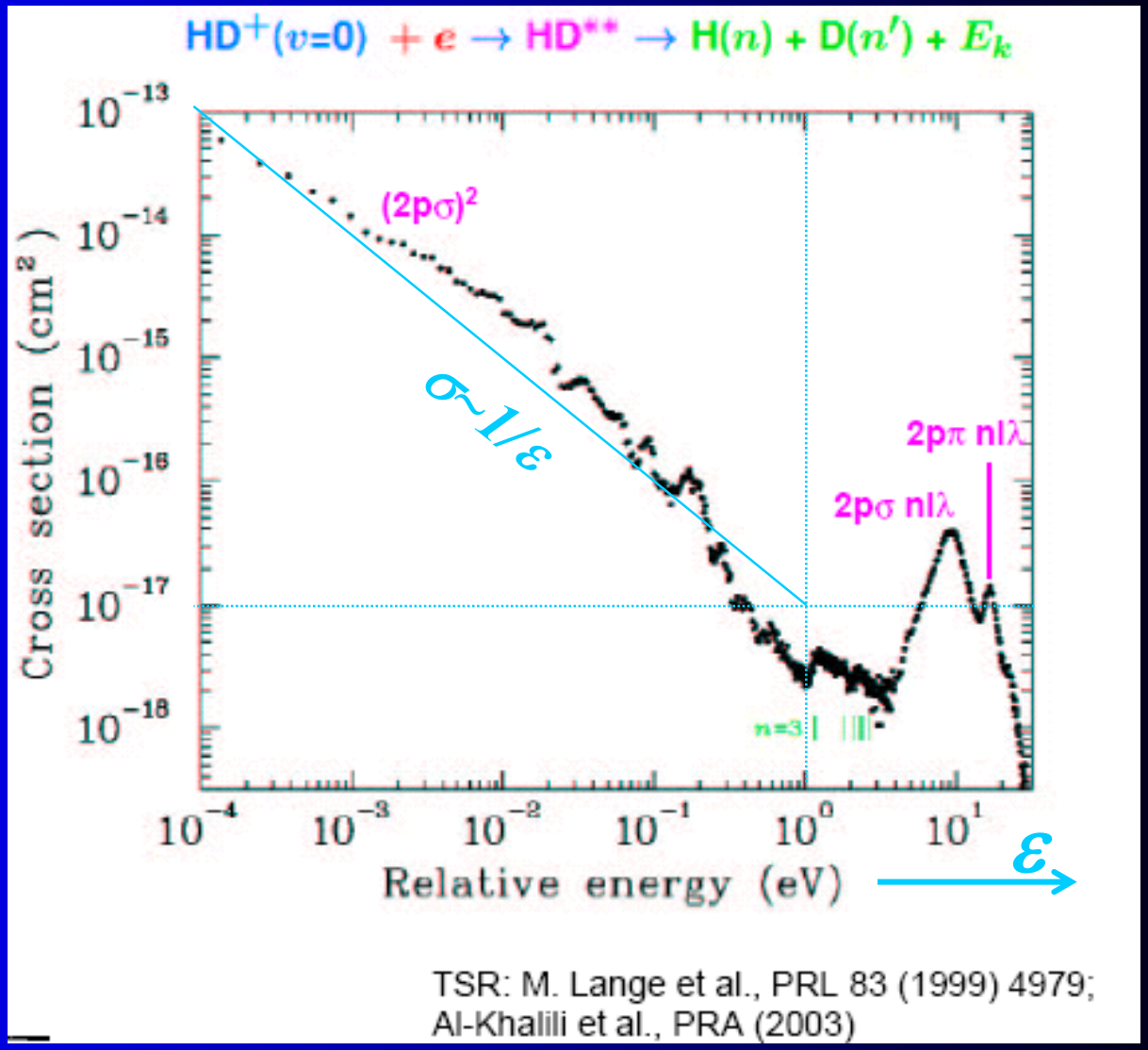

TSR: M. Lange et al., PRL 83 (1999) 4979;
Al-Khalili et al., PRA (2003)

Dissociative recombination HD+

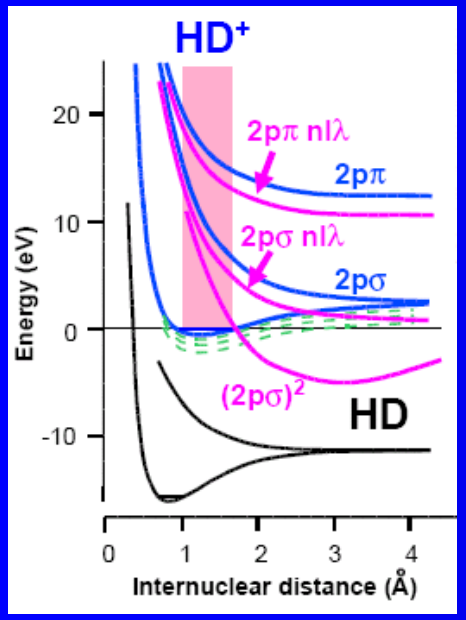

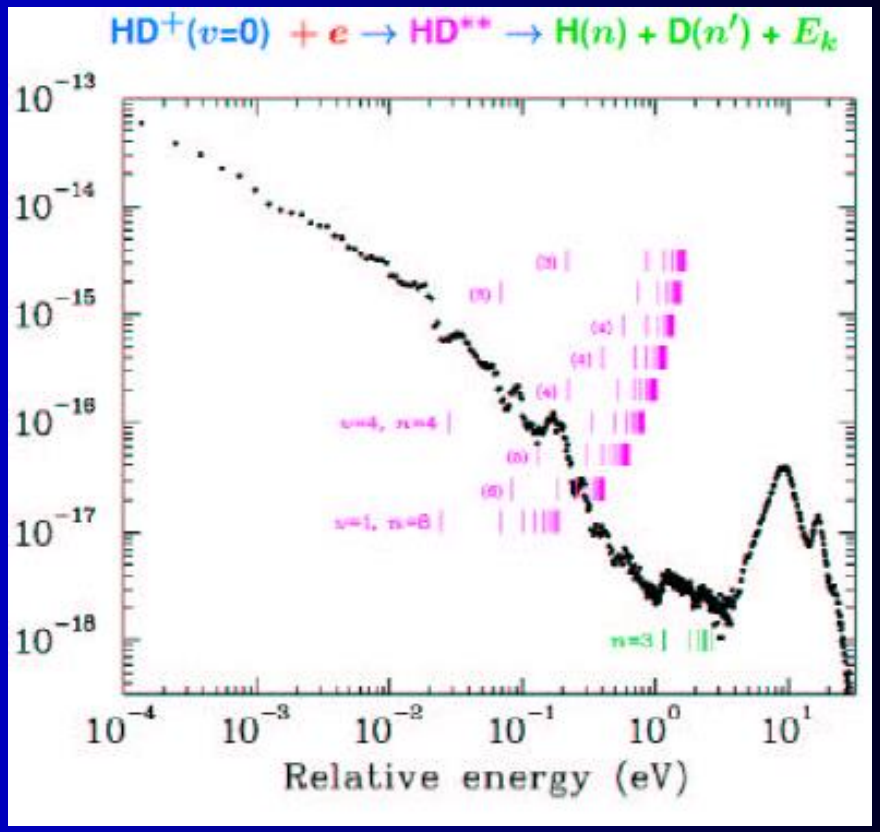

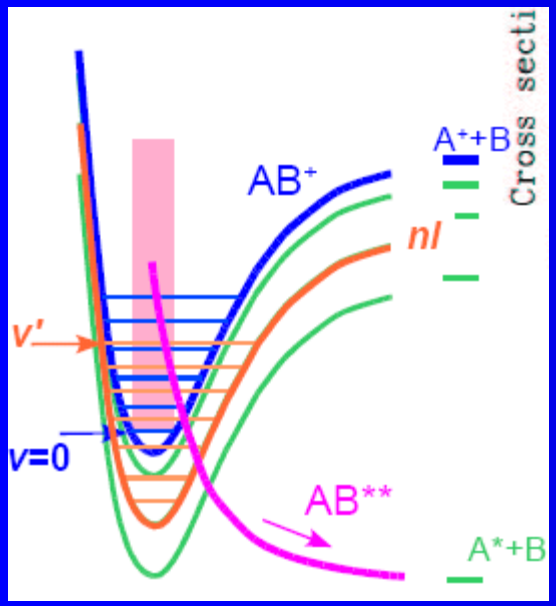

Scan of electron ion relative energy E

Electron temperature kT_{Per}=4meV (30meV for E>0.3eV)

kT_{Par}=0.1meV

Energy resolution ~4….8 meV (E< 0.08eV)

Absolute accuracy of cross section ca. +- 30%

Recombination H_2^+

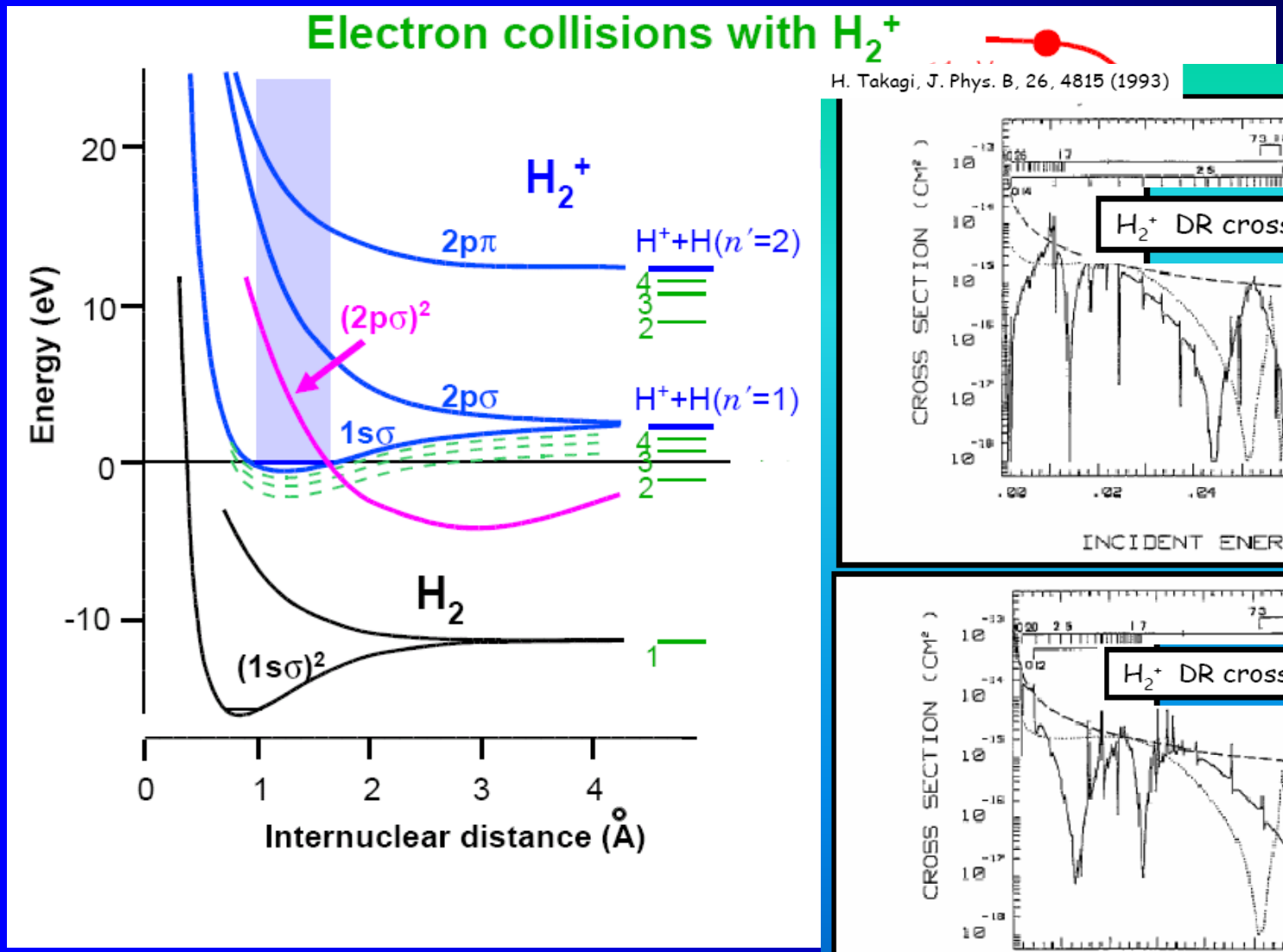

H. Takagi, J. Phys. B, 26, 4815 (1993)

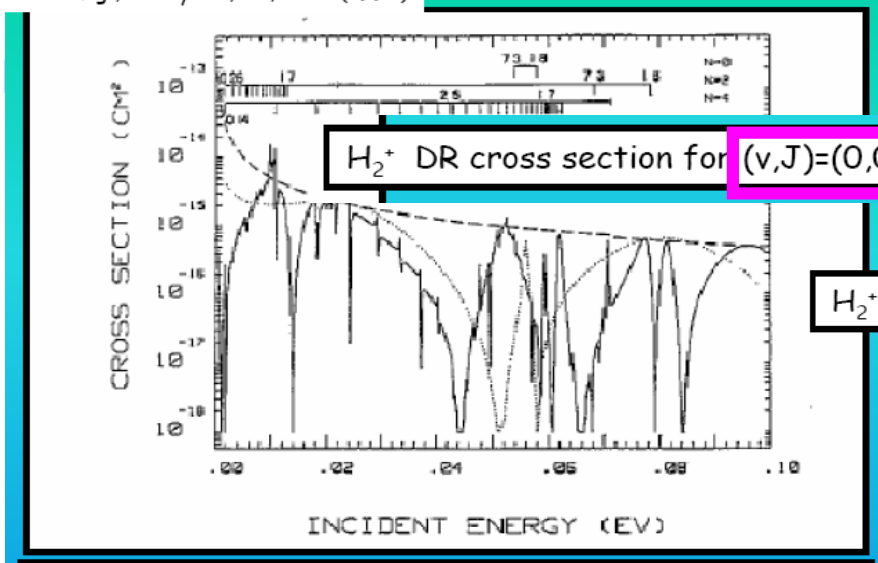

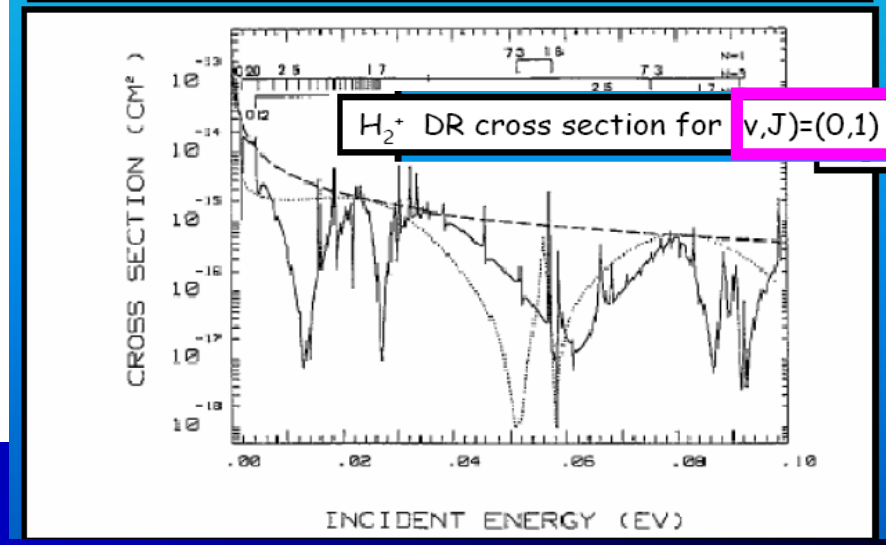

Recombination only one rotational quanta change the whole spectra

H. Takagi, J. Phys. B, 26, 4815 (1993)

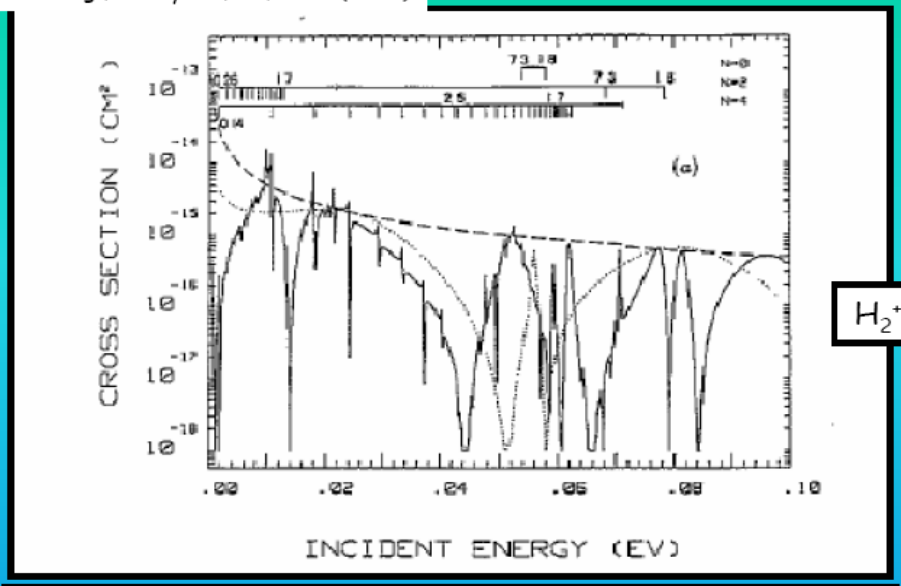

H_2^+ DR cross section for (v,J)=(0,0)

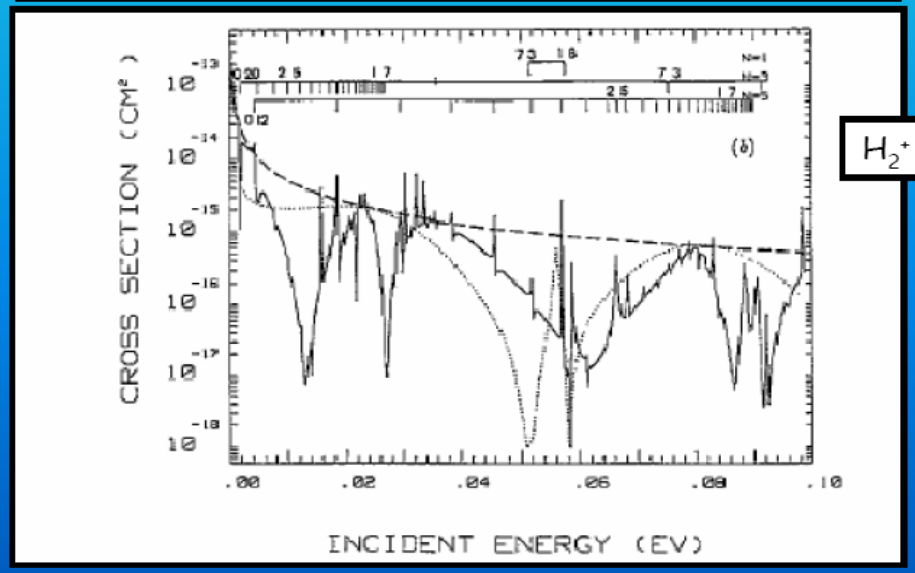

H_2^+ DR cross section for (v,J)=(0,1)

Recombination cross section for a single quantum rotational state of H_2^+ (The simplest molecular ion!)

Only one rotational quanta of excitation changes the whole spectra!!

In fact, these resonances have never been individually observed!

- Position
- Depth
- Shape

teach everything about the dynamics taking place during the dissociation.

D. Zajfman, et al., DR2004 Mosbach

Recombination calculation and theory H_2^+ …..vibrational excitation

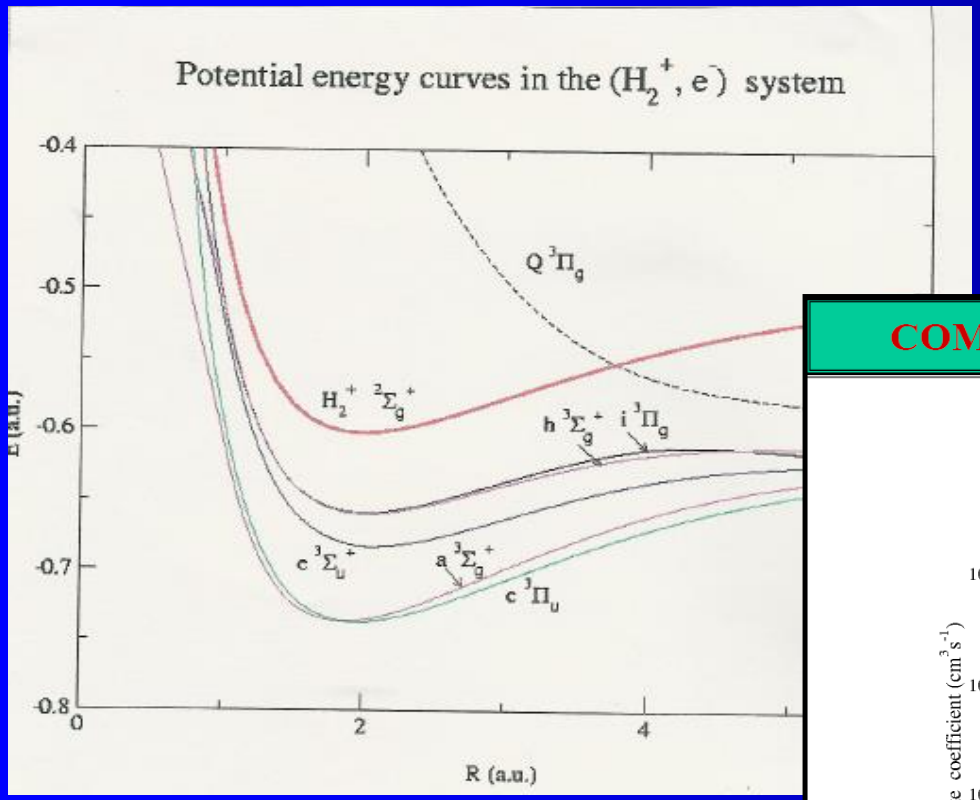

COMPUTATIONS vs MEASUREMENTS: H_2^+/H_2

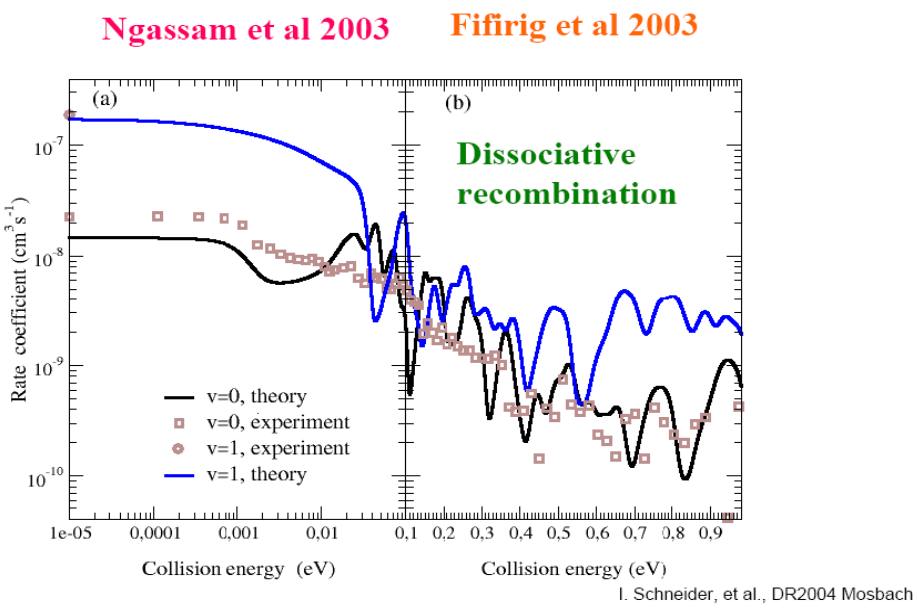

I. Schneider, et al., DR2004 Mosbach

Different energy region

Recombination NO^+

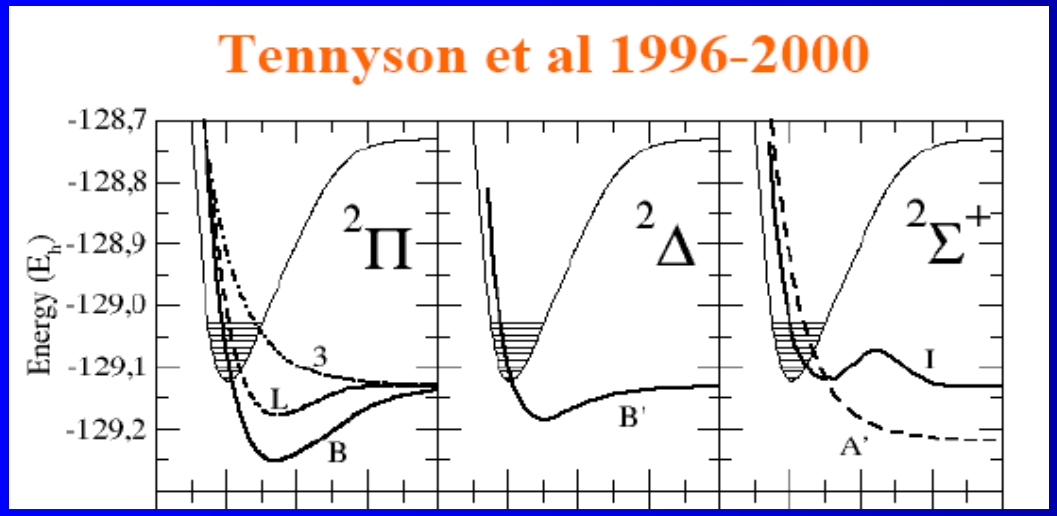

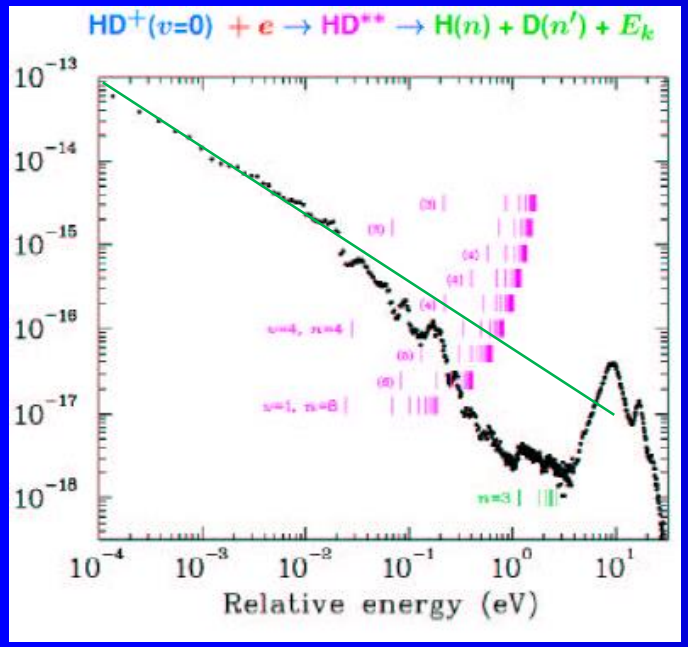

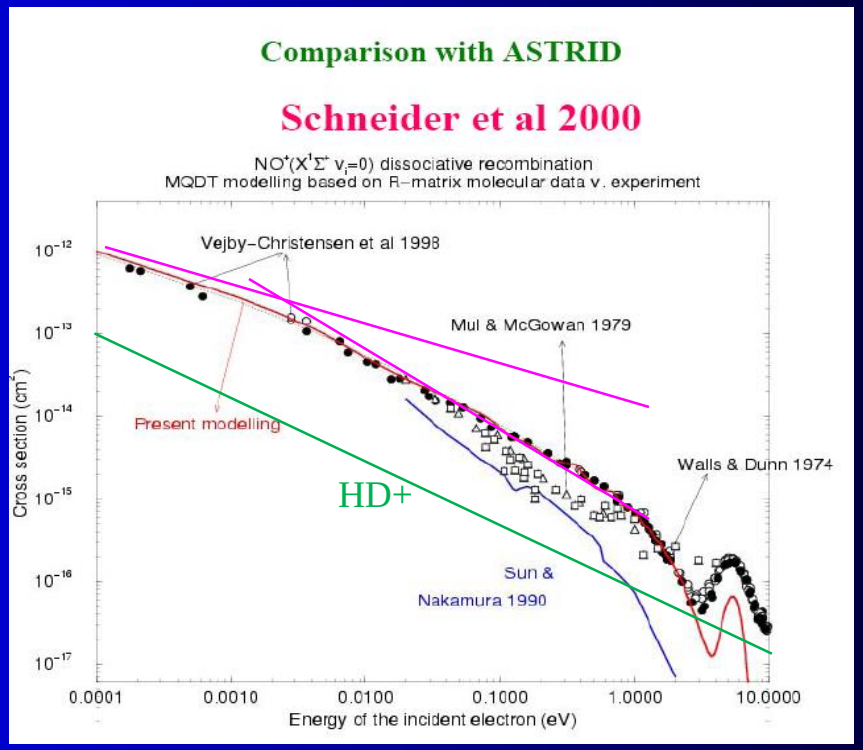

Theoretical background

Dissociative Recombination without a Curve Crossing

Theory predicted: DR rate coefficient is vary small ~ **10^{-11} cm^3s^{-1}**

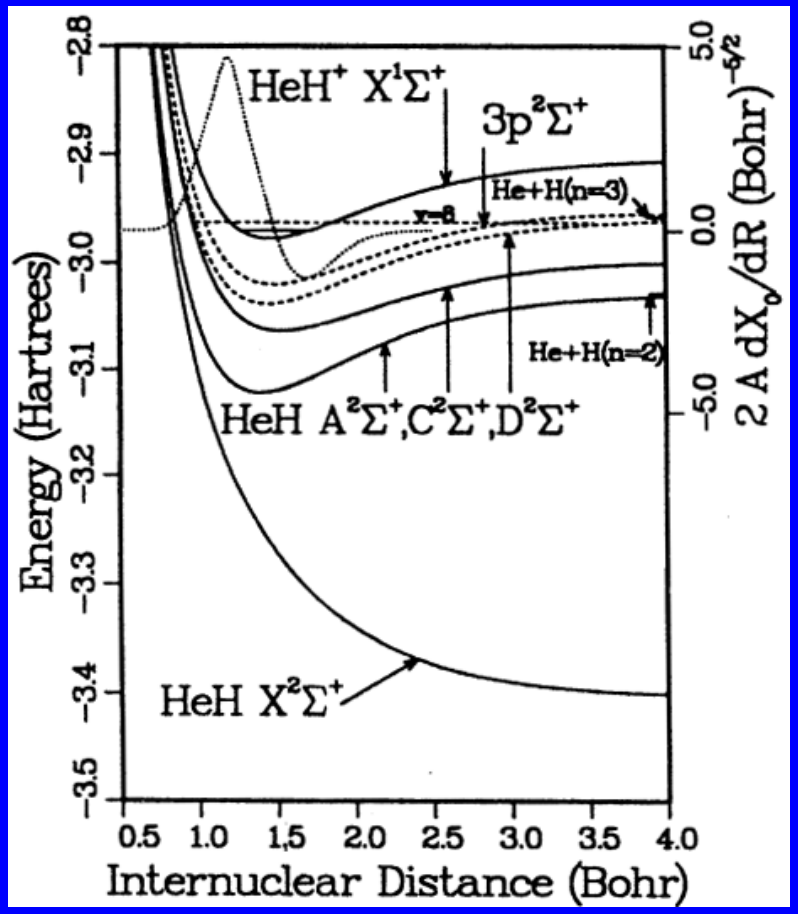

HeH^+ and HCO^+ ions- examples of a non-crossing case. <u>However, experiments gave</u> $\alpha \approx 2\times10^{-8}$ and $\alpha \approx 2 \times10^{-7}$ cm^3s^{-1}

A new mechanism has been proposed!

Multi-step indirect dissociative recombination ("tunneling mode" recombination)

Science REPORTS

2019

Cite as: O. Novotný *et al.*, *Science* 10.1126/science.aax5921 (2019).

Quantum-state-selective electron recombination studies suggest enhanced abundance of primordial HeH^+

Oldřich Novotný[1*], Patrick Wilhelm[1], Daniel Paul[1], Ábel Kálosi[1,2], Sunny Saurabh[1], Arno Becker[1], Klaus Blaum[1], Sebastian George[1,3], Jürgen Göck[1], Manfred Grieser[1], Florian Grussie[1], Robert von Hahn[1], Claude Krantz[1], Holger Kreckel[1], Christian Meyer[1], Preeti M. Mishra[1], Damian Muell[1], Felix Nuesslein[1], Dmitry A. Orlov[1], Marius Rimmler[1], Viviane C. Schmidt[1], Andrey Shornikov[1], Aleksandr S. Terekhov[4], Stephen Vogel[1], Daniel Zajfman[5], Andreas Wolf[1]

[1]Max-Planck-Institut für Kernphysik, Saupfercheckweg 1, 69117 Heidelberg, Germany. [2]Charles University, 18000 Praha, Czech Republic. [3]Universität Greifswald, Institut für Physik, 17487 Greifswald, Germany. [4]Rzhanov Institute of Semiconductor Physics, Novosibirsk 630090, Russia. [5]Weizmann Institute of Science, Rehovot 76100, Israel.

*Corresponding author. Email: oldrich.novotny@mpi-hd.mpg.de

The epoch of first star formation in the early universe was dominated by simple atomic and molecular species consisting mainly of two elements: hydrogen and helium. Gaining insight into this constitutive era requires thorough understanding of molecular reactivity under primordial conditions. We used a cryogenic ion storage ring combined with a merged electron beam to measure state-specific rate coefficients of dissociative recombination, a process by which electrons destroy molecular ions. We found a dramatic decrease of the electron recombination rates for the lowest rotational states of HeH^+, compared to previous measurements at room temperature. The reduced destruction of cold HeH^+ translates into an enhanced abundance of this primordial molecule at redshifts of first star and galaxy formation.

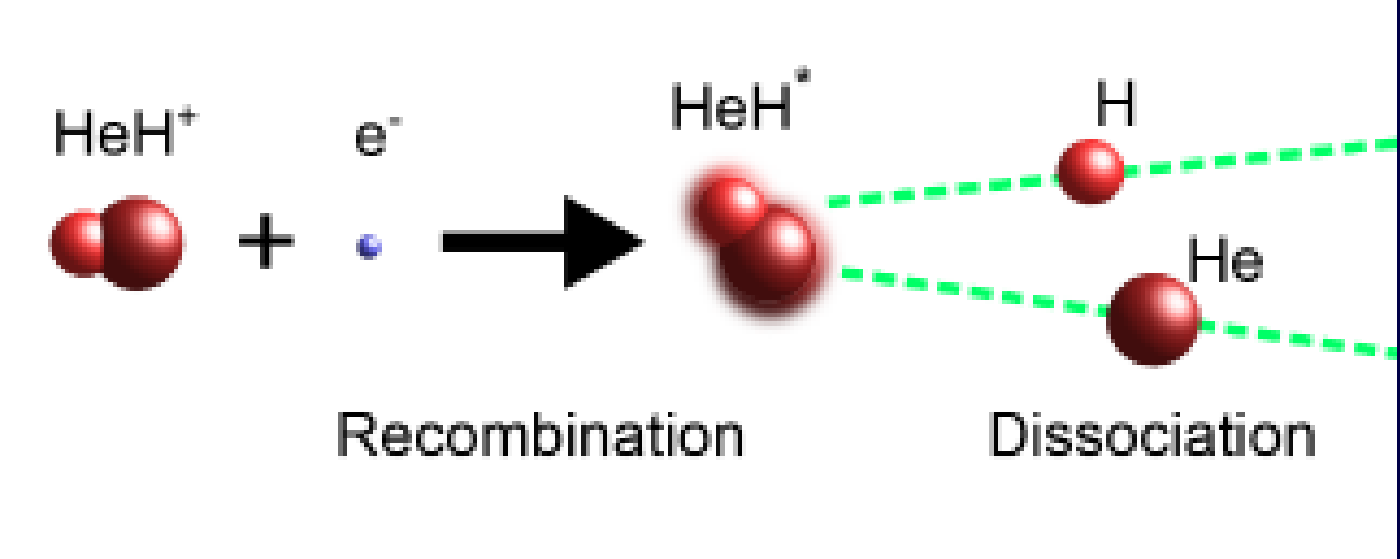

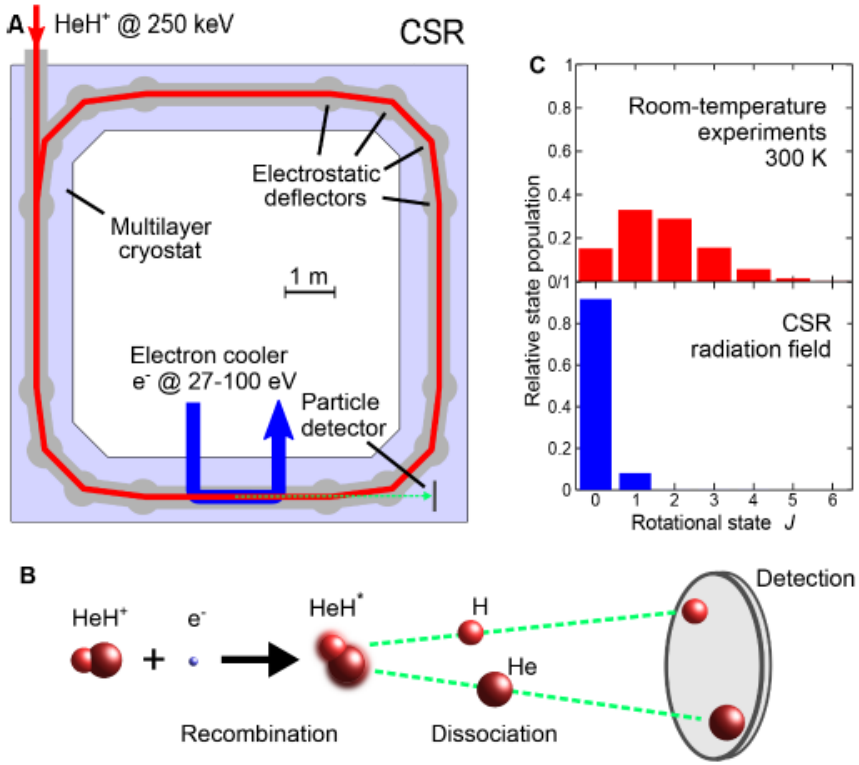

Fig. 1. Dissociative recombination in the cryogenic storage ring CSR. (**A**) Scheme of the CSR ring structure with injected and stored HeH^+ ion beam (red), merged electron beam (blue), reaction products (green) and particle detector. (**B**) Reaction scheme and position-sensitive detection of coincident fragments. (**C**) Equilibrium rotational state populations of HeH^+ for previous studies (300 K) and the estimated radiation field in the CSR.

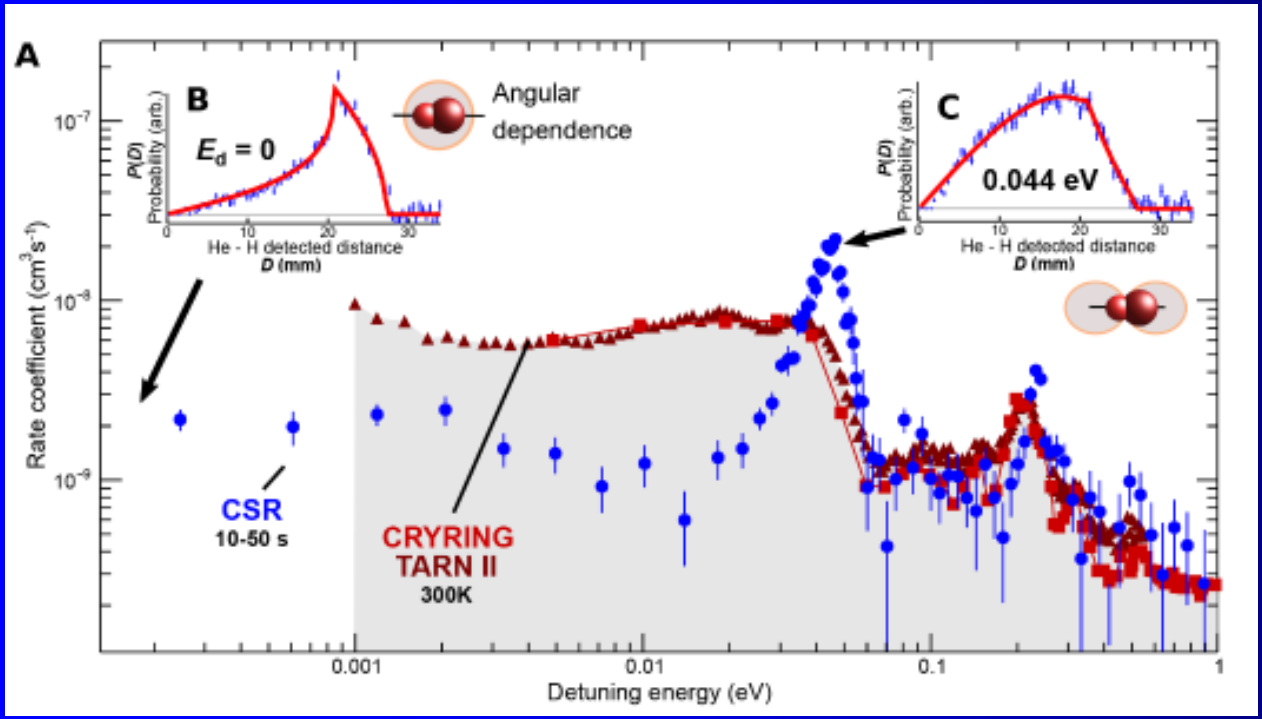

Fig. 2. DR for rotationally cold HeH^+. (A) Blue dots: merged-beams rate coefficient α_{DR} as a function of the detuning energy E_d after relaxation to >50% $J = 0$ (this experiment, 10 s < t < 50 s, mean ± SD); absolute scaling uncertainty ±20% (SEM). Red symbols: room-temperature data from Ref. (*11*) (squares, absolute scaling uncertainty ±10% SEM) and from Ref. (*12*) (triangles, scaled to Ref. (*11*) at 0.03 eV). (B) Fragment distance distribution projected into the detector plane for $E_d = 0$ (blue) with fit (*19*) for isotropic angular distribution (red). (C) Projected fragment distance distribution for $E_d = 0.044$ eV (blue) with fit (*19*) for a $|Y_{10}|^2$ angular distribution of the fragments (red). The angular dependences in (B) and (C) are indicated schematically.

Fig. 4. Rotational-state selective DR rates for HeH^+. (A) Merged-beams rate coefficients $\alpha^J_{DR}(E_d)$ for $J \leq 2$ and average for $J \geq 3$ (mainly 3 and 4; mean ± SD). The dashed lines mark the shift of the maximum as J increases. (B) Full lines: single-J plasma rate coefficients $\alpha^J_{DR,pl}(T_{pl})$ for $J \leq 2$ and average for $J \geq 3$ (mainly 3 and 4; mean with shaded areas as ± SD). Dotted: fully thermal rate coefficient $\alpha_{DR,therm}(T_{rot} = T_{pl})$. Dashed-dotted: values applied in early-universe models (*21*, *22*) and astrochemistry databases (*23*–*25*). See (*19*) for further discussion, numerical fitting functions and parameters.

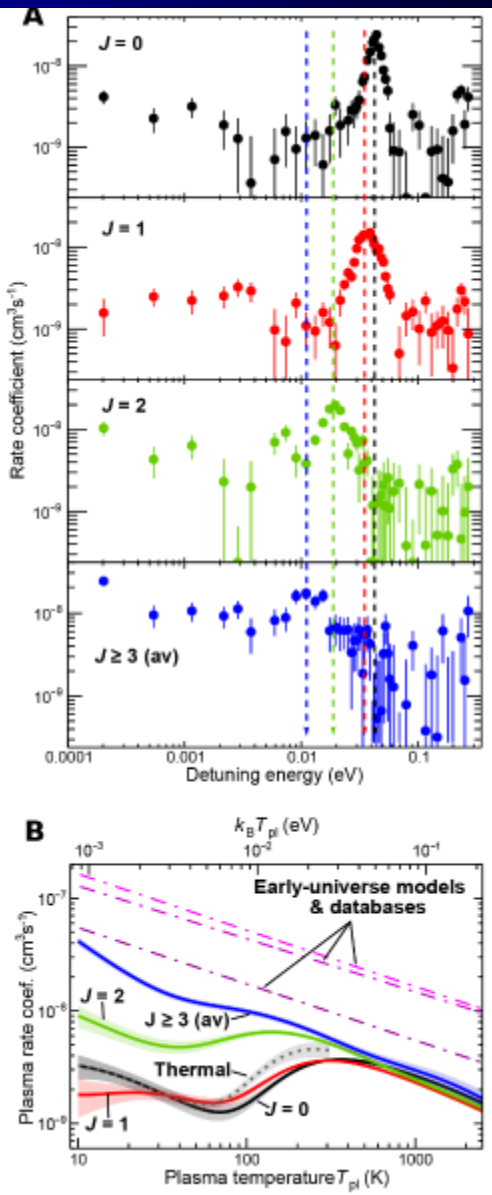

Dissociative recombination of N_2H^+ ions with electrons in the temperature range of 80–350 K

Cite as: J. Chem. Phys. **152**, 024301 (2020); https://doi.org/10.1063/1.5128330
Submitted: 18 September 2019 . Accepted: 19 December 2019 . Published Online: 08 January 2020

Dmytro Shapko, Petr Dohnal, Miroslava Kassayová, Ábel Kálosi, Serhiy Rednyk, Štěpán Roučka, Radek Plašil, Lucie D. Augustovičová, Rainer Johnsen, Vladimír Špirko, and Juraj Glosík

$$N_2H^+ + e^- \xrightarrow{\alpha_{bin}} \text{neutral products}$$

Recombination of N_2H^+ ions with electrons was studied using a stationary afterglow with cavity ring-down spectrometer. We probed in situ the time evolutions of number densities of different rotational and vibrational states of recombining N_2H^+ ions and determined the thermal recombination rate coefficients for N_2H^+ in the temperature range of 80 – 350 K. The newly calculated vibrational transition moments of N_2H^+ are used to explain the different values of recombination rate coefficients obtained in some of the previous studies. No statistically significant dependence of the measured recombination rate coefficient on the buffer gas number density was observed.

I. INTRODUCTION

N_2H^+, an important interstellar ion, has been observed in different interstellar environments such as dark and translucent clouds[1,2], protostellar cores[3], protoplanetary disks[4] and is considered to play a role in the atmospheric chemistry of Titan[5]. N_2H^+ serves as an important tracer for N_2 in dark clouds, therefore detailed information on production and destruction processes of N_2H^+ could help with the prediction of N_2 abundance in this environment. N_2H^+ in the interstellar medium is mainly produced in proton transfer from H_3^+ to N_2 and its main destruction mechanisms are proton transfer to CO and dissociative recombination with electrons[6].

$$N_2H^+ + e^- \xrightarrow{\alpha_{bin}} \text{neutral products}$$

II. EXPERIMENT

The recombination rate coefficients[7,32] are measured in a stationary afterglow (SA) in conjunction with cavity ring-down spectroscopy (CRDS) to monitor the decay of the densities of different rotational and vibrational states of N_2H^+ ions. The plasma is generated in a pulsed microwave discharge in a fused silica tube (inner diameter ≈ 1.3 cm). The microwave generator is equipped with an external fast high-voltage switch to cut off the power to the magnetron within a fall time of less than 30 µs. A low microwave power in the range of 10 – 25 W, with ≈ 40% duty cycle, is used to avoid excessive heating of the gas during the discharge. The discharge tube temperature (T_{tec}) is measured by a thermocouple outside of the discharge and can be varied between 80 and 350 K.

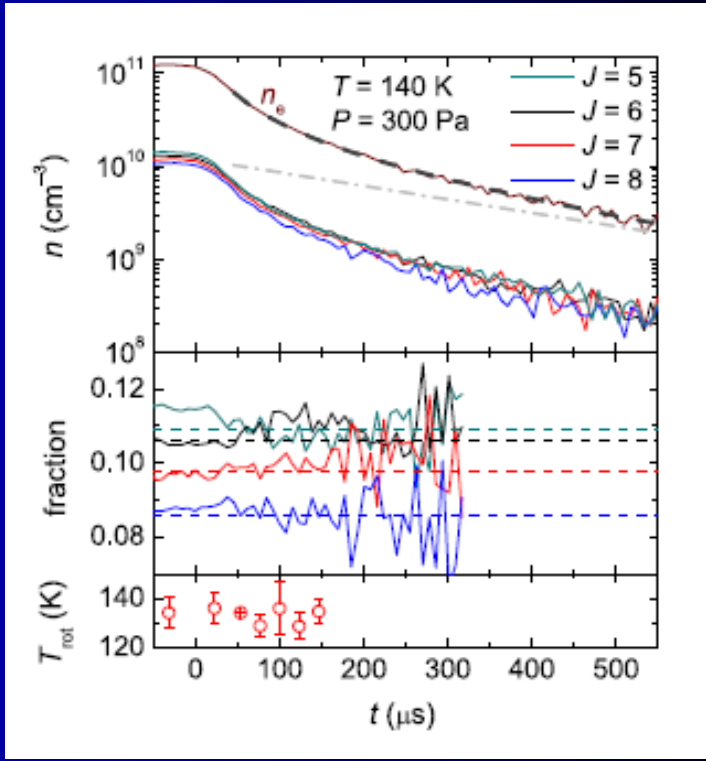

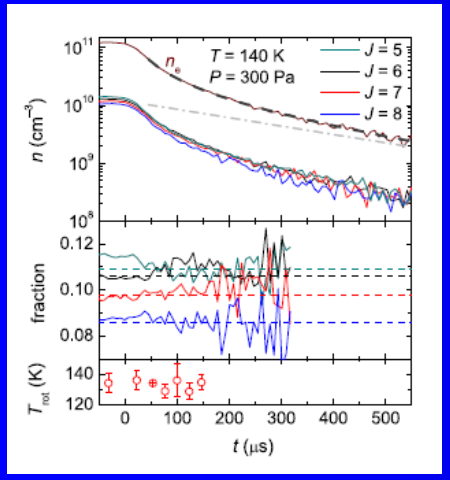

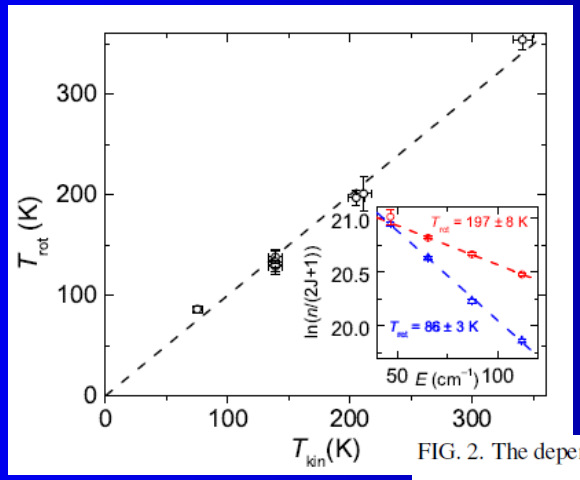

FIG. 2. The dependence of the rotational temperature measured during the discharge on kinetic temperature. All the displayed data were obtained in helium buffer gas. Insert: An example of the Boltzmann plots used for determination of the rotational temperature obtained at T = 200 K and T = 78 K.

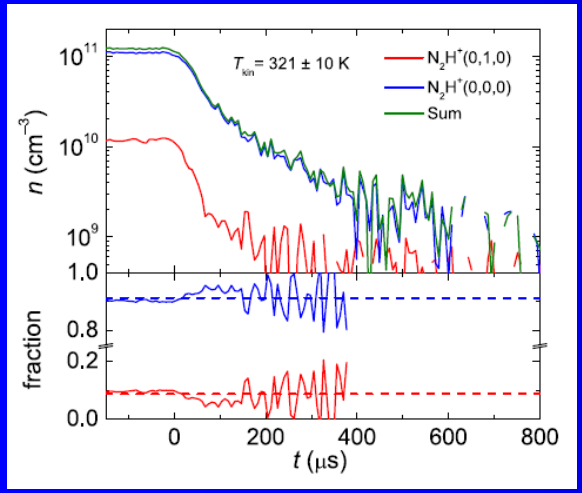

FIG. 3. An example of measured time evolutions of number densities of N_2H^+ ions in the ground and the first excited vibrational state. The lower panel shows the relative fractions of the vibrational states and the dashed lines denote the corresponding fraction in thermal equilibrium at temperature of 321 K. The particular vibrational states number densities were calculated from the measured number densities of the J = 6 rotational state of the ground vibrational state and of J = 9 state of the (01^10) vibrational state under the assumption of the same rotational temperature in both vibrational states.

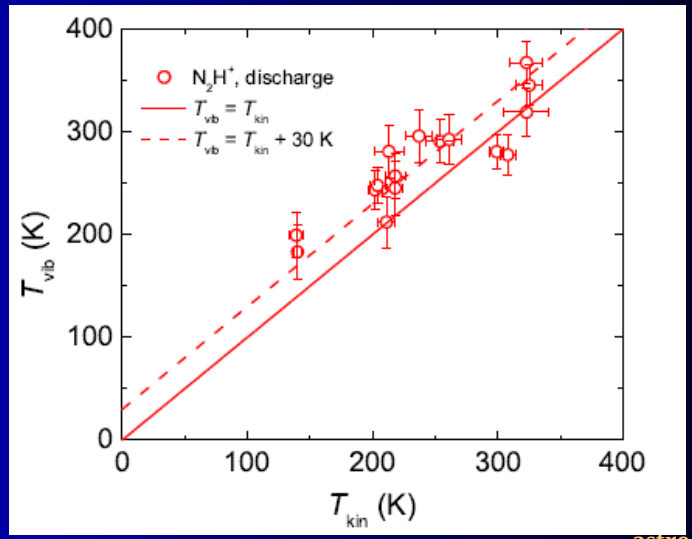

FIG. 4. Dependence of the measured vibrational temperature T_{vib} on kinetic temperature T_{kin} of the N_2H^+ ions measured in the discharge. The kinetic temperature was obtained from the Doppler broadening of the P(6) line of the (200) ← (000) vibrational band of N_2H^+. It was assumed that the rotational temperature of (000) and (010) states is equal to T_{kin}. The vibrational temperature was then evaluated from the P(6) line of the (200) ← (000) vibrational band and from the $R(9)^f$ line of the (210) ← (010) vibrational band of the N_2H^+ ion. The full line denotes equality of $T_{vib} = T_{kin}$ and the dashed line indicates $T_{vib} = T_{kin}$ + 30 K. The displayed errors are statistical errors of the fits.

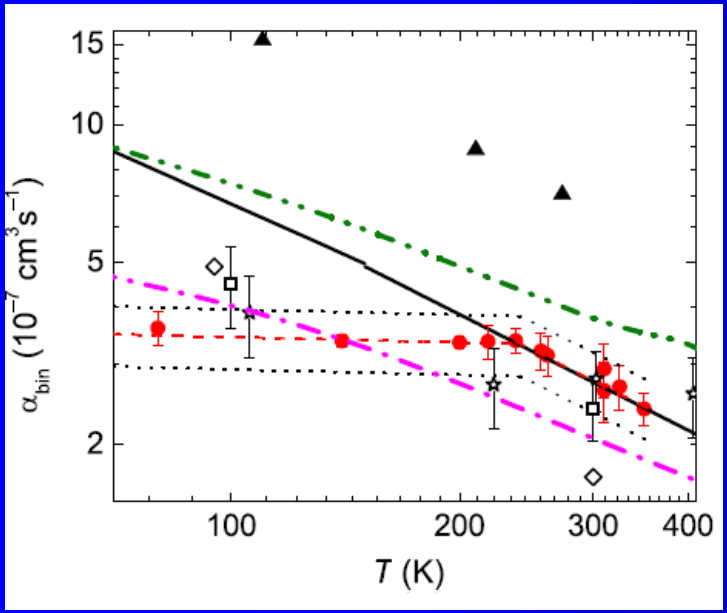

FIG. 8. The temperature dependence of the measured recombination rate coefficients of N_2H^+ (full circles, the value of α_{bin} at 350 K was obtained in H_2 buffer gas, for the rest of the data points, helium buffer gas was used) compared to values obtained in previous experiments. Rhomboids: FALP[11], squares: FALP[13], stars: FALP[14], triangles: stationary afterglow with absorption spectroscopy[17], full line: ion storage ring[6], double-dot-dashed line: merged beams[8] and to recent theoretical calculations by Fonseca dos Santos[21] (dot-dashed line, the rate coefficient was calculated from the cross sections for the direct and indirect recombination process in ref.[21]). The dashed line denotes fit to the data: $\alpha_{N_2H^+} = (2.81 \pm 0.04) \times 10^{-7}(T/300)^{-(0.81\pm0.10)}$ cm^{3}s^{-1} for $T > 240$ K and $\alpha_{N_2H^+} = (3.29 \pm 0.04) \times 10^{-7}(T/300)^{-(0.06\pm0.02)}$ cm^{3}s^{-1} otherwise. The dotted lines show 15% deviation from the fitted value (estimated systematic error of the measurement reflects mainly the uncertainty in the effective discharge column length and in the calculated vibrational transition moments).

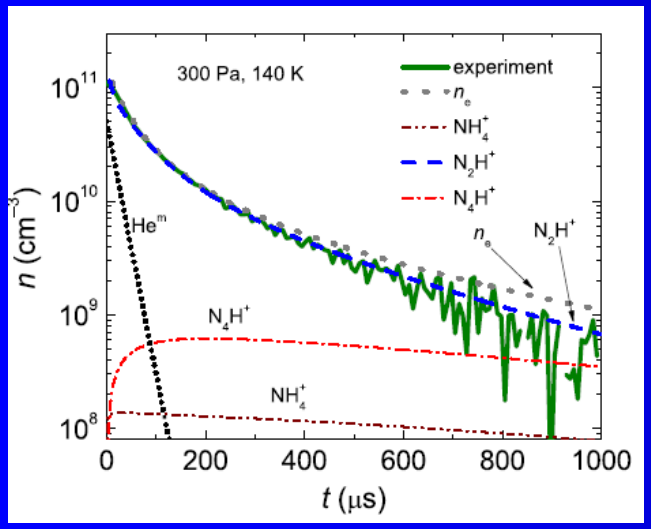

FIG. 9. Time evolution of the measured overall number density of N_2H^+ ions (full line) compared to the results obtained from the model of chemical kinetics. The data were obtained at T = 140 K, [He] = 1.5×10^{17} cm^{-3}, [Ar] = 2.5×10^{14} cm^{-3}, $[H_2] = 5 \times 10^{14}$ cm^{-3} and $[N_2] = 4 \times 10^{13}$ cm^{-3} (same as in Figure 1) and $[NH_3] = 5 \times 10^{11}$ cm^{-3}. $[He^m](t = 0) = 1/3\, n_e(t = 0)$.

Ternary recombination

Ternary electron assisted recombination

$$Ar^+ + e + e \rightarrow Ar + e$$

$$\frac{dn_e}{dt} = \frac{d[Ar^+]}{dt} = -K_e[Ar^+]n_e^{\ 2} = -\alpha_{eff}[Ar^+]n_e$$

Collisional Radiative Recombination CRR

$$\alpha_{eff} = K_e n_e$$

Ternary neutral assisted recombination

$$Ar^+ + e + He \rightarrow Ar + He$$

$$\frac{dn_e}{dt} = \frac{d[Ar^+]}{dt} = -K_M[Ar^+]n_e[He] = -\alpha_{eff}[Ar^+]n_e$$

$$\alpha_{eff} = K_M[He]$$

$Ar^+ + e^- + e^-$

$H^+ + e^- + e^-$

Anti hydrogen formation

Colisional Radiative Recombination -CRR

$$\frac{dn_e}{dt} = -K_{CRR}\ [Ar^+]n_e^2 - \frac{n_e}{\tau_D} = -K_{CRR}\ n_e^3 - \frac{n_e}{\tau_D}$$

$$\alpha_{CRR} = K_{CRR}\, n_e$$

Kvantovka na každý deň

$H^+ + e^- + e^- \rightarrow H + e^-$

PRL 98, 133201 (2007) PHYSICAL REVIEW LETTERS week ending 30 MARCH 2007

Three-Body Recombination of Atomic Ions with Slow Electrons

S. X. Hu
Laboratory for Laser Energetics, University of Rochester, 250 East River Road, Rochester, New York 14623, USA

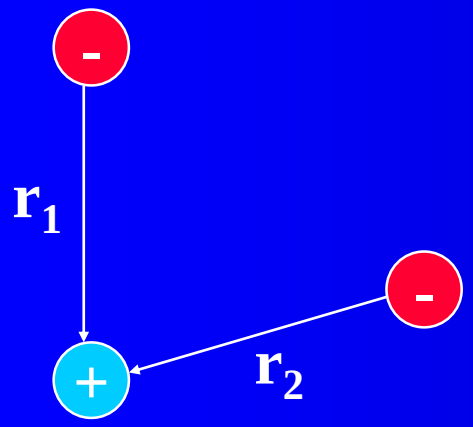

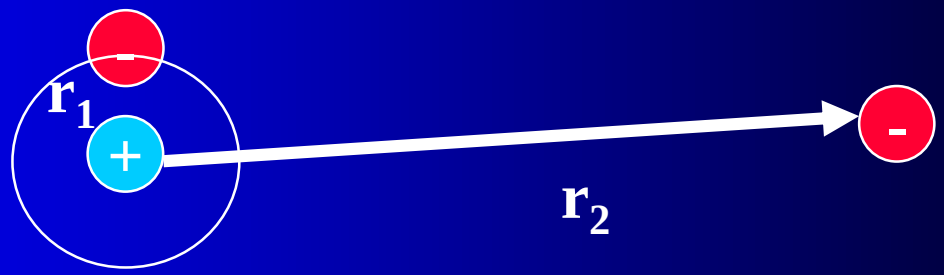

We consider the simplest TBR in the case of hydrogen formation, in which two free electrons interact with a proton. To investigate the three-body interaction dynamics, we numerically solve the six-dimensional (6D) time-dependent Schrödinger equation, which has the following form (atomic units are used throughout):

$$i\frac{\partial}{\partial t}\Phi(\mathbf{r}_1,\mathbf{r}_2,t) = \left[-\frac{1}{2}(\Delta_{\mathbf{r}_1}+\Delta_{\mathbf{r}_2}) - \frac{1}{r_1} - \frac{1}{r_2} + \frac{1}{|\mathbf{r}_1-\mathbf{r}_2|}\right]\Phi(\mathbf{r}_1,\mathbf{r}_2,t), \qquad (1)$$

where $\mathbf{r}_1$ and $\mathbf{r}_2$ are the position vectors of each electron, with respect to the proton. We obtain a more tractable solution by using the close-coupling recipe [12]: expanding the 6D wave function $\Phi(\mathbf{r}_1,\mathbf{r}_2|t)$ in terms of bipolar spherical harmonics $Y^{LS}_{l_1 l_2}(\Omega_1,\Omega_2)$, $\Phi(\mathbf{r}_1,\mathbf{r}_2|t) = \sum_{LS}\sum_{l_1 l_2}[\Psi^{(LS)}_{l_1 l_2}(r_1,r_2|t)/r_1 r_2]Y^{LS}_{l_1 l_2}(\Omega_1,\Omega_2)$, for a specific symmetry (LS). We can also expand the Coulomb repulsion term $1/|\mathbf{r}_1-\mathbf{r}_2|$ in terms of spherical harmonics. Substituting these expansions into the above Schrödinger Eq. (1) and integrating over the angles Ω_1 and Ω_2 yields a set of coupled partial differential equations with only two radial variables r_1 and r_2 left:

$$i\frac{\partial}{\partial t}\Psi_j(r_1,r_2|t) = [\hat{T}_1+\hat{T}_2+\hat{V}_c]\Psi_j(r_1,r_2|t) + \sum_k \hat{V}^I_{j,k}(r_1,r_2|t)\Psi_k(r_1,r_2|t), \qquad (2)$$

where the partial-wave index j runs from 1 to the total number N of partial waves used for expansion. In Eq. (2),

Kvantovka na každý deň

$$i\frac{\partial}{\partial t}\Psi_j(r_1, r_2|t) = [\hat{T}_1 + \hat{T}_2 + \hat{V}_c]\Psi_j(r_1, r_2|t) + \sum_k \hat{V}^I_{j,k}(r_1, r_2|t)\Psi_k(r_1, r_2|t), \qquad (2)$$

$H^+ + e^- + e^- \rightarrow H + e^-$

$$P_{nl}(E_2) = 2\sum_{LS}\sum_{l_2}\left|\int dr_1 \int dr_2 \phi^*_{nl}(r_1)\phi^*_{k_2 l_2}(r_2)\Psi^{(LS)}_{ll_2}(r_1, r_2, t = t_f)\right|^2,$$

K_E=0.1 eV

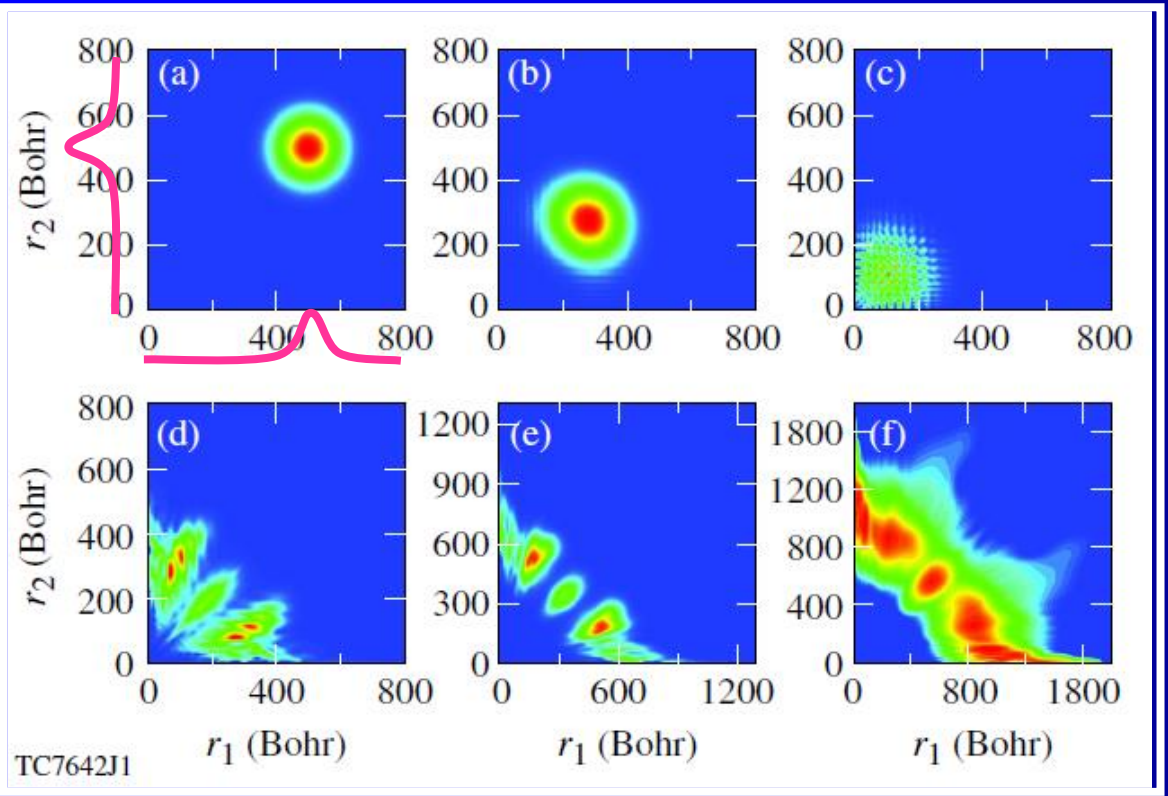

FIG. 1 (color online). Snapshots of electron probability distribution on the plane spanned by the radial coordinates r_1 and r_2 for different times: (a) $t = 0.0$ fs, (b) $t = 60$ fs, (c) $t = 100$ fs, (d) $t = 150$ fs, (e) $t = 194$ fs, and (f) (in log scale) $t = 260$ fs.

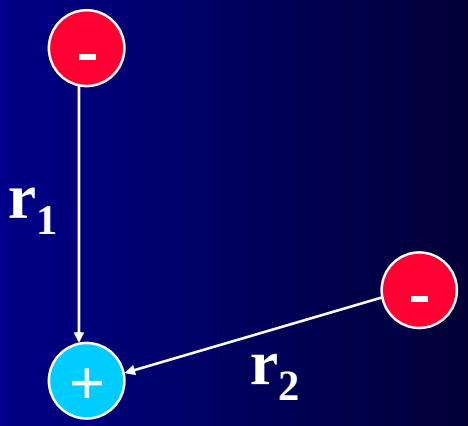

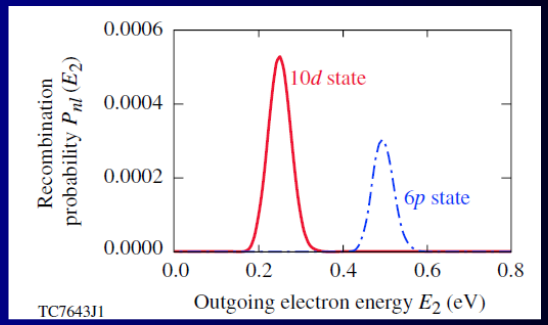

Thus, for the case of $K_E = 0.1$ eV considered in Figs. 1 and 2, the total system energy is about $E_{tot} \sim 0.12$ eV instead of $2K_E$. Hence, when one electron recombines to the $10d$ state ($|E_{10d}| \approx 0.136$ eV) of the H atom, the outgoing electron takes an initial total energy of 0.12 eV plus $|E_{10d}|$, thereby $P_{10d}(E_2)$ peaks at $E_2 \sim 0.256$ eV, as shown by the (red) solid line of Fig. 2. Similar energy conservation is also well satisfied for the recombination to the $6p$ state, as is illustrated by the (blue) dash-dotted line in Fig. 2. Our quantum calculations unambiguously reveal the essential feature of a TBR process.

Kvantovka na každý deň

$H^+ + e^- + e^- \rightarrow H + e^-$

$K_E = 0.1$ eV

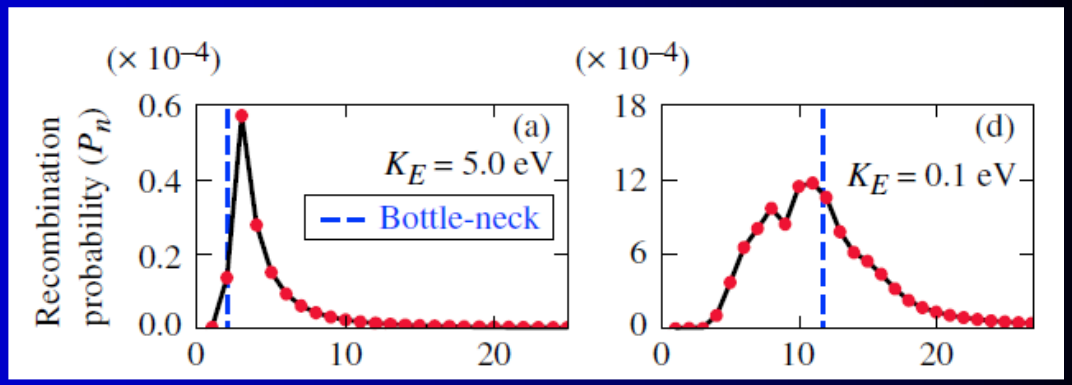

FIG. 3 (color online). The recombination probability P_n as a function of the energy level n, for different electron kinetic energies K_E marked in each panel.

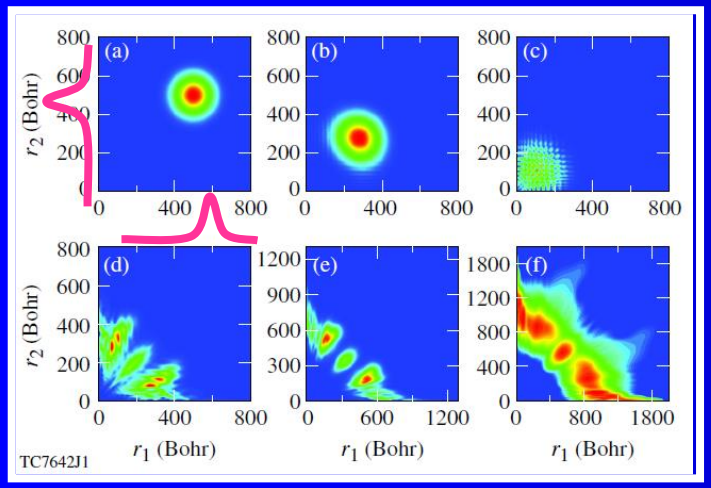

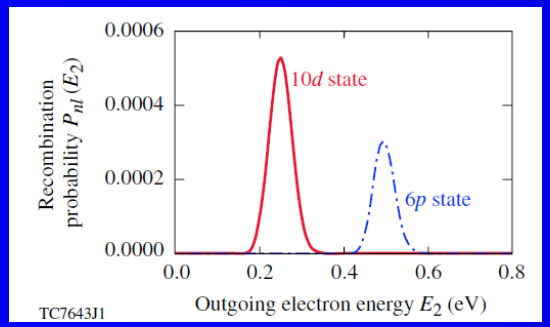

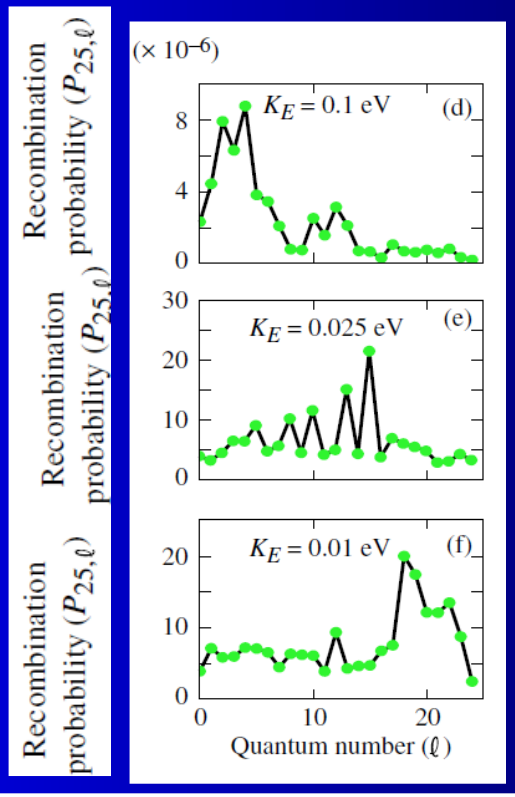

FIG. 4 (color online). The recombination probability $P_{n=25,l}$ as a function of the angular-momentum quantum number l, for different electron kinetic energies K_E marked in each panel.

$Ar^+ + e^- + e^-$

$H^+ + e^- + e^-$

$H^- + e^+ + e^+$

Anti hydrogen formation

$$\frac{dn_e}{dt} = -K_{CRR}\,[Ar^+]\,n_e^2 - \frac{n_e}{\tau_D} = -K_{CRR}\,n_e^3 - \frac{n_e}{\tau_D}$$

$$\alpha_{CRR} = 3.8\times10^{-9}T_e^{-4.5}n_e + 1.55\times10^{-10}T_e^{-0.63} + 6\times10^{-9}T_e^{-2.18}n_e^{0.37}\,\mathrm{cm^3s^{-1}}$$

$$K_{CRR} = 3.8\times10^{-9}T_e^{-4.5}\,\mathrm{cm^6s^{-1}}$$

$$\alpha_{CRR} = K_{CRR}\,n_e$$

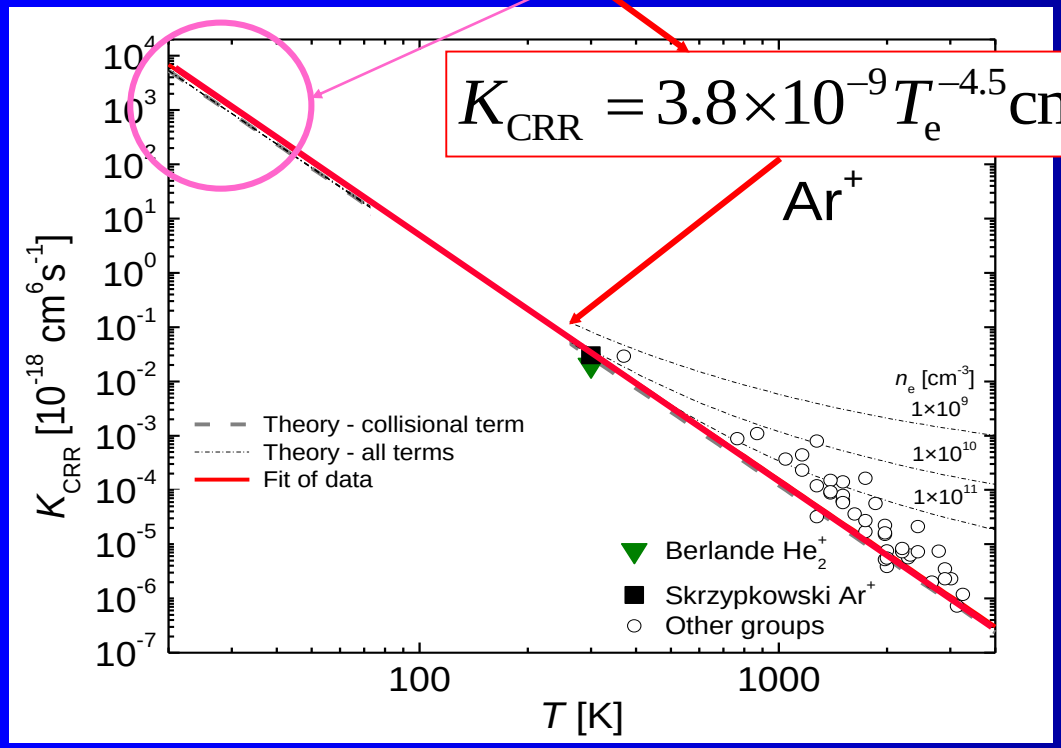

$Ar^+ + e^- + e^-$

$$\frac{dn_e}{dt} = -K_{CRR}\,[Ar^+]n_e^2 - \frac{n_e}{\tau_D} = -K_{CRR}\,n_e^3 - \frac{n_e}{\tau_D}$$

$$\alpha_{\mathrm{CRR}} = 3.8\times10^{-9}T_{\mathrm{e}}^{-4.5}n_{\mathrm{e}} + 1.55\times10^{-10}T_{\mathrm{e}}^{-0.63} + 6\times10^{-9}T_{\mathrm{e}}^{-2.18}n_{\mathrm{e}}^{0.37}\,\mathrm{cm}^3\mathrm{s}^{-1}$$

$$K_{\mathrm{CRR}} = 3.8\times10^{-9}T_{\mathrm{e}}^{-4.5}\,\mathrm{cm}^6\mathrm{s}^{-1}$$

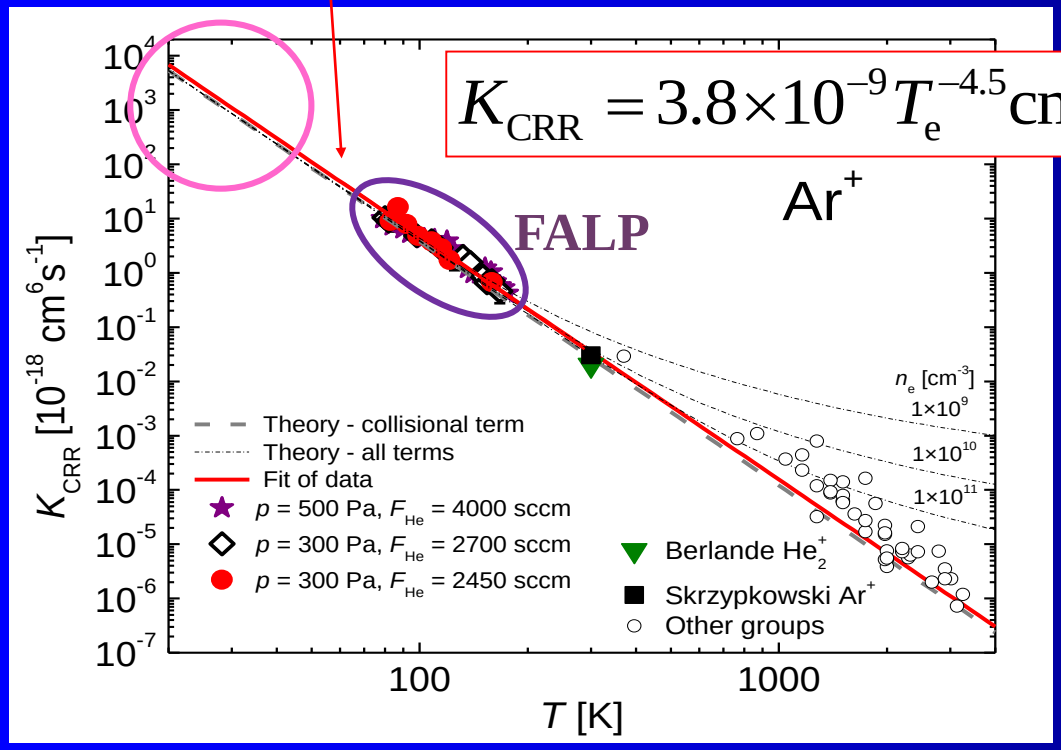

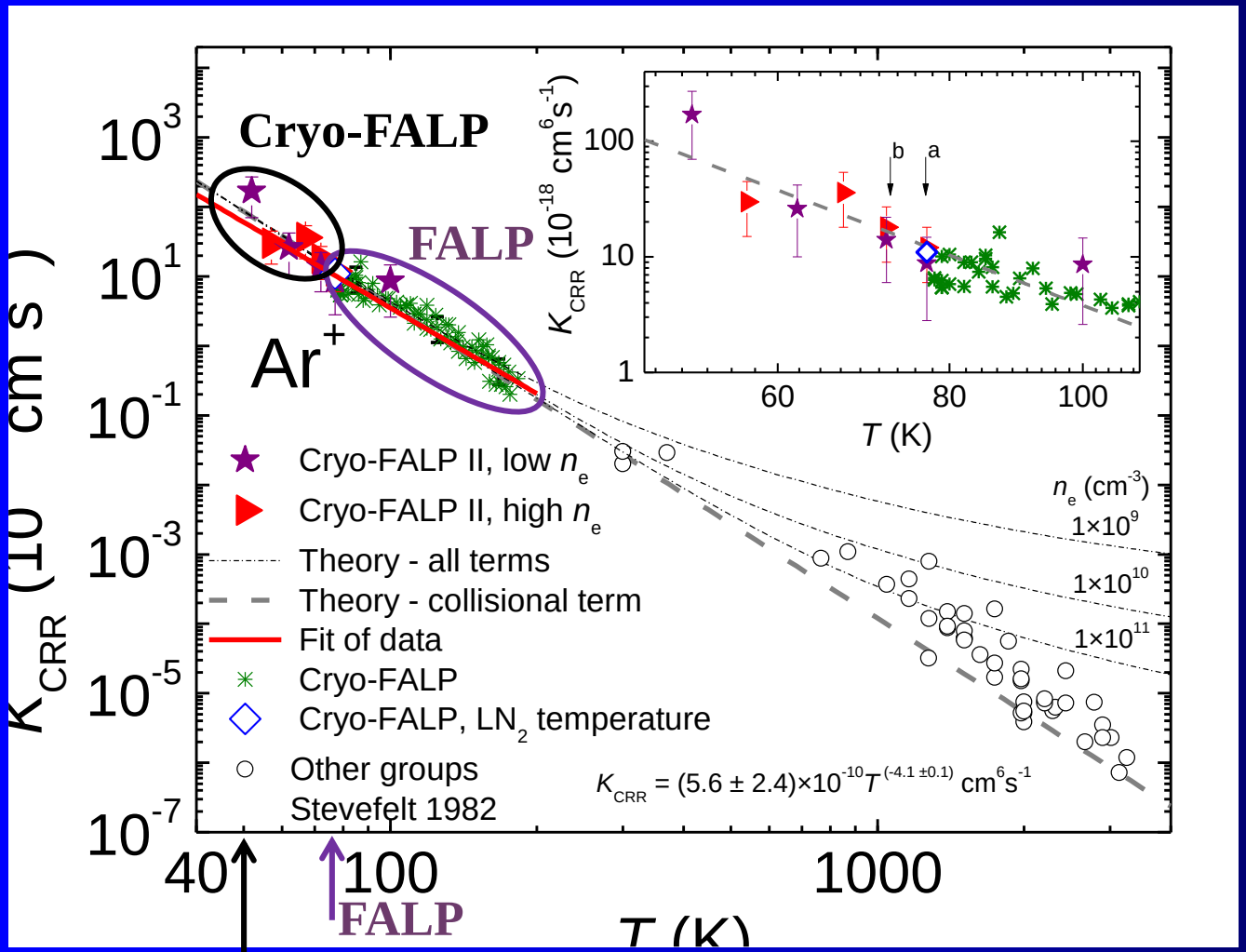
Cryo-FALP
FALP
Ar+
Cryo-FALP II, low ne
Cryo-FALP II, high ne
Theory - all terms
Theory - collisional term
Fit of data
Cryo-FALP
Cryo-FALP, LN2 temperature
Other groups
Stevefelt 1982
ne (cm-3)
1×10^9
1×10^10
1×10^11
KCRR = (5.6 ± 2.4)×10^-10 T^(-4.1 ±0.1) cm^6s^-1
KCRR (10^-18 cm^6s^-1)
T (K)
b
a
FALP
Cryo-FALP

Recombination of H_3^+

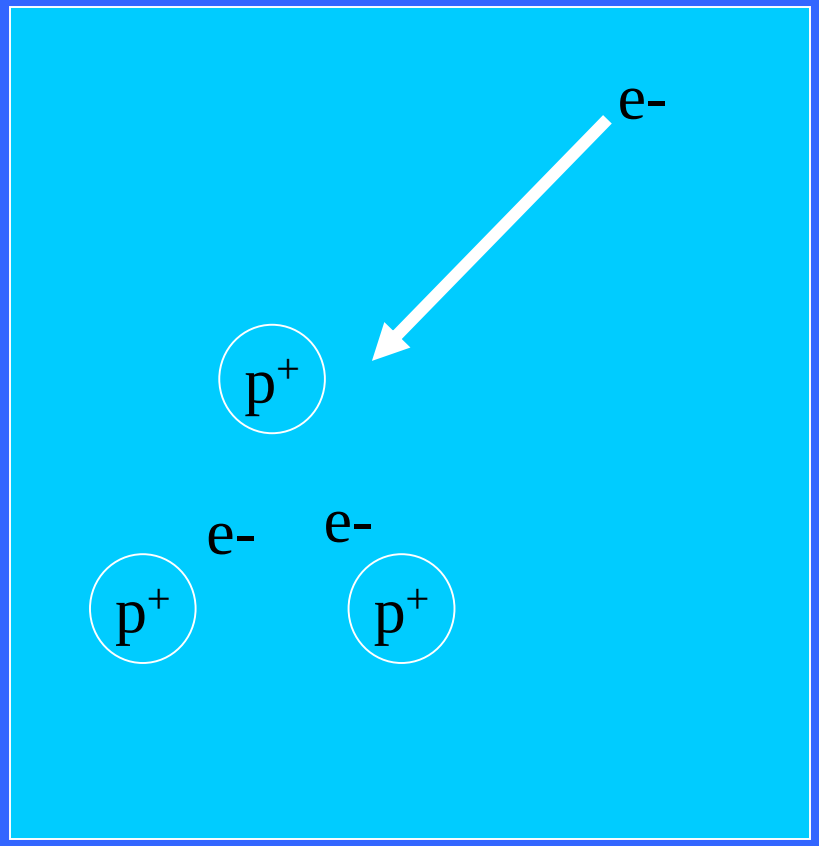

$$H_3^+ + e^- \rightarrow H + H + H$$

$$\rightarrow H_2 + H$$

$$\rightarrow H_3^* \quad (?)$$

Tunneling dissociative recombination

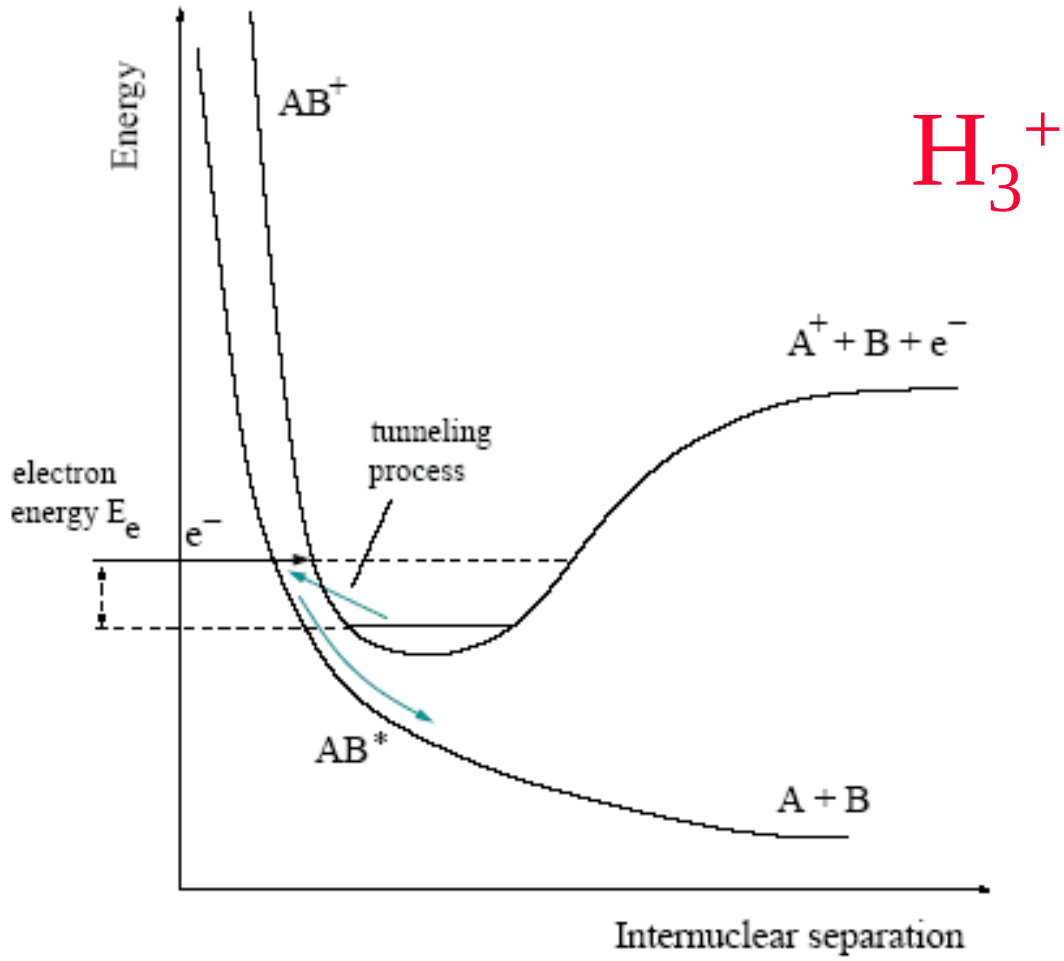

Figure 4.3: *Sketch of tunneling mode dissociative recombination.*

Tunneling dissociative recombination

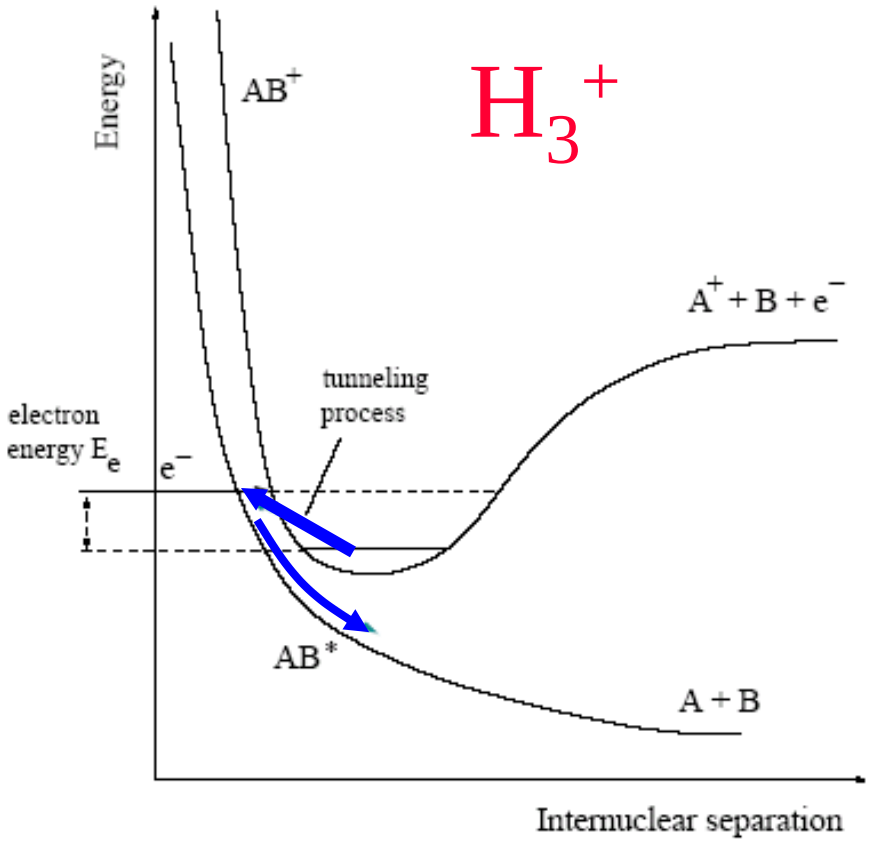

Figure 4.3: *Sketch of tunneling mode dissociative recombination.*

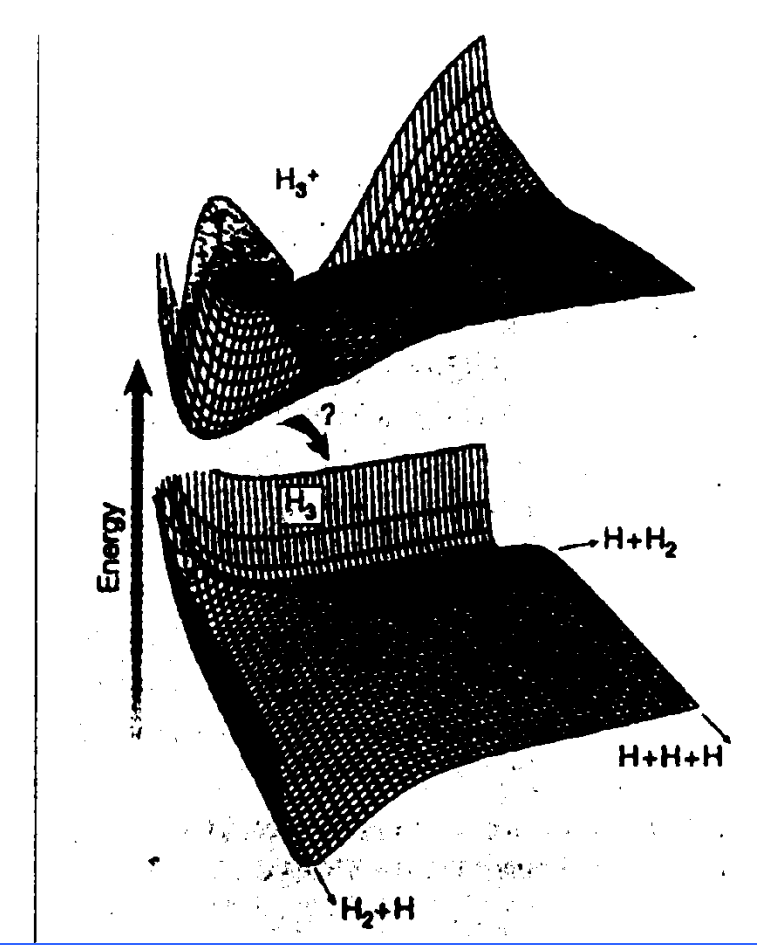

Dissociative recombination of H_3^+. Relevant potential curves

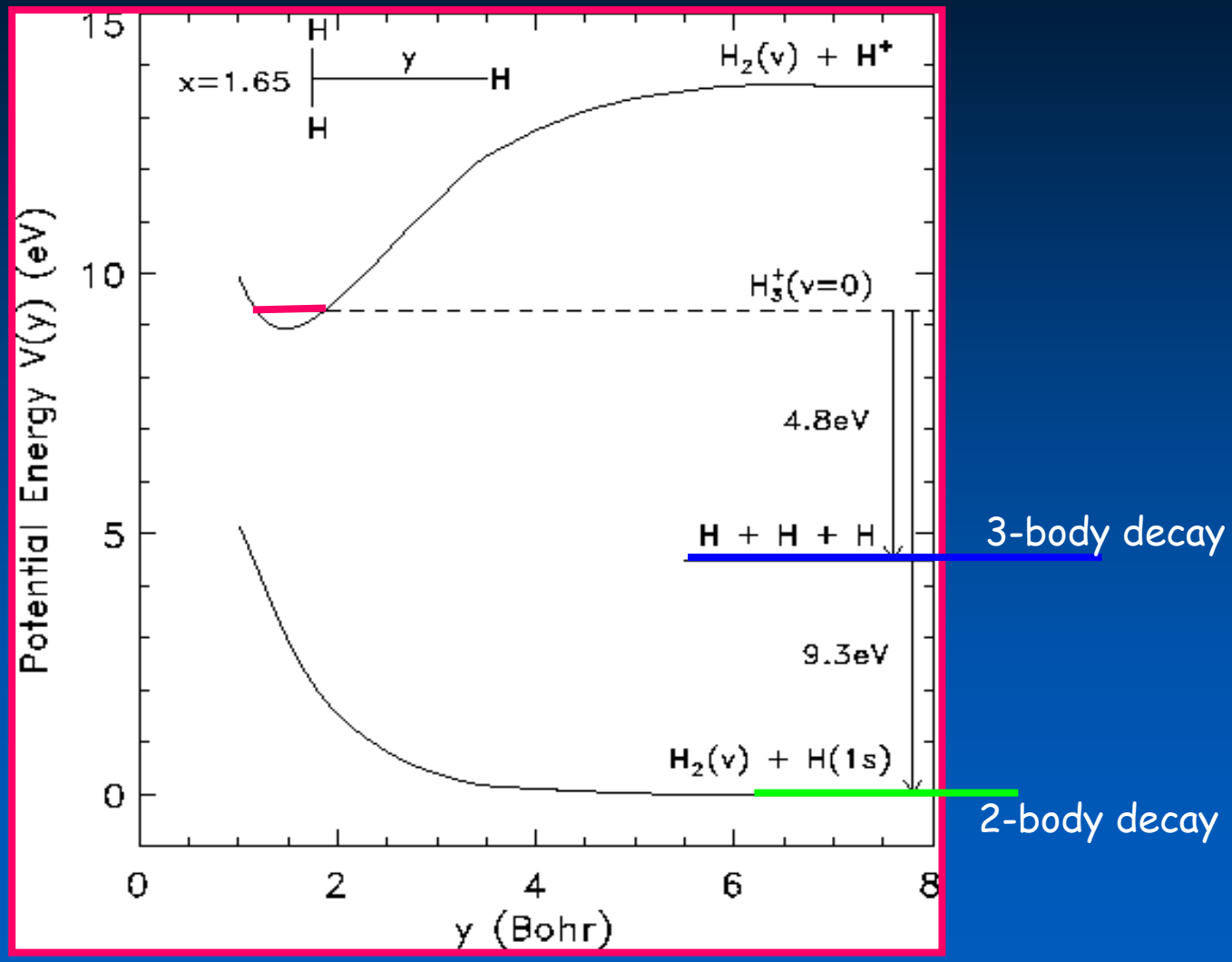

Dissociative recombination of H_3^+

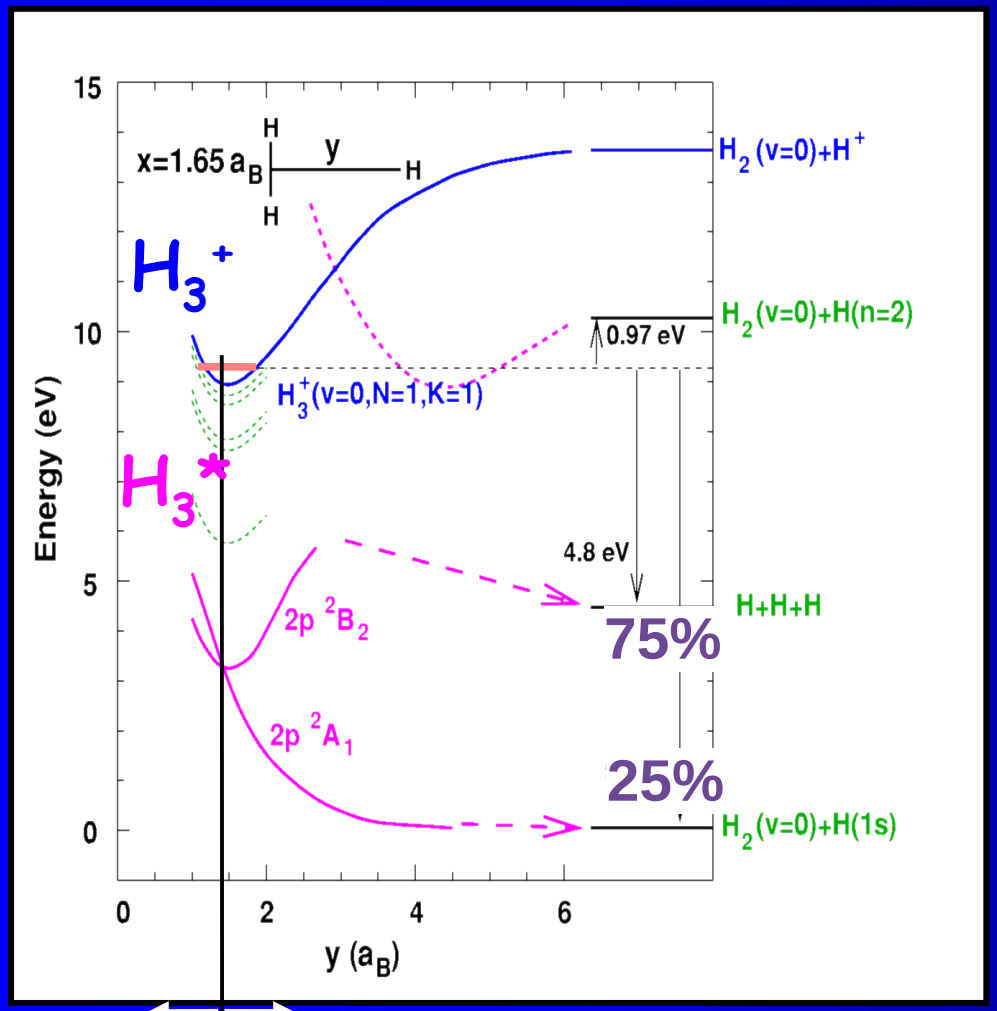

Symmetric deformation

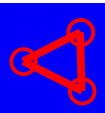

Remote curve crossing

Electron capture via Jahn-Teller coupling of electronic and ro-vibrational motion

Prototype system for electron capture and dissociation mechanisms in polyatomic species

Dissociative recombination of H_3^+

Prototype system for electron capture and dissociation mechanisms in polyatomic species

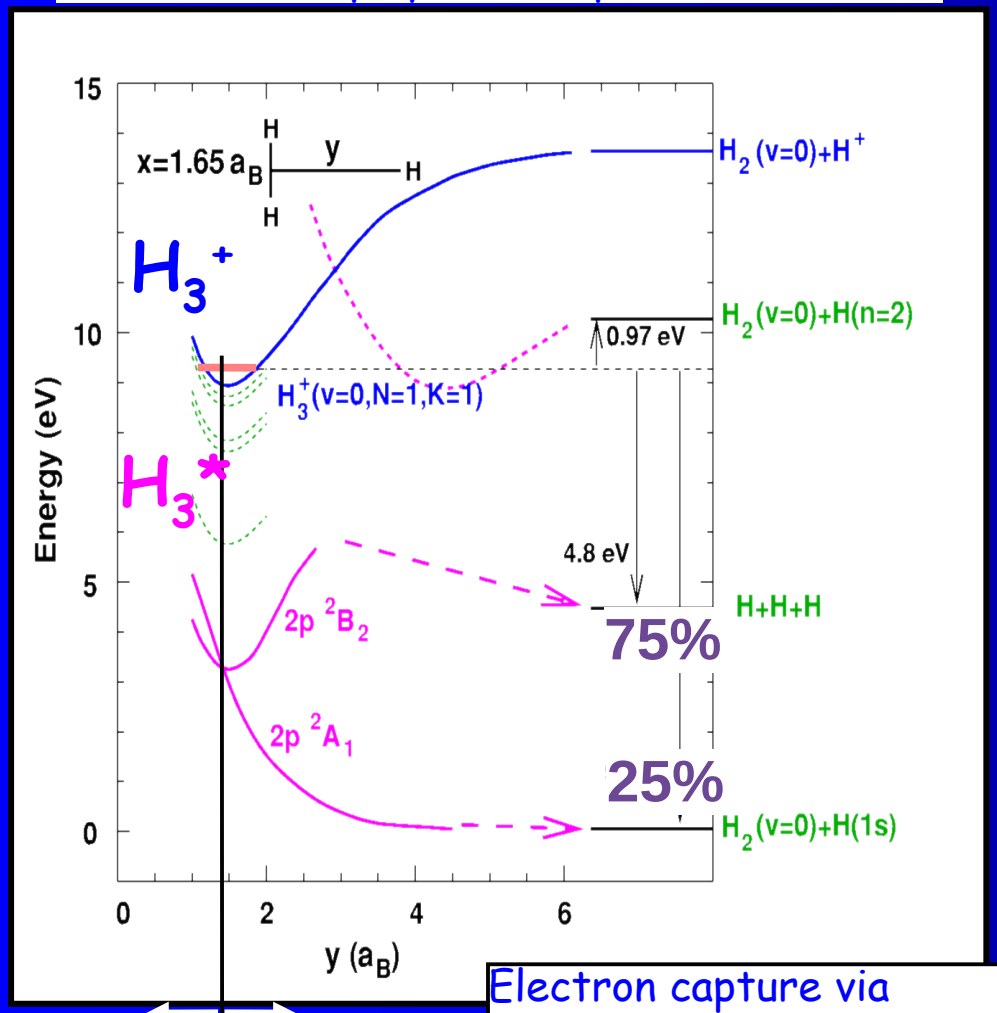

Symmetric deformation

Electron capture via Jahn-Teller coupling of electronic and ro-vibrational motion

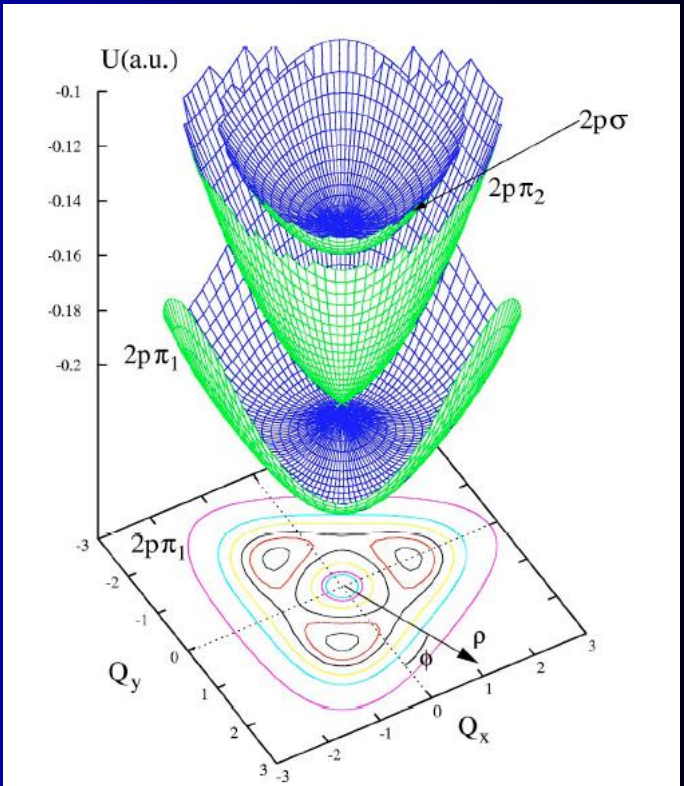

FIG. 4. The figure demonstrates how the Jahn-Teller effect produces a high rate of dissociative recombination. One $2p\sigma$ potential surface and two $2p\pi$ potential surfaces [47] of the neutral molecule are shown. The conical intersection is produced by Jahn-Teller coupling. When an electron arrives, it scatters first into a low-lying vibrationally excited Rydberg state $\{01^1\}$. Then, after the nuclei vibrate, the system finds its way with high probability into a $2p\pi$ state having high vibrational excitation, near the point of conical intersection. The contour plot at the bottom of the figure represents the lowest $2p\pi_1$ surface. All three potential surfaces are shown in the reduced 2D space of dimensionless normal coordinates. The coordinates used here are the normal asymmetric Q_x, Q_y coordinate, with ρ and ϕ their polar components [17,18]. The third vibrational coordinate—the symmetric stretch coordinate Q_1—is kept constant for this graph.

2004-7

PHYSICAL REVIEW A **68**, 012703 (2003)

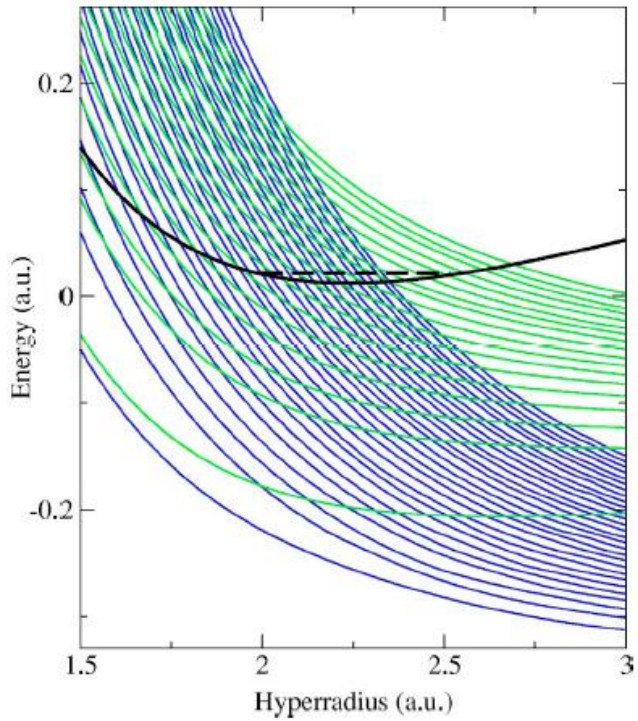

FIG. 1. The problem of DR of H_3^+ in the hyperspherical adiabatic approximation. The lowest hyperspherical adiabatic potential (thick full line) of the H_3^+ and number of hyperspherical adiabatic potentials of the neutral molecule (thin lines). Lower family of lines (darker lines) dissociate to the H_2+H channel; the upper family (lighter lines) dissociate to the H+H+H channel. To calculate hyperspherical adiabatic curves we used the three-dimensional H_3^+ potential from Ref. [48] and the H_3 potential from Refs. [35–37]. Since the density of hyperspherical states is high, only every tenth H_3 potential curve is shown in the figure. The dashed line shows the position of the ground vibrational level of the ion, which is the only one populated in the relevant experiments.

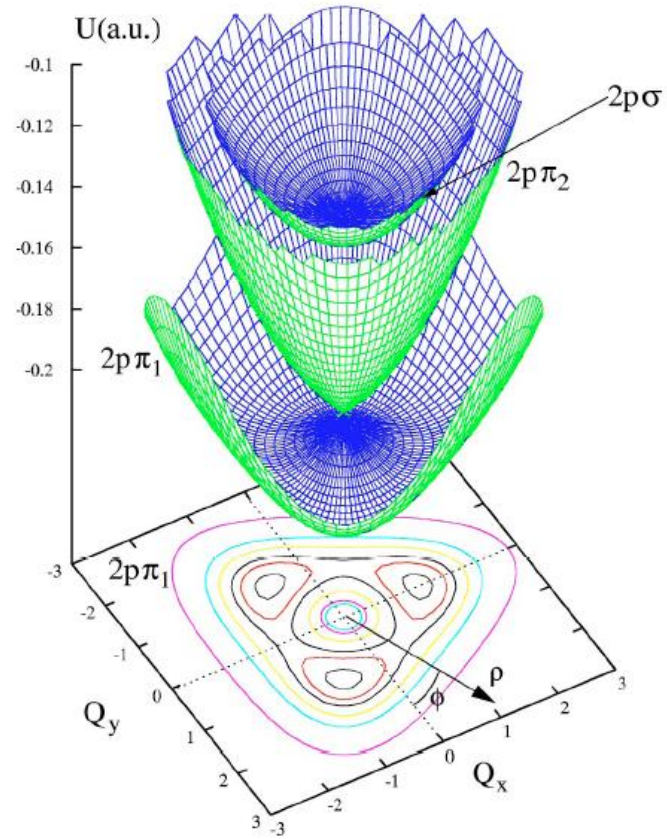

FIG. 4. The figure demonstrates how the Jahn-Teller effect produces a high rate of dissociative recombination. One $2p\sigma$ potential surface and two $2p\pi$ potential surfaces [47] of the neutral molecule are shown. The conical intersection is produced by Jahn-Teller coupling. When an electron arrives, it scatters first into a low-lying vibrationally excited Rydberg state $\{01^1\}$. Then, after the nuclei vibrate, the system finds its way with high probability into a $2p\pi$ state having high vibrational excitation, near the point of conical intersection. The contour plot at the bottom of the figure represents the lowest $2p\pi_1$ surface. All three potential surfaces are shown in the reduced 2D space of dimensionless normal coordinates. The coordinates used here are the normal asymmetric Q_x, Q_y coordinate, with ρ and ϕ their polar components [17,18]. The third vibrational coordinate—the symmetric stretch coordinate Q_1—is kept constant for this graph.

$e^- + H_3^+$

Capture

Autoionization

H_3^* resonant state(s)

predissociation

To get high recombination rate, we need

(a) efficient capture

(b) predissociation faster than auto-ionization

Cosmic-ray ionisation rate $\gamma \sim 3\times10^{-17} s^{-1}$

Dense Clouds

Barnard 68 (João Alves)

Formation

$$H_2 \xrightarrow{h\nu} H_2^+ \xrightarrow{H_2} H_3^+$$

$$d[H_3^+]/dt \sim \gamma.[H_2]$$

Diffuse Clouds

Cygnus OB2 (POSS)

a) DENSE CLOUDS:

$H_3^+ + CO$ $\quad d[H_3^+]/dt \sim -k_{CO} x [H_3^+] x [CO]$

$(k_{CO}=2\times10^{-9} cm^3 s^{-1})$

$[H_3^+]=\gamma/k_{CO} \cdot [H_2]/[CO]=$ **$\sim 1\times10^{-4} cm^{-3}$**

~OK with observation

b) DIFFUSE CLOUDS:

$H_3^+ + e^-$ $\quad d[H_3^+]/dt \sim -\alpha_{DR} [H_3^+][e^-]$

$\alpha_{DR}=2\times10^{--7} cm^3 s^{-1} x (T/300)^{-0.65}$ (the value from 2005)

$[H_3^+]=\gamma/\alpha_{DR} \cdot [H_2]/[C]=$ **$\sim 1\times10^{-7} cm^{-3}$**

~ NO with observation

… history is repeating itself ….

$$H_3^+ + e^- \Rightarrow H + H_2, 3H$$

RSDM 2012

DR 2013

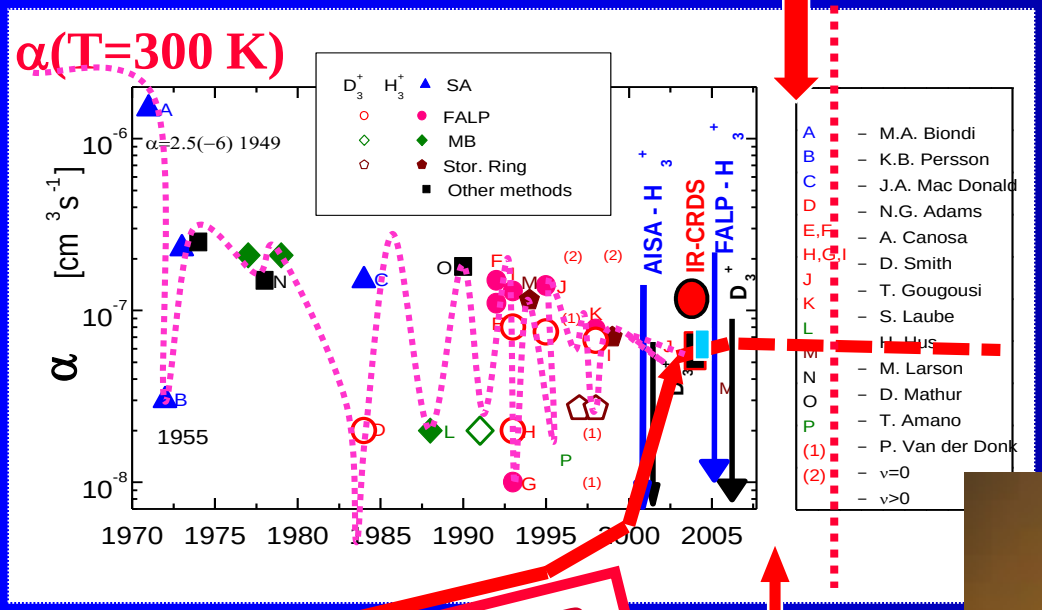

THEORY OF DR

Doubts 2011

"Presently no rate coefficient measurement with a confirmed temperature below 300 K exists".

Petrignani *et al.* Phys. Rev. A (2011)

and … history repeated itself .

M. Larsson et al, CP Letters (2008)

… One remaining problem is to understand the plasma afterglow experiments.

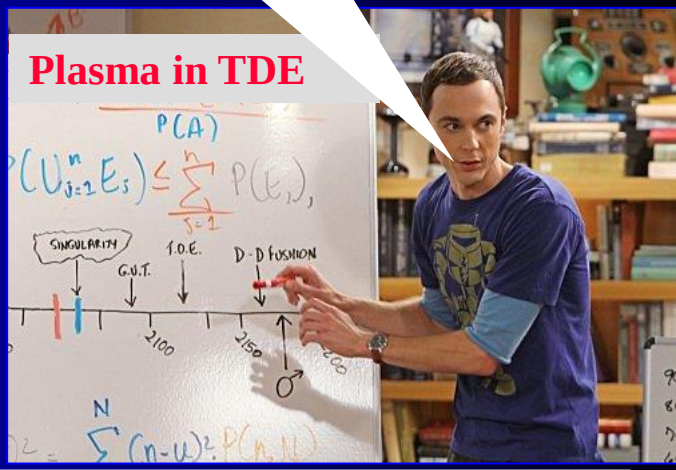

…. many times it was concluded, that the task was finished….

… and the caravan is on its way

p/o

The battle ship enters the stage

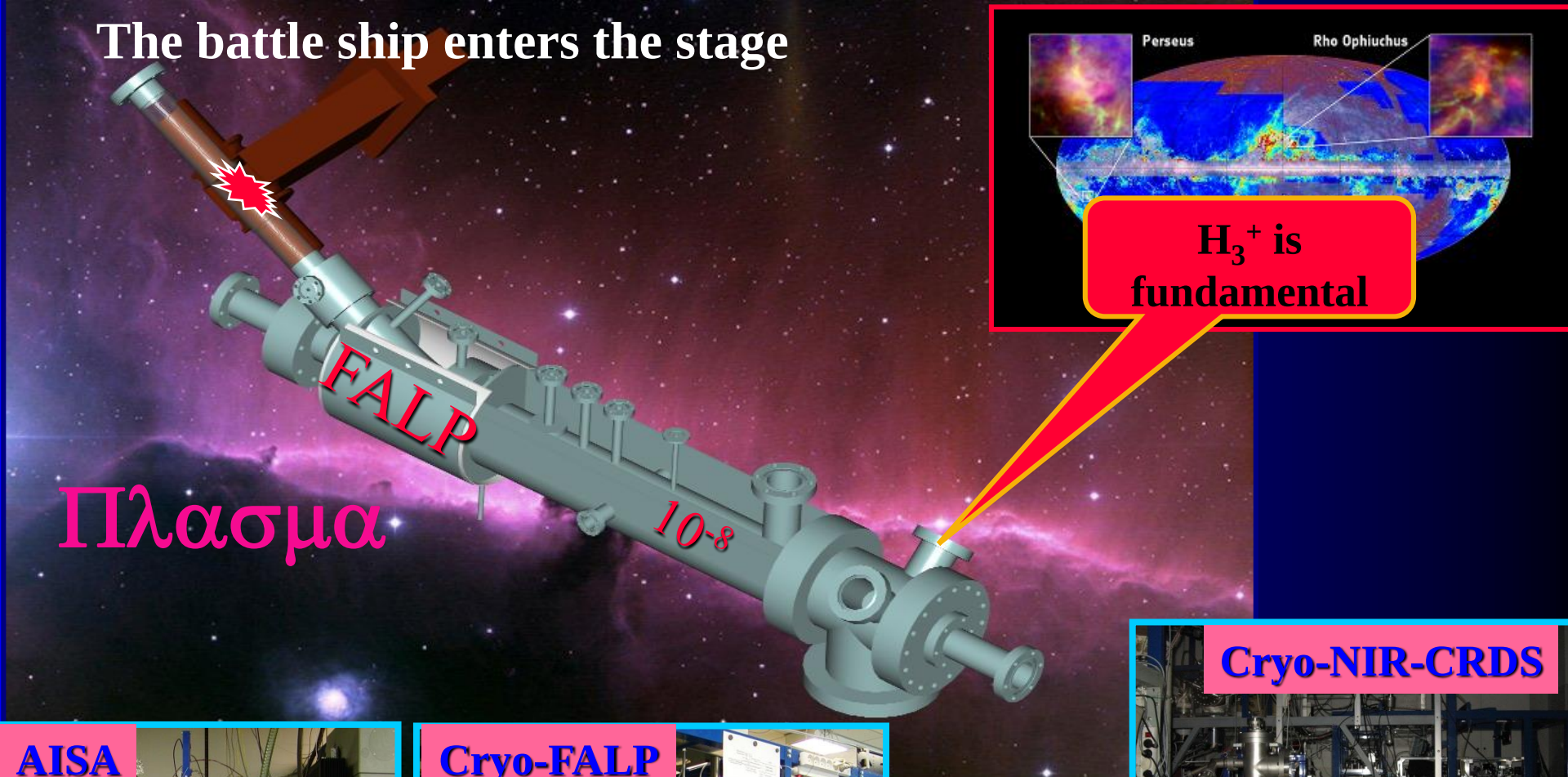

H_3^+ is fundamental

AISA

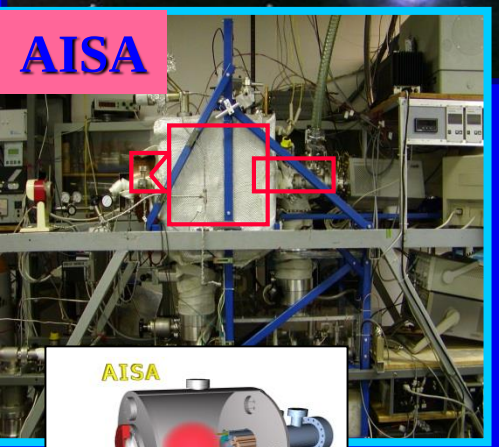

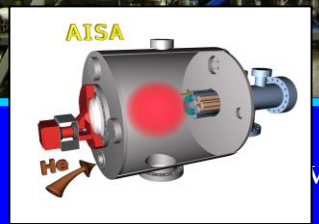

Cryo-FALP

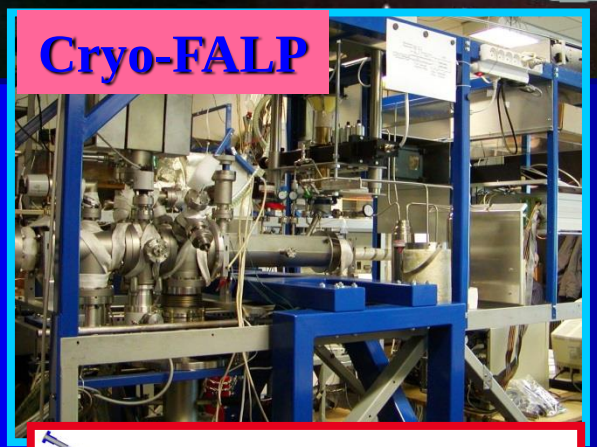

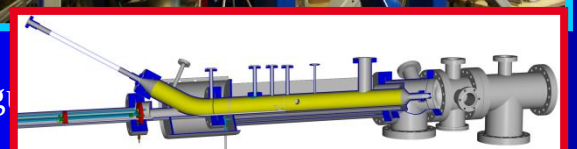

Cryo-NIR-CRDS

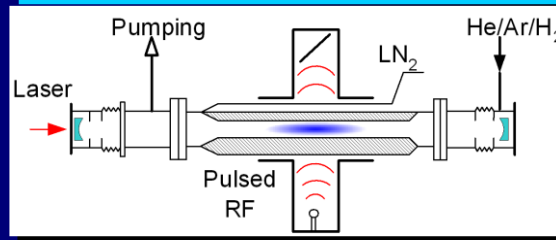

Pressure dependence

Pulsed (stationary) afterglow

Discharge pulse

microwave, UV, x-ray, e-beam

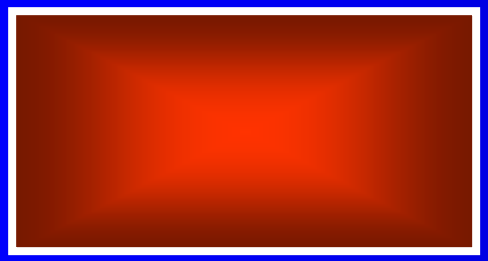

Plasma chamber
He: ~ 1 –20 Torr
Ar: 10 to 30 %
+ molecules

Measure $n_e(t)$

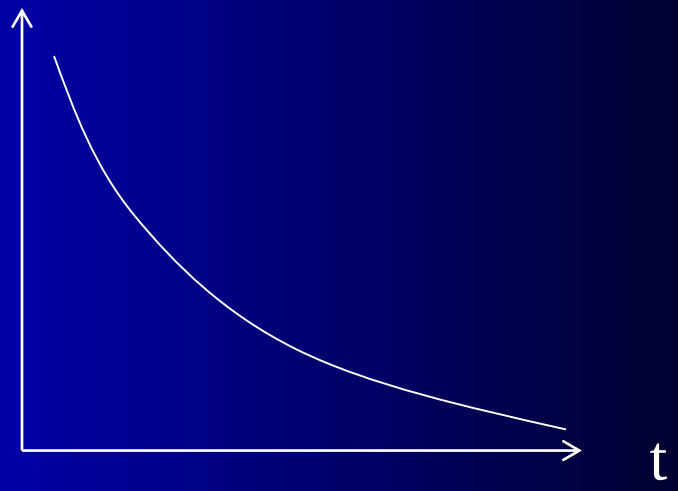

Get:

$$\frac{dn_e}{dt} = -\alpha n_e^{\ 2} + (diffusion)$$

$$n_e(t) = \frac{n_{e0}}{1 + \alpha n_{e0} t}$$

We measure effective – apparent binary recombination rate coefficient

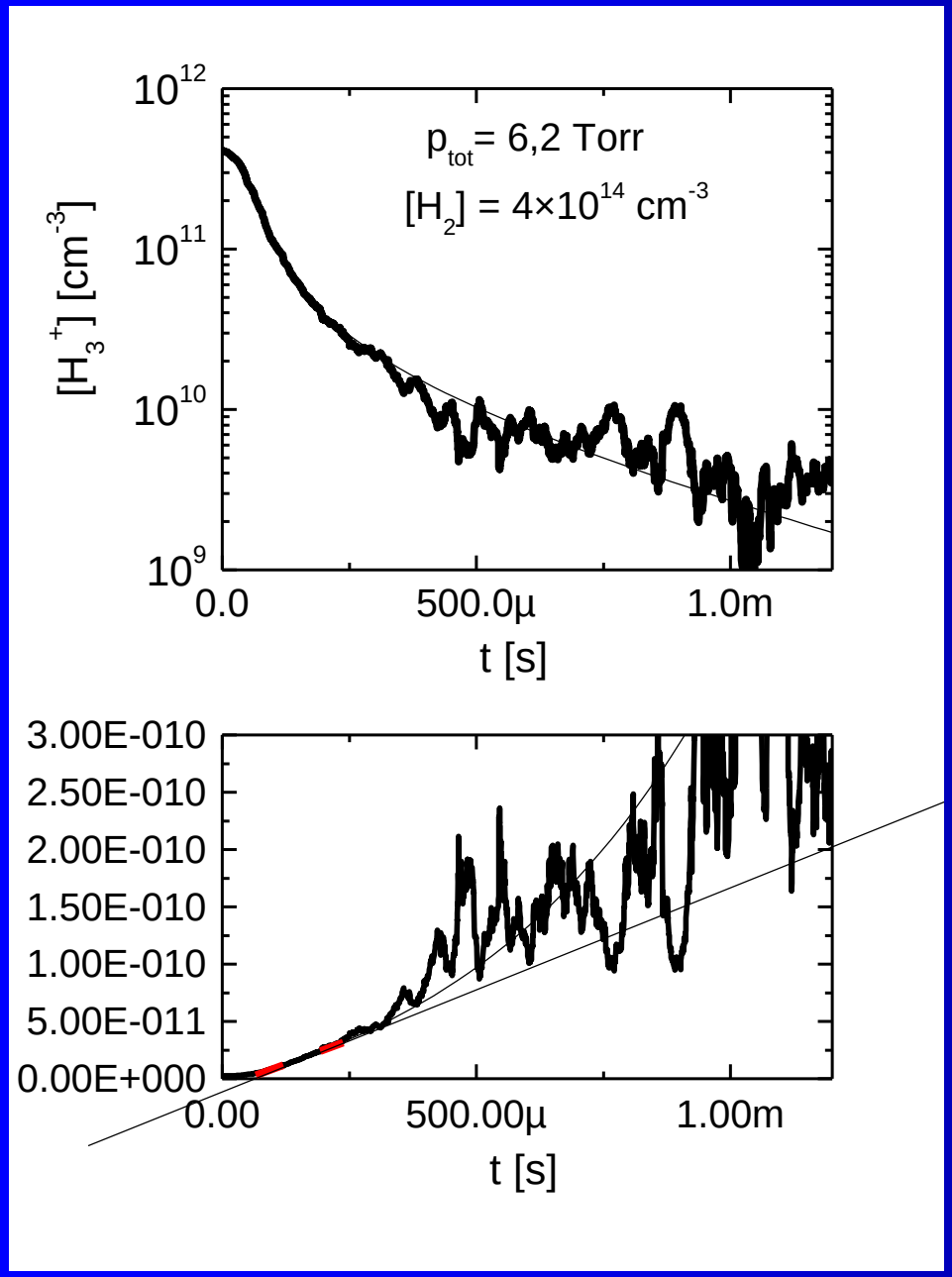

Quasineutral H_3^+ dominated plasma

$$\frac{\mathrm{d}n_\mathrm{e}}{\mathrm{d}t} = -\alpha_\mathrm{eff} n_\mathrm{e}^2 - \frac{n_\mathrm{e}}{\tau_\mathrm{L}}$$

$$\frac{1}{[H_3^+]} = \frac{1}{[H_3^+]_0} + \alpha t$$

We measure effective – apparent binary recombination rate coefficient

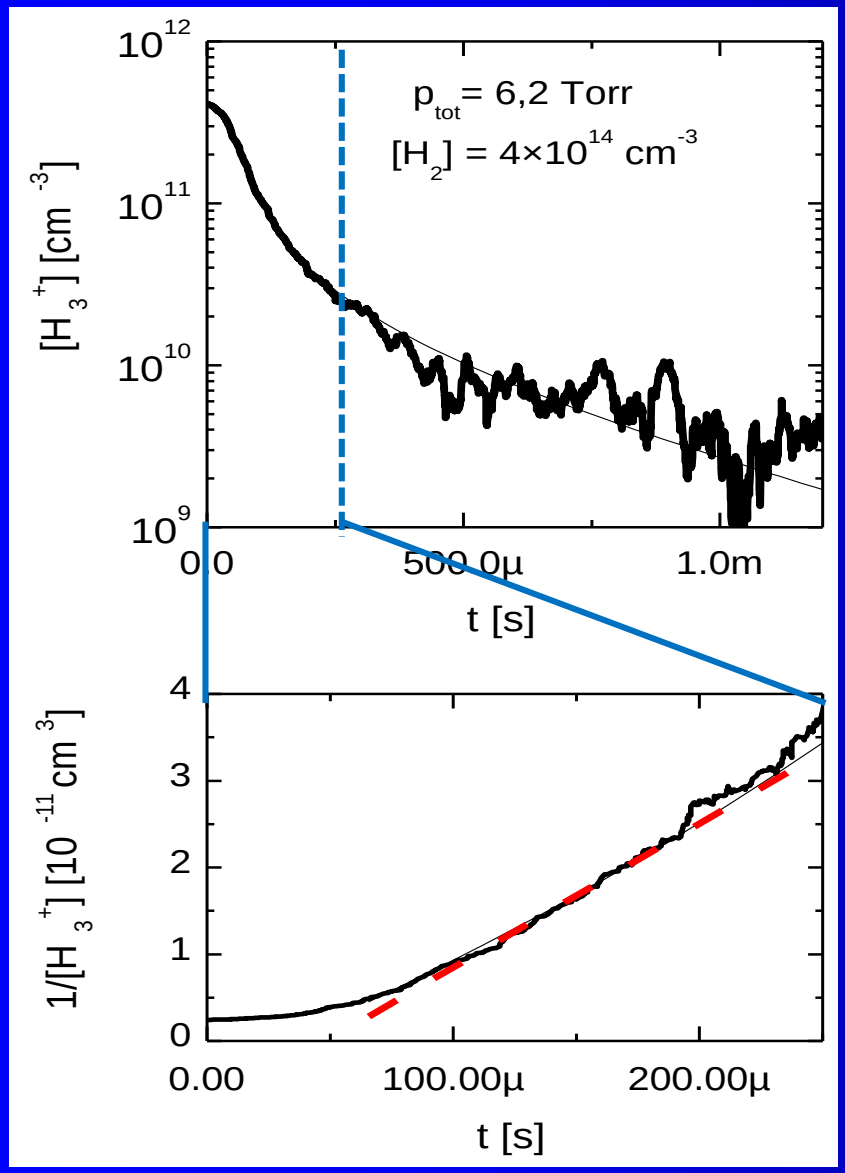

Quasineutral H_3^+ dominated plasma

$$\frac{\mathrm{d}n_\mathrm{e}}{\mathrm{d}t} = -\alpha_\mathrm{eff} n_\mathrm{e}^2 - \frac{n_\mathrm{e}}{\tau_\mathrm{L}}$$

$$\frac{1}{[H_3^+]} = \frac{1}{[H_3^+]_0} + \alpha t$$

Decay in diffusion and recombination governed plasma

$$\frac{dn_e}{dt} = -\alpha\, n_e^2 - \frac{D_a}{\Lambda^2} n_e$$

$$\frac{1}{n_e} = \alpha\, \frac{\exp(\nu t) - 1}{\nu_D} + \frac{1}{n_0} \exp(\nu_D t)$$

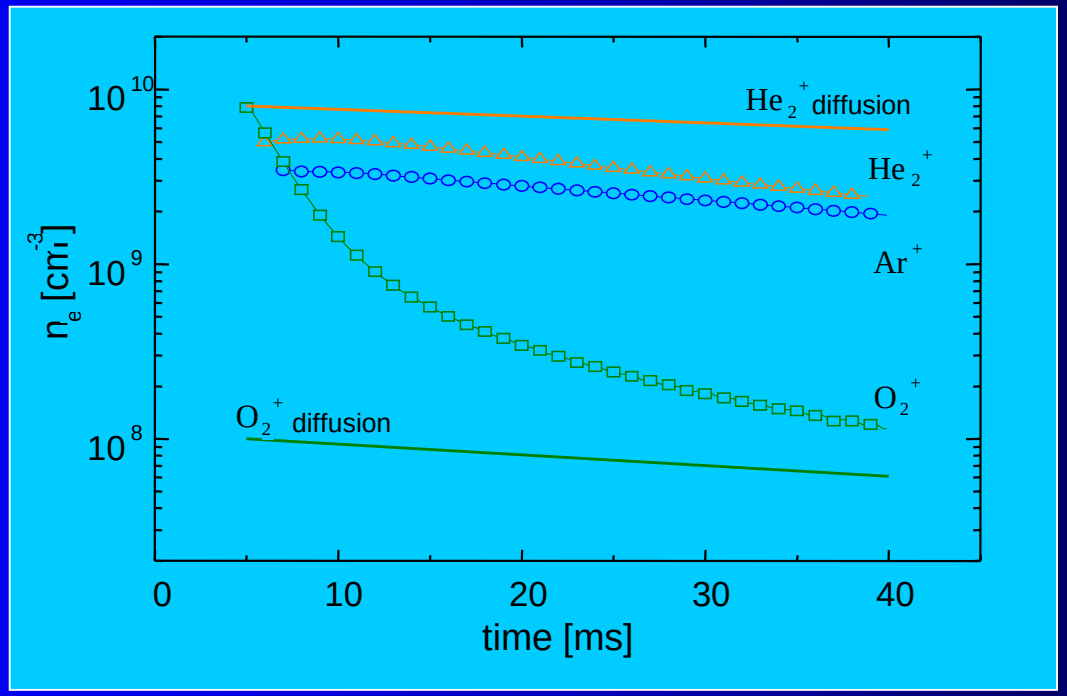

Decay in diffusion and recombination governed plasma

$$\frac{dn_e}{dt} = -\alpha\, n_e^2 - \frac{D_a}{\Lambda^2} n_e$$

$$\frac{1}{n_e} = \alpha\, \frac{\exp(\nu t) - 1}{\nu_D} + \frac{1}{n_0} \exp(\nu_D t)$$

Limit for t -->0

$$\frac{1}{n_e} = \alpha\, \frac{(1 + \nu_D t) - 1}{\nu_D} + \frac{1}{n_0}(1 + \nu_D t)$$

$$\frac{1}{n_e} = \alpha t + \frac{1}{n_0}(1)$$

Limit for large t

$$\frac{1}{n_e} = \left(\frac{\alpha}{\nu_D} + \frac{1}{n_0}\right) \exp(\nu_D t)$$

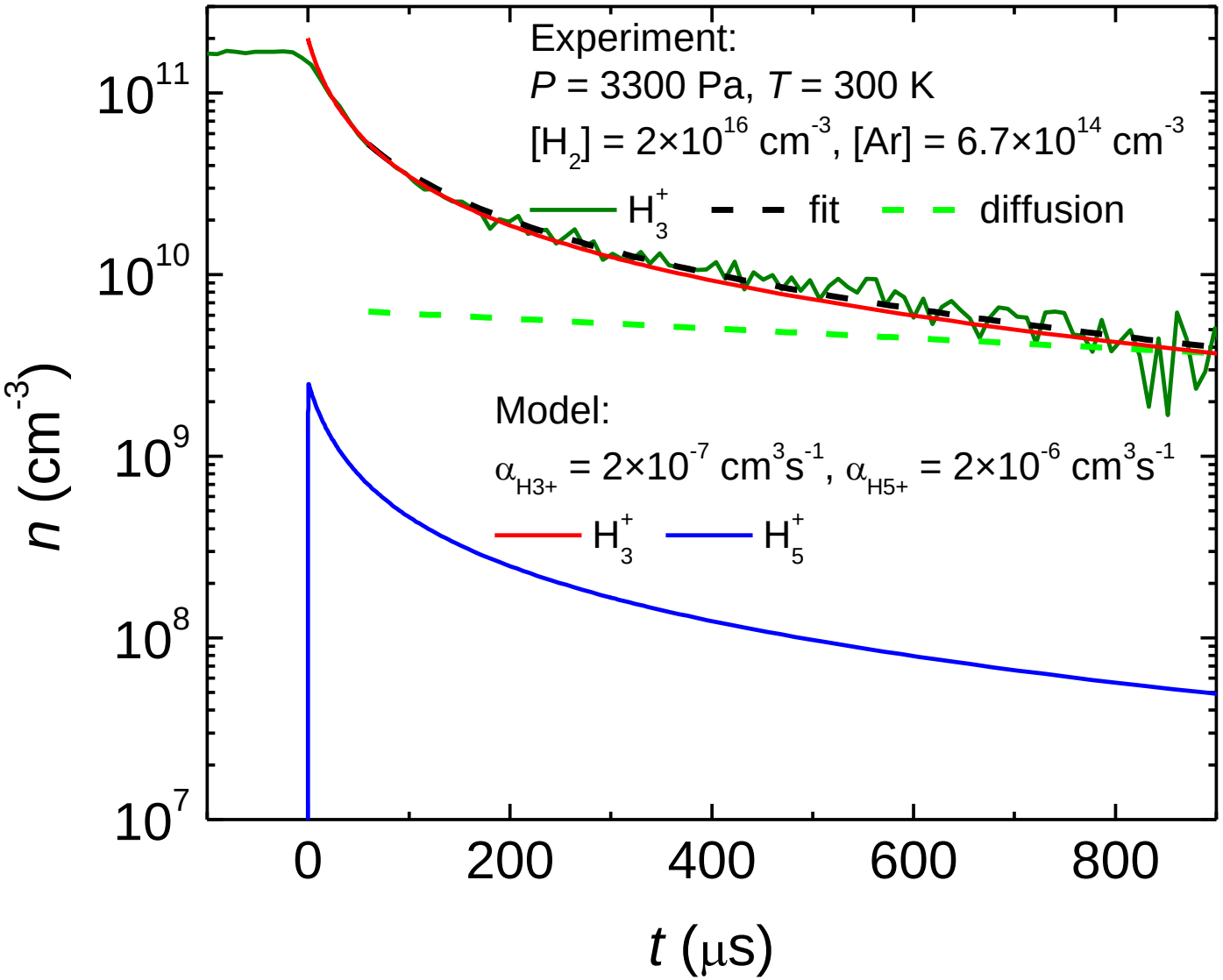

Srovnani modelu a experimentu. Pocatecni podminka: $[H_3^+] = n_e = 2\times10^{11}$ cm^{-3}.

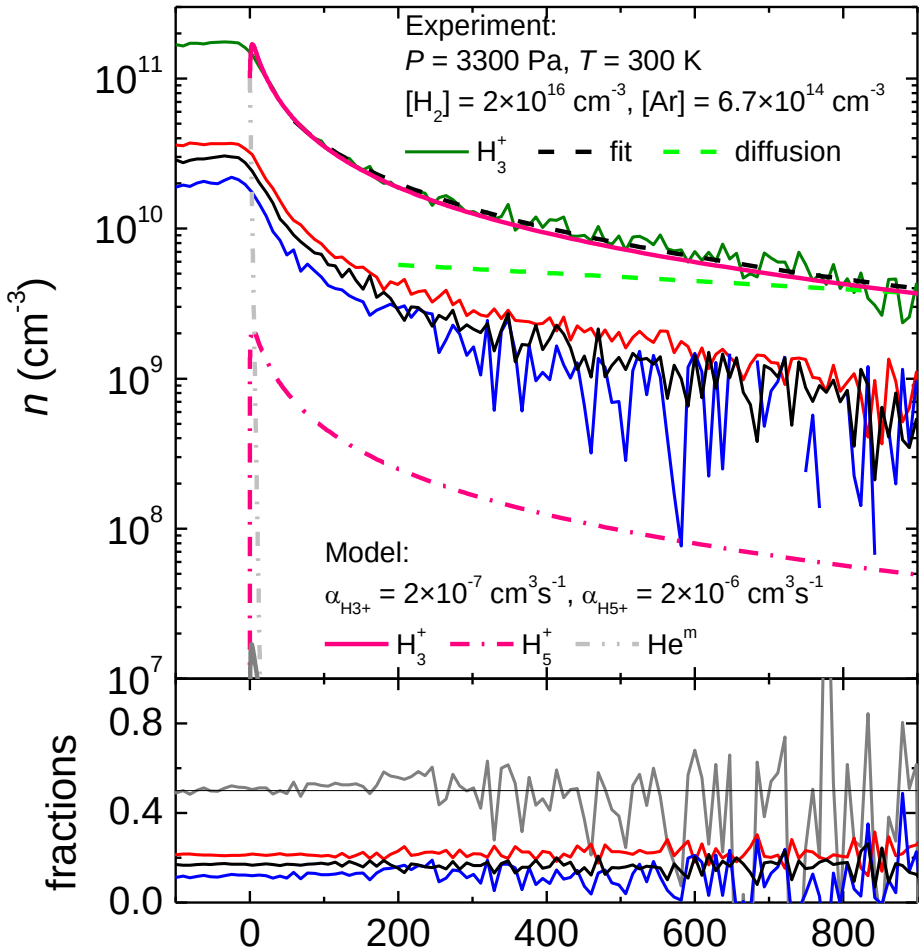

$$\frac{dn_e}{dt} = -[\alpha_1 n_1(t) + \alpha_2 n_2(t)]n_e$$

$$\Rightarrow \alpha_{eff}(t) = [\alpha_1 f_1(t) + \alpha_2 f_2(t)]$$

$$f_1 + f_2 = 1$$

Model + data. Pocatecni podminka: $n_e = He^m = [H_3^+]$.
Poznamka. Namerene τ difuznich ztrat 1.6 ms. Teoreticke τ pri danem tlaku je 1.8 ms (odpovida cca 4×10^{10} cm^{-3} koncentraci necistot (pri 2×10^{-9} cm^3s^{-1} rychlosti reakce H_3^+ s necistotami). Namerena koncentrace vody $[H_2O] = 5\times10^{10}$ cm^{-3} ($[He] = 8\times10^{17}$ cm^{-3}).

If there are 2 or more ion species, the fast recombining species disappears first

$$\frac{dn_e}{dt} = -[\alpha_1 n_1(t) + \alpha_2 n_2(t)]n_e$$

$$\Rightarrow \alpha_{eff}(t) = [\alpha_1 f_1(t) + \alpha_2 f_2(t)]$$

$$f_1 + f_2 = 1$$

Formation of H_3^+ in $He/Ar/H_2$ mixture

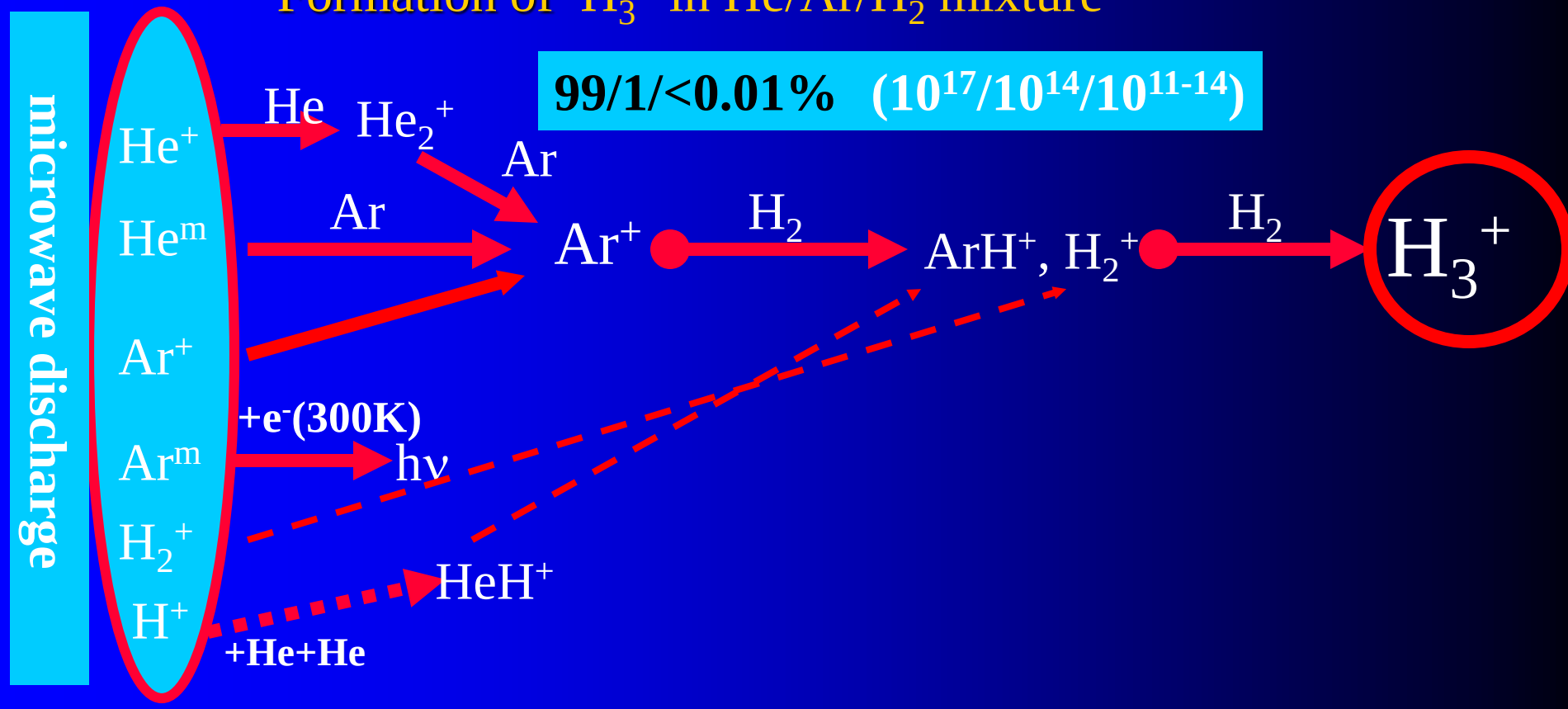

FORMATION:

Ion molecule reactions during the early afterglow

VT - AISA

$$dn_i/dt=-\alpha n_i n_e$$

He/Ar/H_2

$\alpha(T)$

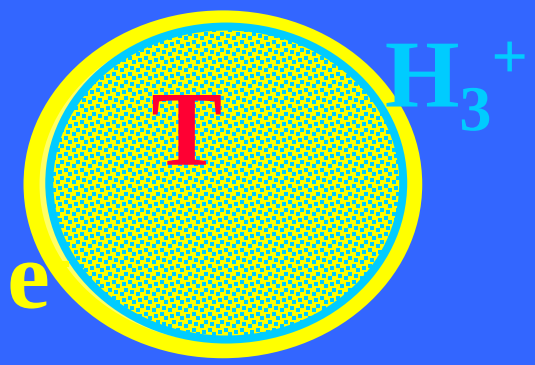

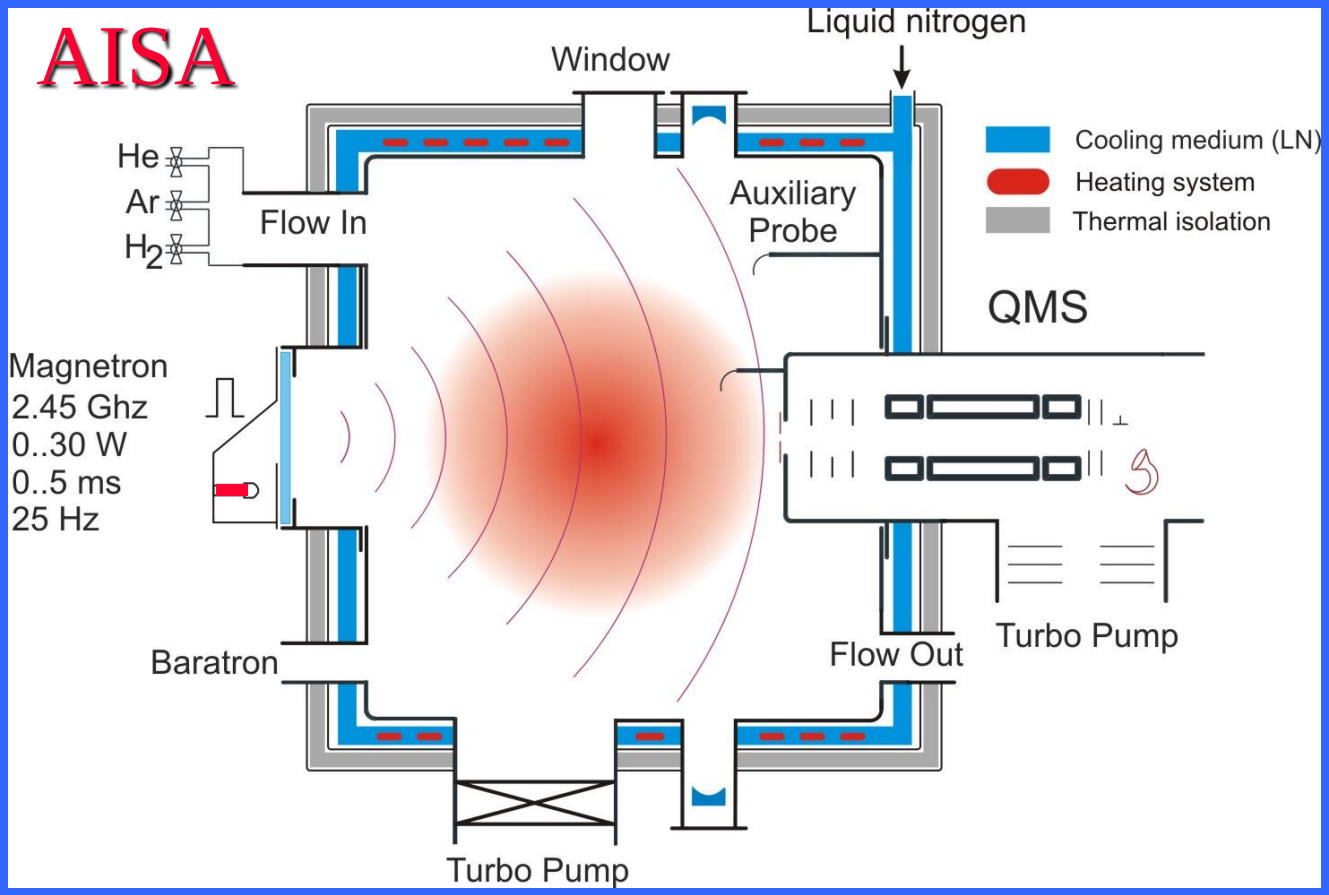

40 cm diameter
UHV - 10^{-9} Torr
External magnetron
2 Torr of He/Ar/H_2

PULSED STATIONARY AFTERGLOW

20-100ms decay

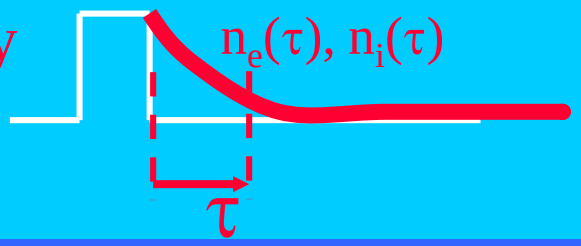

Formation of H_3^+ in $He/Ar/H_2$

99/1/<0.01% ($10^{17}/10^{14}/10^{11-14}$)

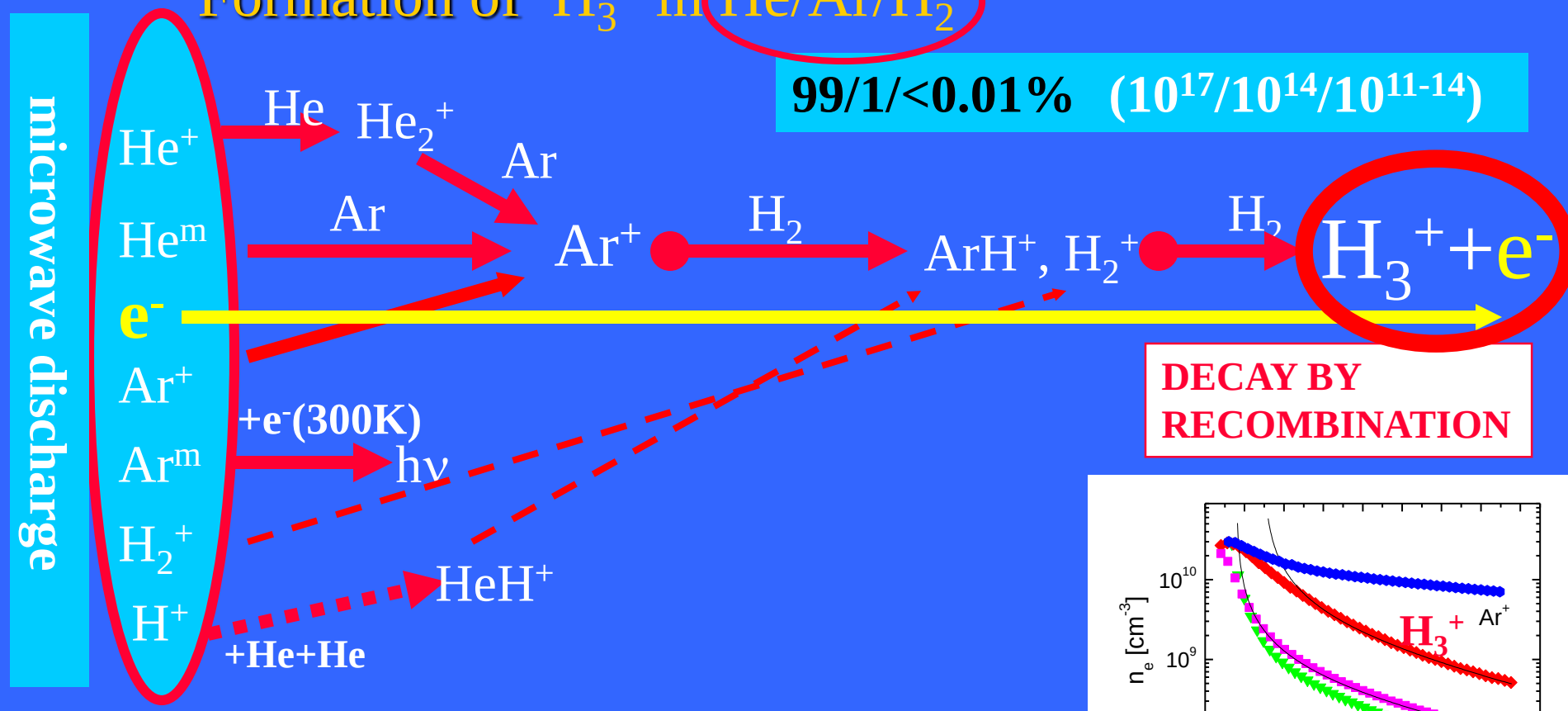

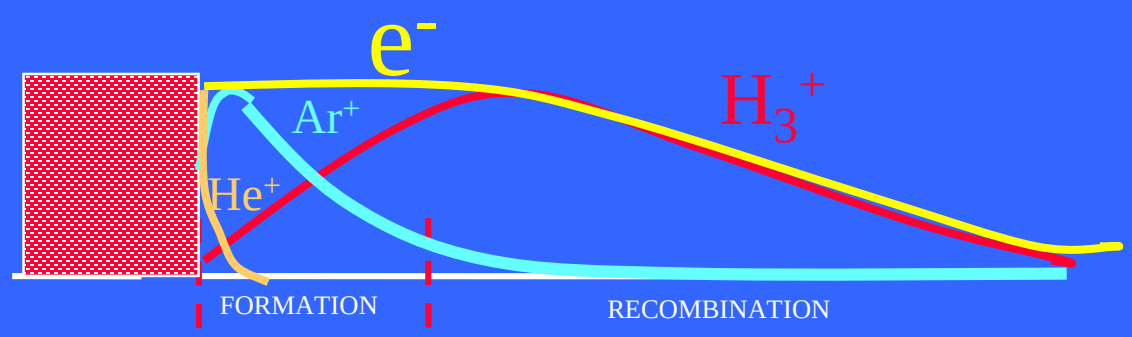

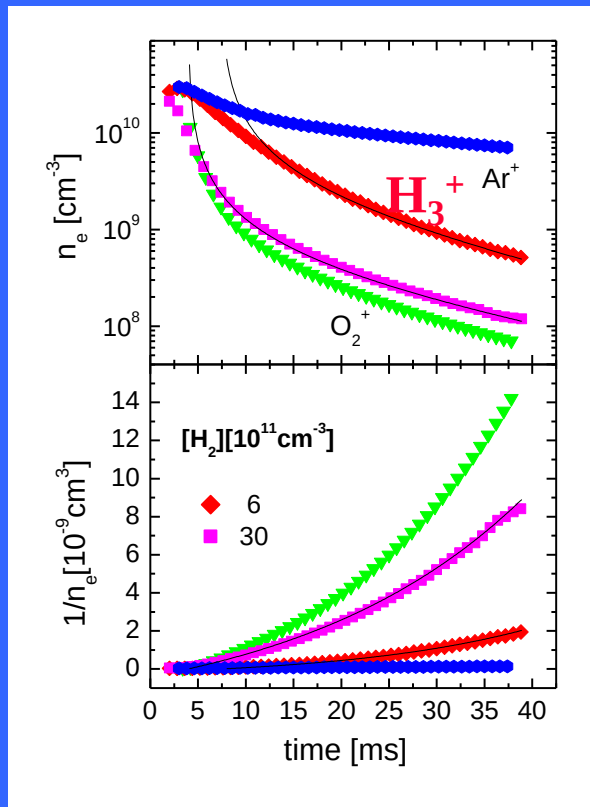

Time resolved mass spectra

Formation of H_3^+ in $He/Ar/H_2$ mixture

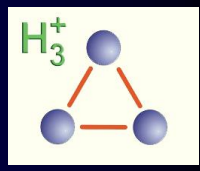

$10^{17}/10^{14}/10^{11}$

microwave discharge

He^+, He^m, Ar^+, Ar^m, H_2^+

$\xrightarrow{Ar} Ar^+ \xrightarrow{H_2} ArH^+, H_2^+ \xrightarrow{H_2} H_3^+$

Changes due to the ion molecule reactions during the early afterglow

He/Ar

He/Ar/H_2

He/Ar/D_2

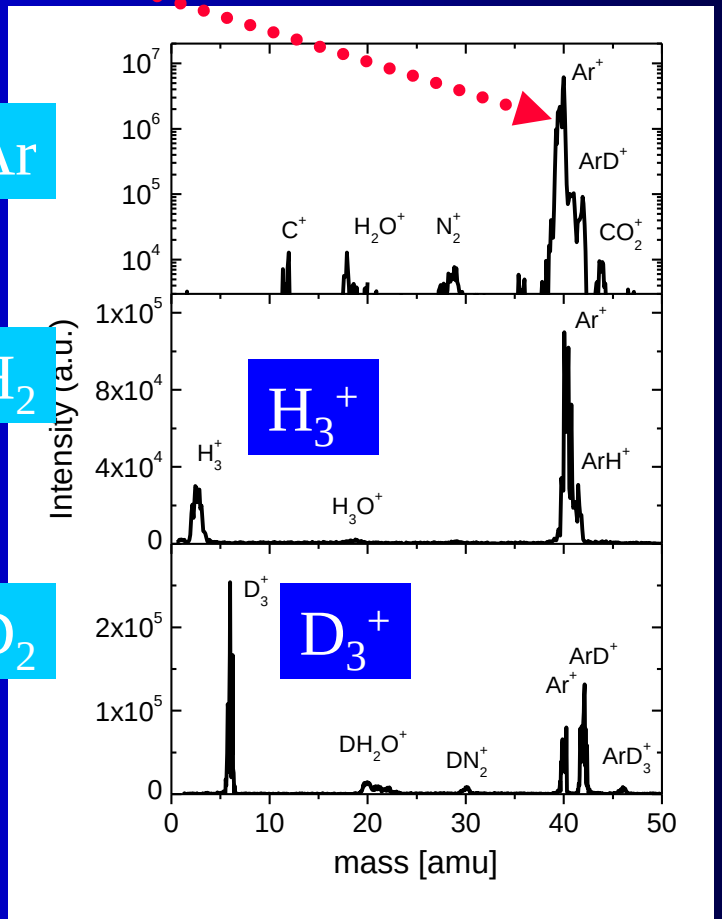

Recombination

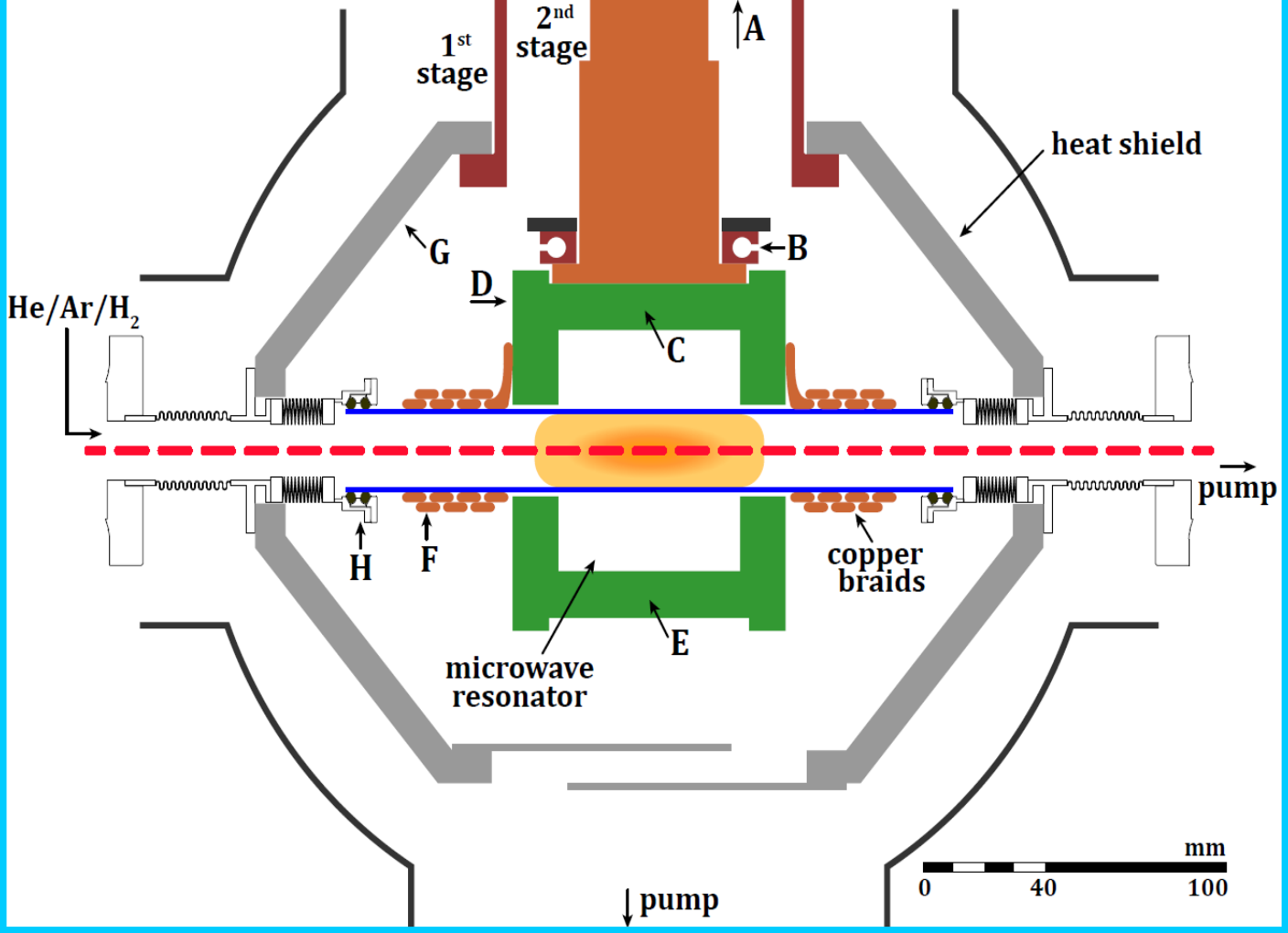

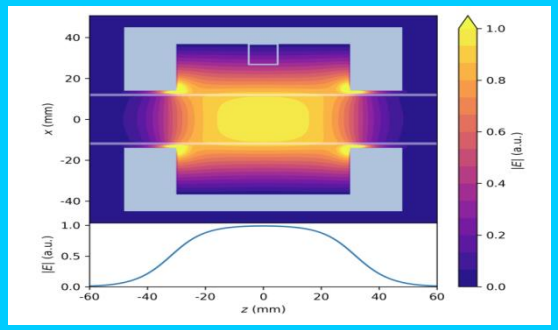

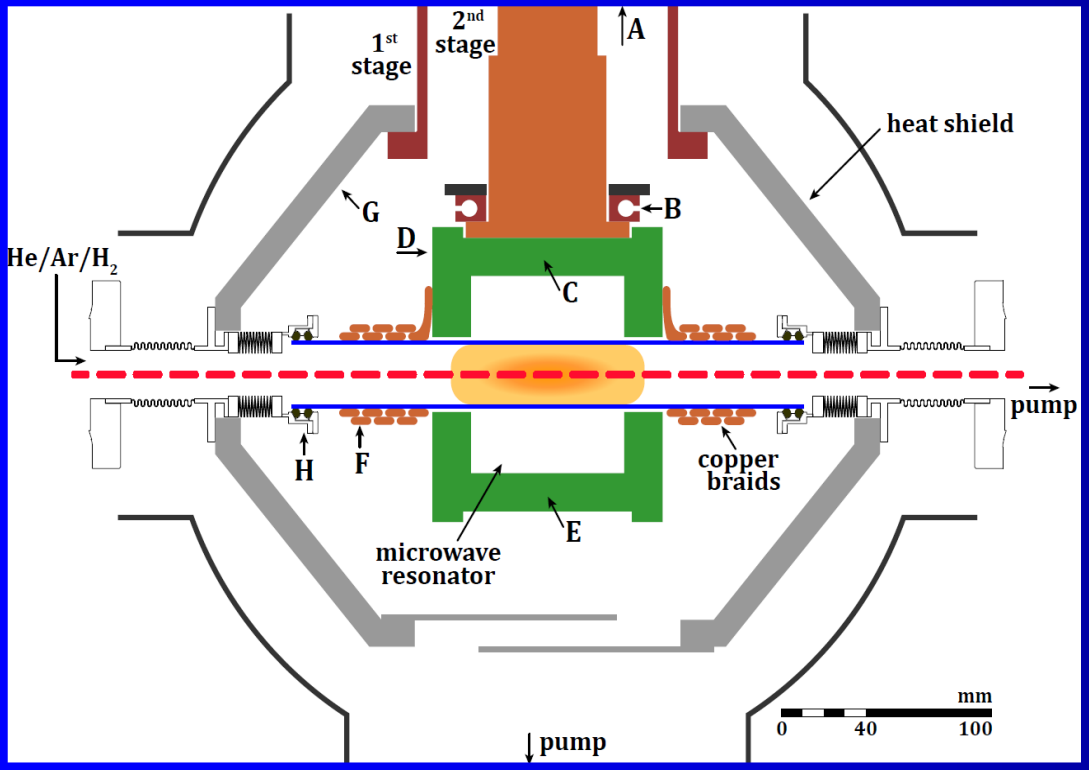
1st stage
2nd stage
A
heat shield
G
B
D
He/Ar/H2
C
pump
H
F
copper braids
E
microwave resonator
mm
0
40
100
pump

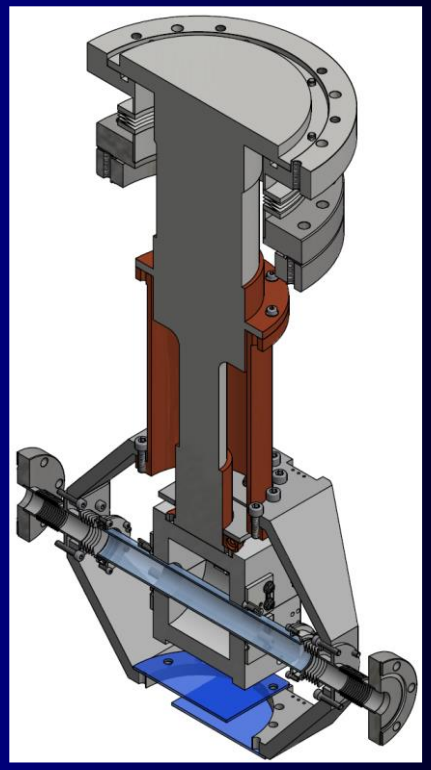

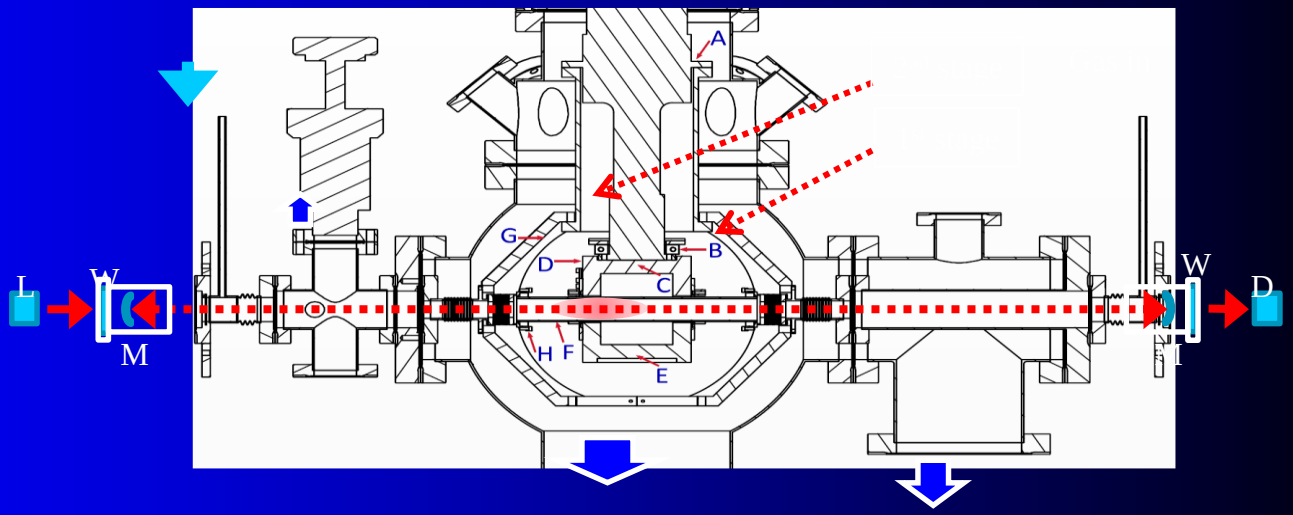
A
G
B
D
C
H
F
E
L
W
M
W
D
I

Recombination

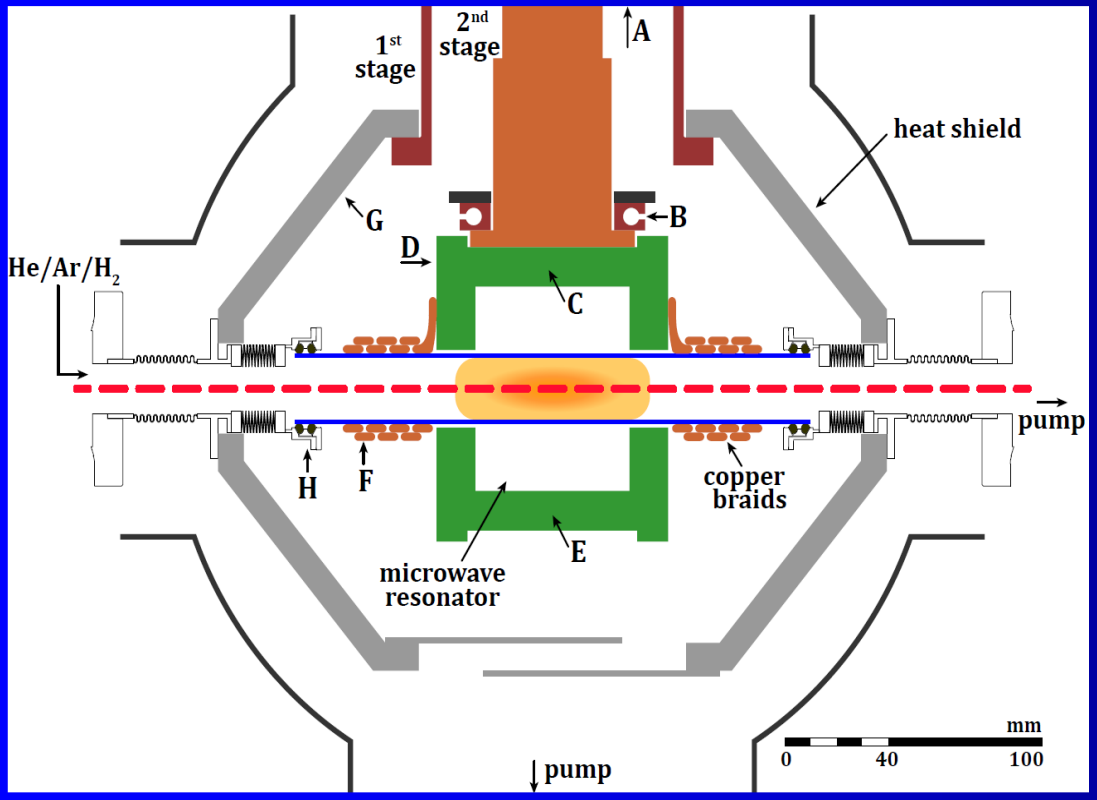

Recombination

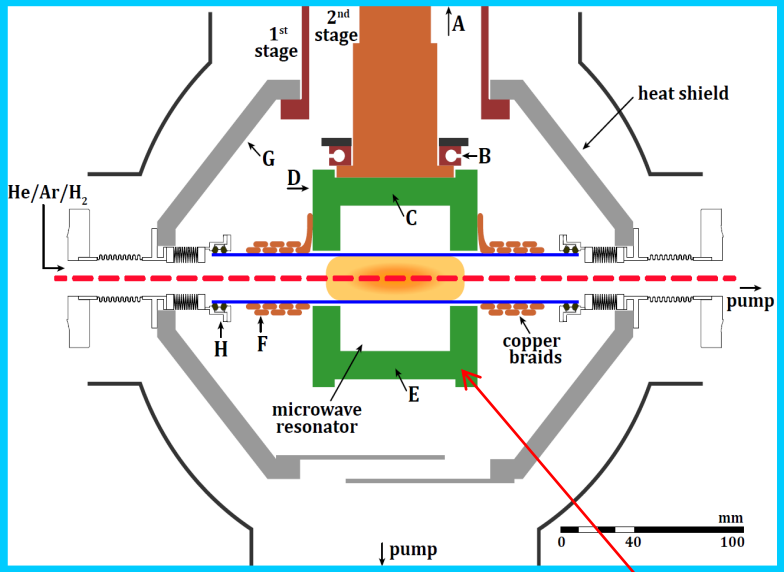

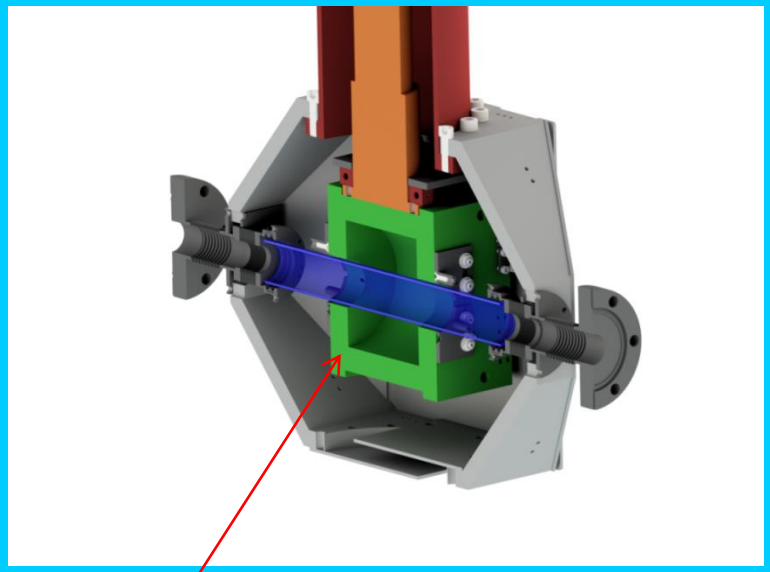

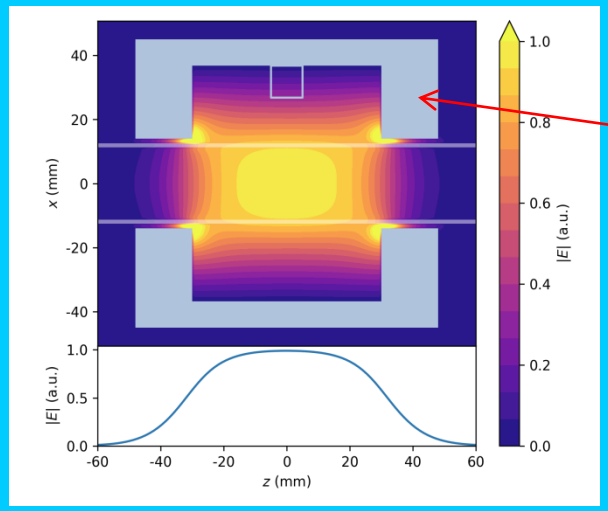

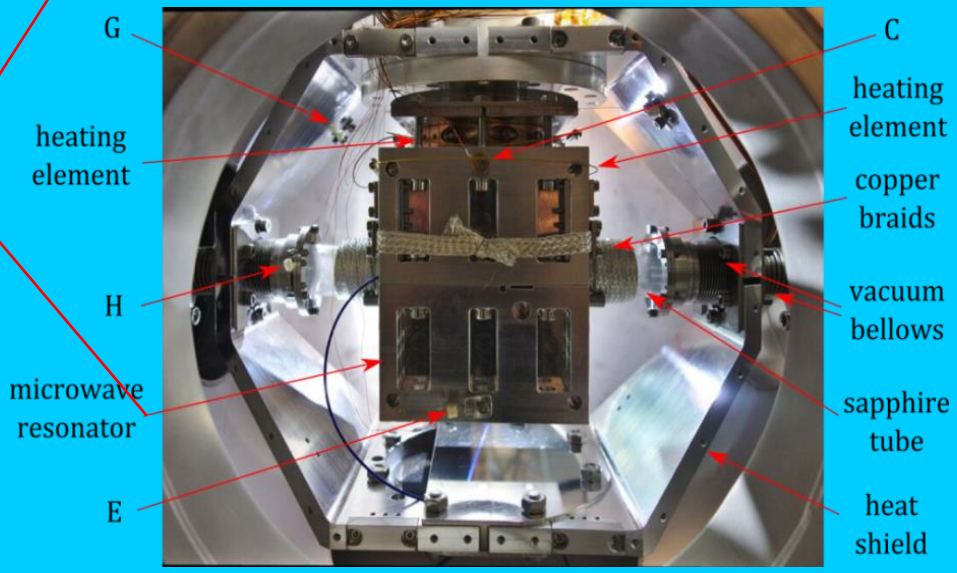

Recombination

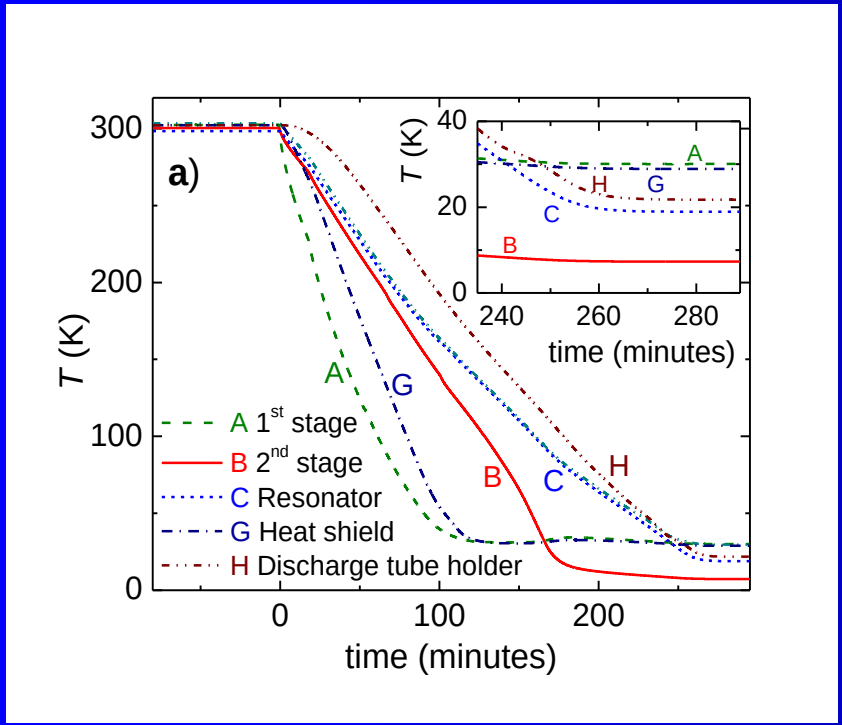

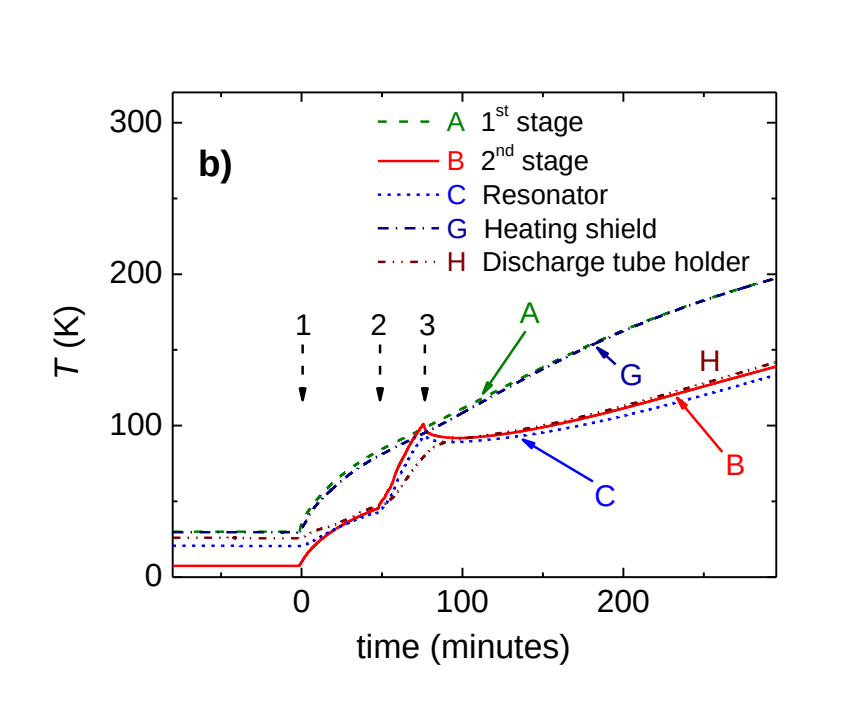

Recombination

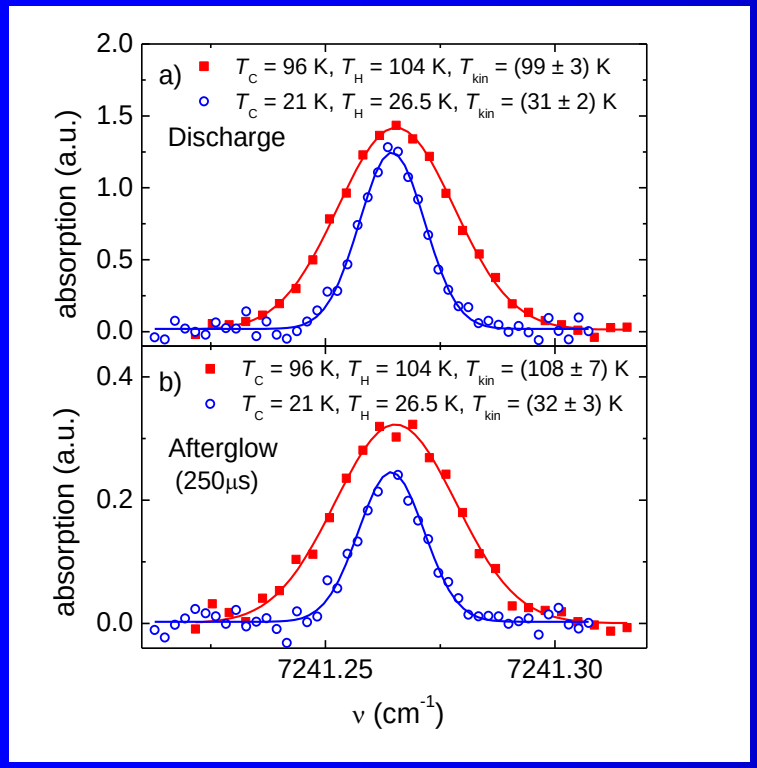

Examples of H_3^+ absorption line profiles

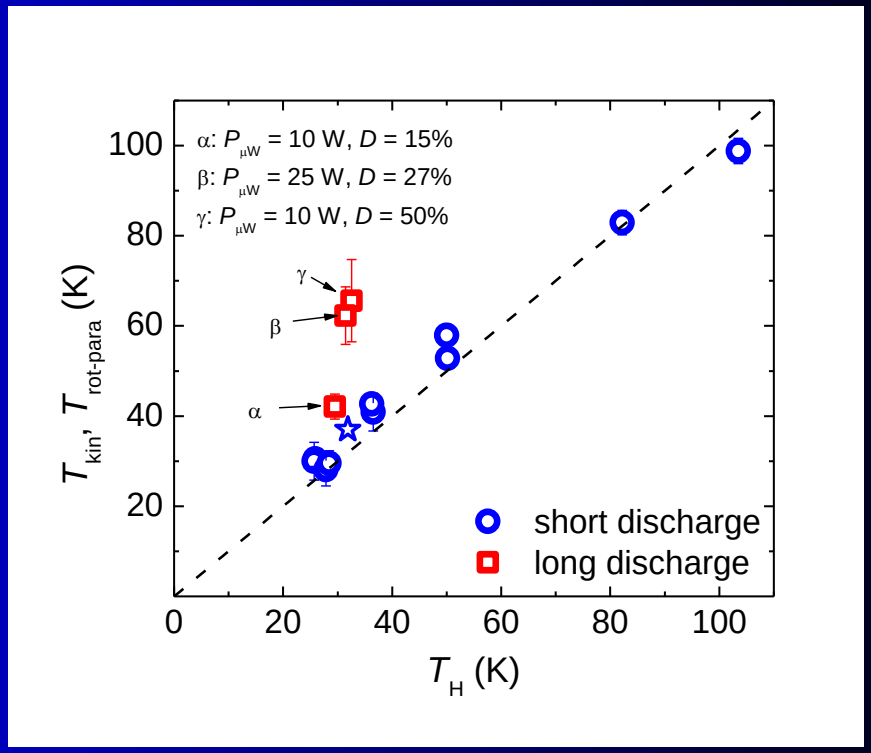

The dependence of the kinetic temperature (T_{kin}) of H_3^+ ions on the temperature T_H (temperature of the discharge tube holder.

RECOMBINATION

FLOWING AFTERGLOW

Diffusion in FA

Diffusion losses
Ambipolar diffusion

$$[A^+] = [A^+]_0 \exp(-Dt/\Lambda^2) = [A^+]_0 \exp(-Dpt/p\Lambda^2) = [A^+]_0 \exp(-D_0 p_0 L/vp\Lambda^2)$$

$$\sim [A^+]_0 \exp(-D_0 p_0 L/vp\Lambda^2) \sim [A^+]_0 \exp(-const.L/Q)$$

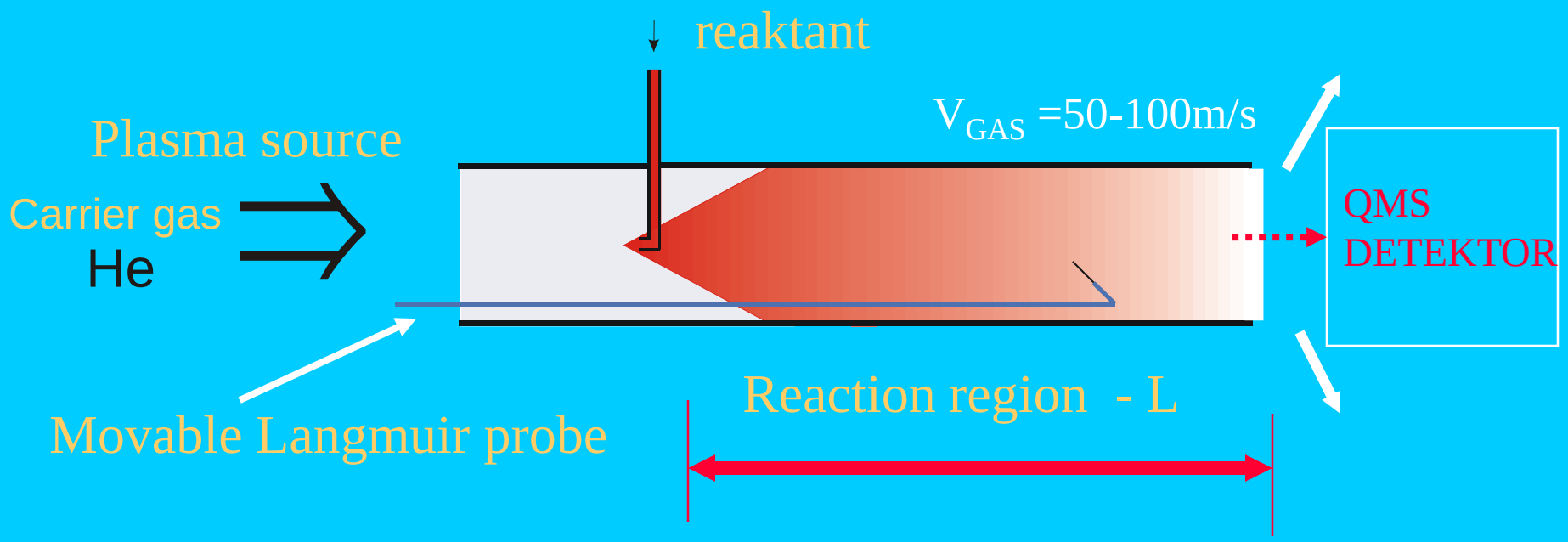

$$[A^+] \sim [A^+]_0 \exp(-const.L/Q)$$

FLOWING AFTERGLOW

Ion-molecule reactions

FA

FA	**E.E.Ferguson, Fehsenfeld, ~1965**
FALP	**J. Hasted, D. Smith, N. Adams, ….**

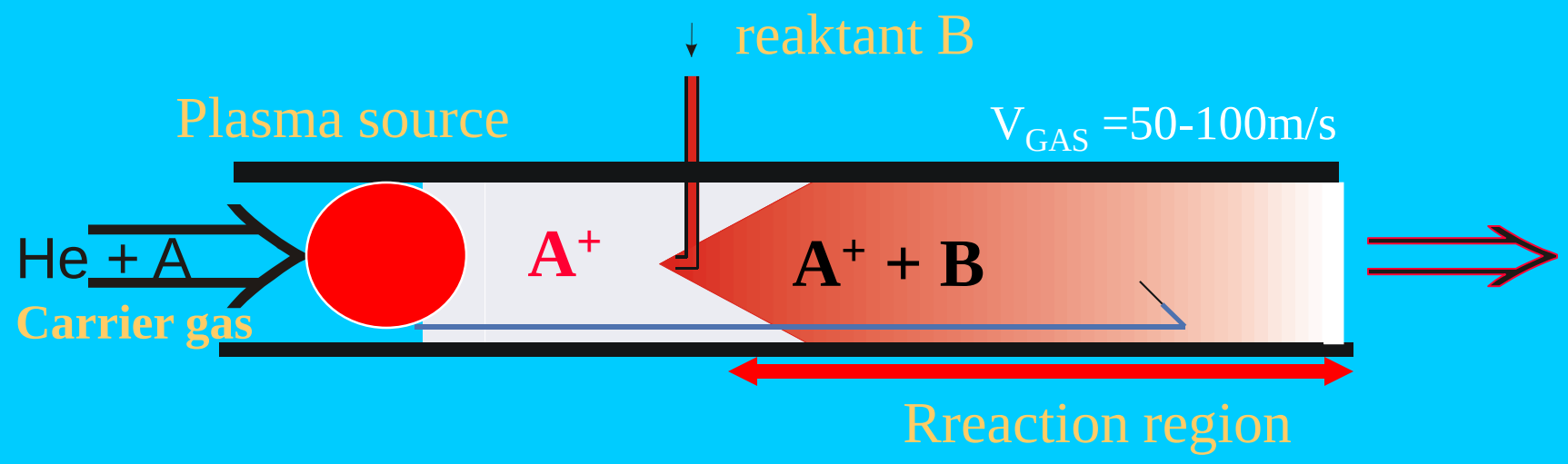

$$A^+ \quad + \quad B \xrightarrow{k} \quad products,$$

$$d[A^+]/dt = -k[B][A^+], \qquad at\ [A^+] << [B]$$

$$[A^+] = [A^+]_0 \exp(-k[B]t) = [A^+]_0 \exp(-k[B]L_0/v)$$

SIFT

, D. Smith, N. Adams, ….

Flowing Afterglow Langmuir Probe - FALP

Recombination
Attachment

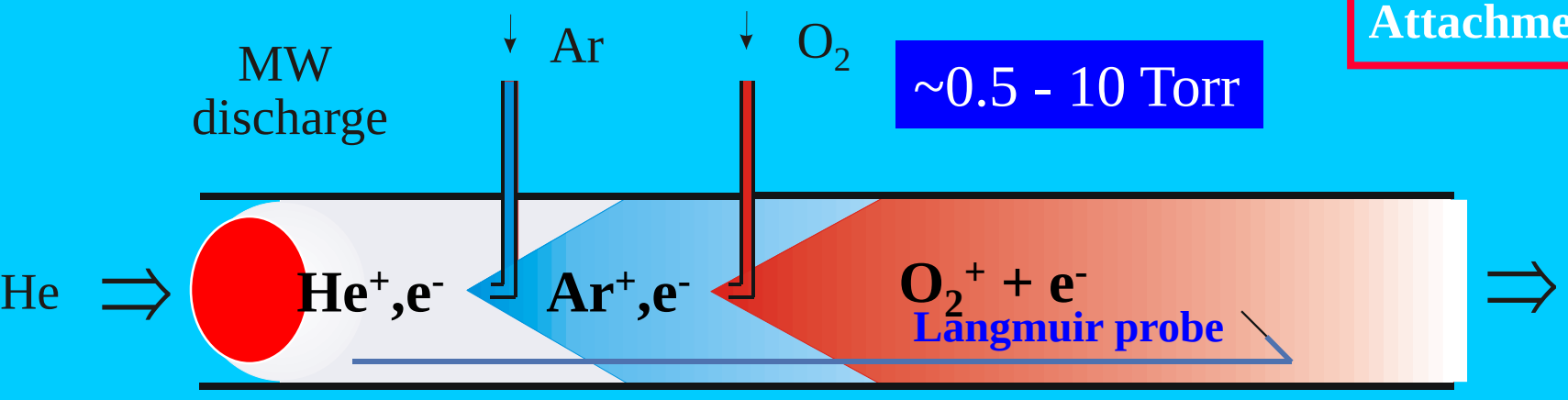

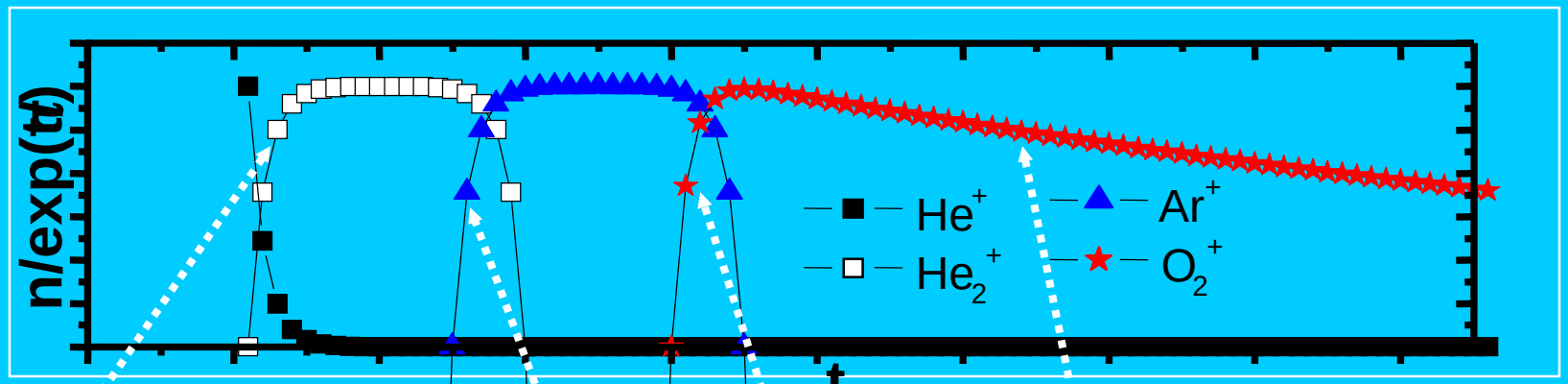

$He^+ + 2He \rightarrow He_2^+ + He$

$He_2^+ + Ar \rightarrow Ar^+ + 2He$

$He^m + Ar \rightarrow Ar^+ + He$

$Ar^+ + O_2 \rightarrow O_2^+ + Ar$

Diffusion, IMR
Recombination

FALP - Formation of H_3^+ in He/Ar/H_2 mixture

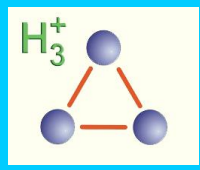

microwave discharge

He^+
He^m
He_2^+

$\xrightarrow{Ar}$ Ar^+ $\xrightarrow{H_2}$ ArH^+, H_2^+ $\xrightarrow{H_2}$ H_3^+

Ar

H_2

He

T_e ~2eV

$T_e = T_i = T_G$ = 300K

FALP - RECOMBINATION OF H_3

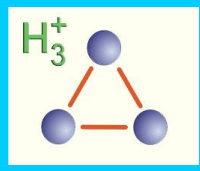

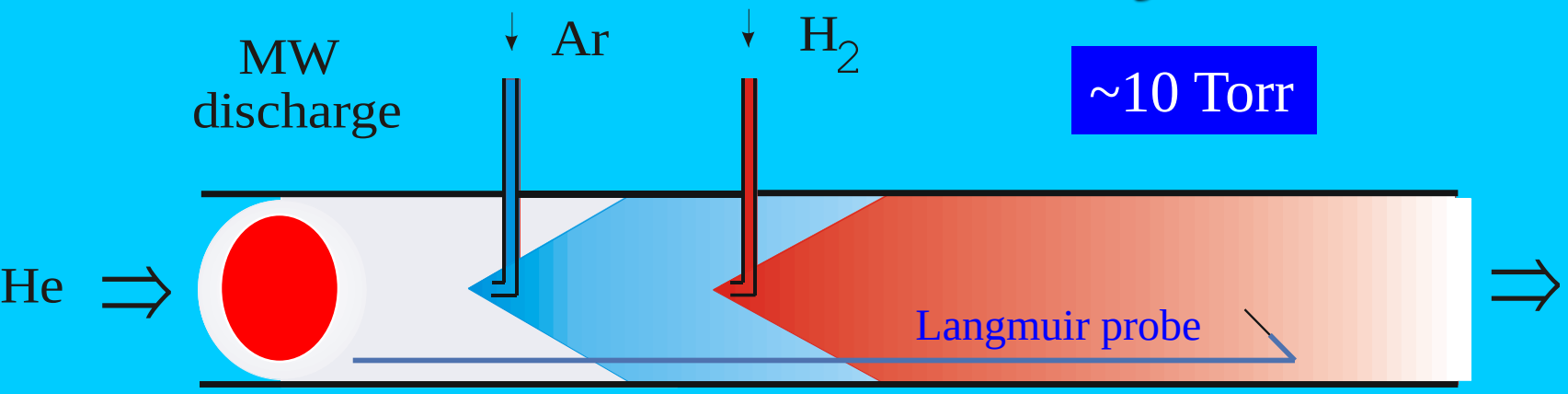

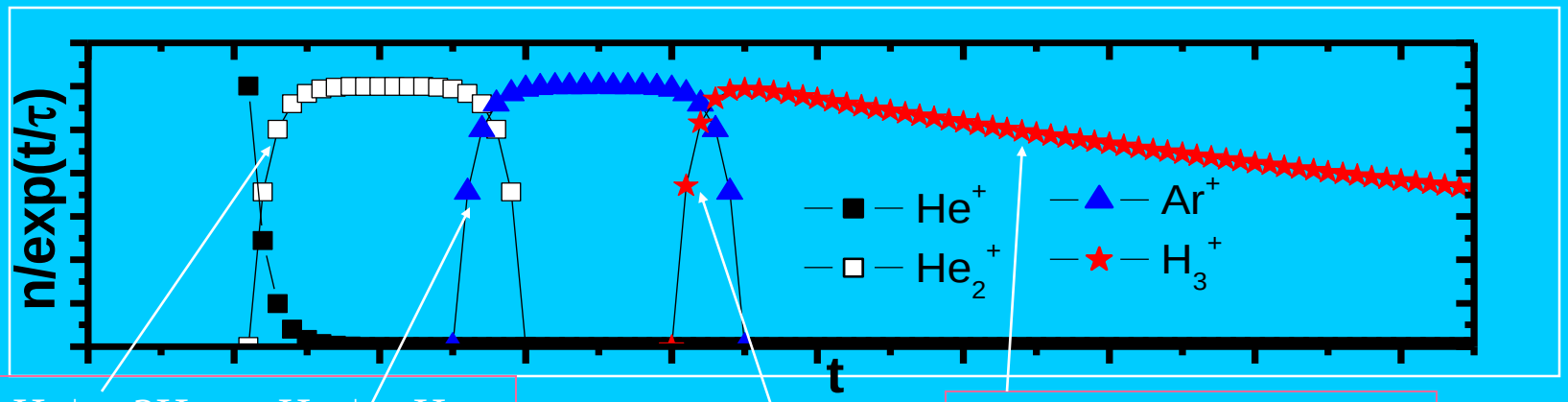

$He^+ + 2He \rightarrow He_2^+ + He$

$He_2^+ + Ar \rightarrow Ar^+ + 2He$

$He^m + Ar \rightarrow Ar^+ + He$

$Ar^+ + H_2 \rightarrow ArH^+ \ldots$

$ArH^+ + H_2 \rightarrow H_3^+ \ldots$

$H_3^+ + H_2 + He \rightarrow H_5^+ \ldots$

$H_3^+ + e^- \rightarrow \ldots$

$H_5^+ + e^- \rightarrow \ldots$

FALP High pressure UHV version - PRAGUE

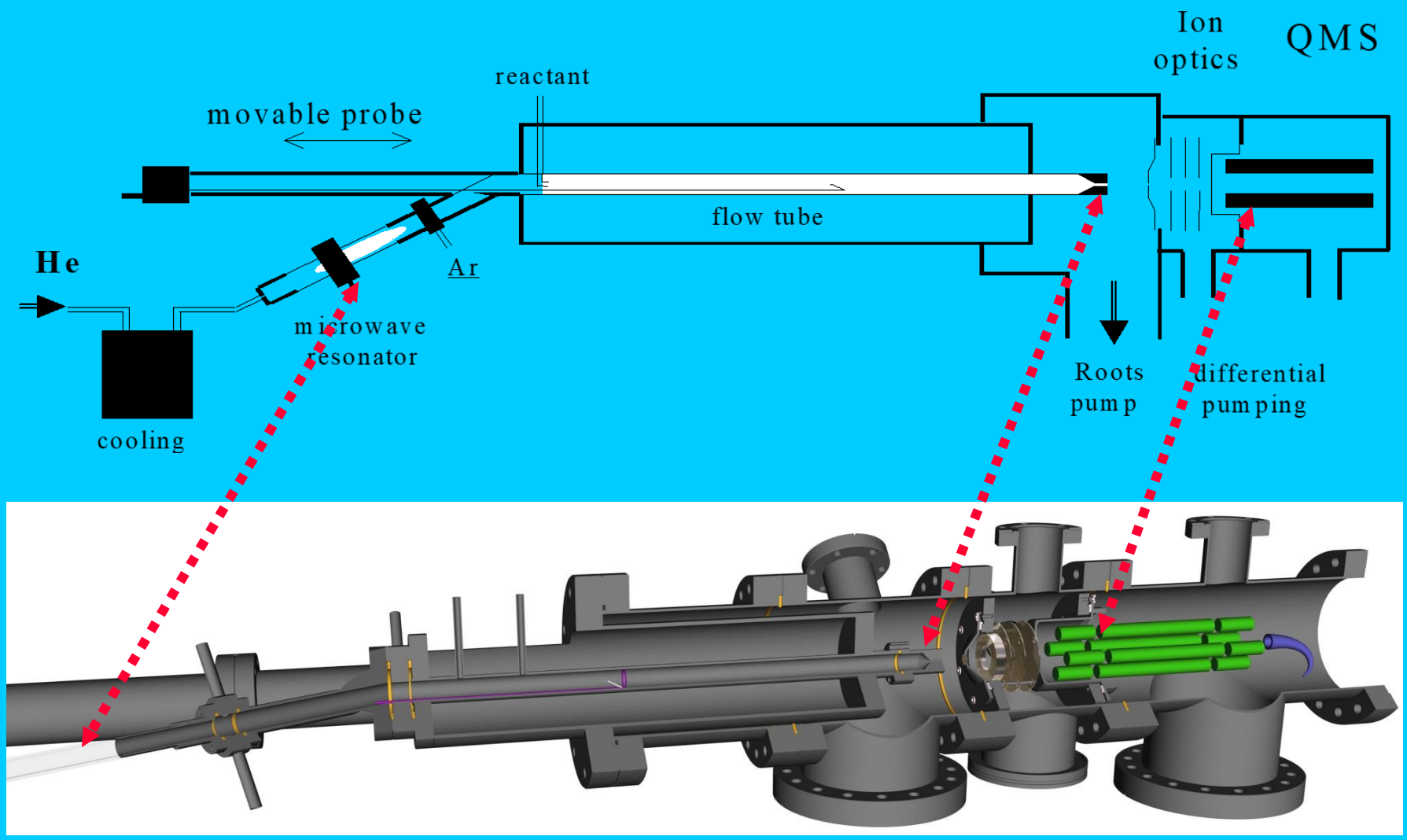

FALP – Ion detection system

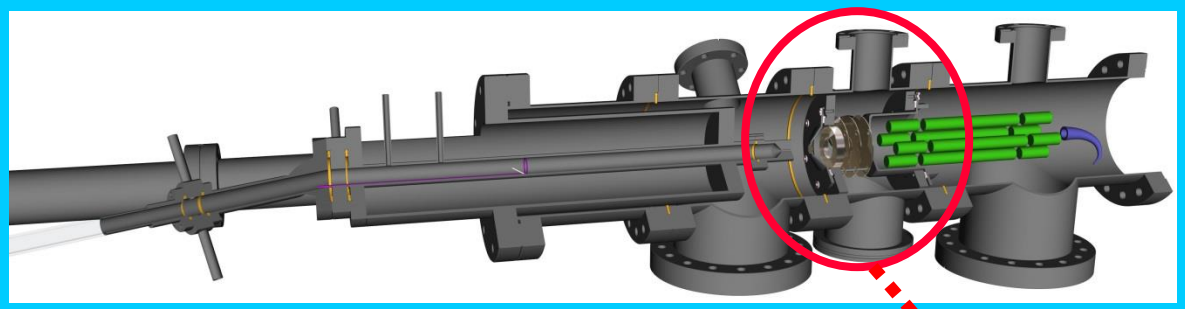

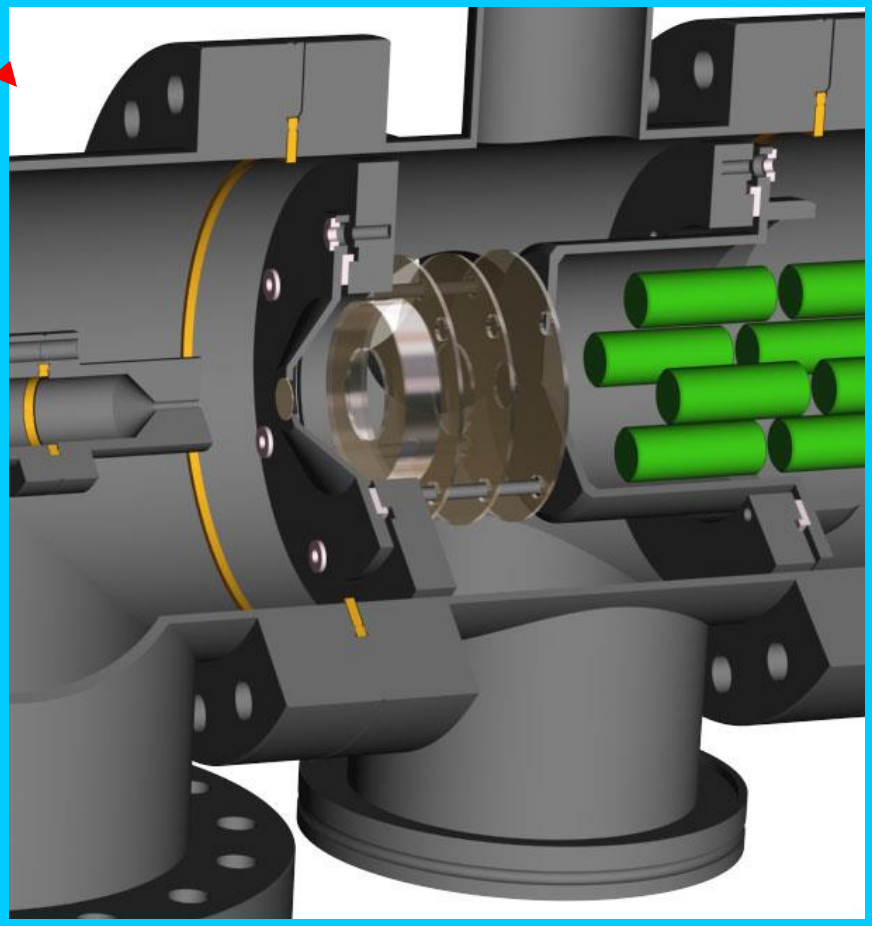

CRESU

The CRESU technique at Rennes

Carrier gas (He, Ar or N_2) + reactants

Kinetics of Reaction in Supersonic Uniform Flows (CRESU)

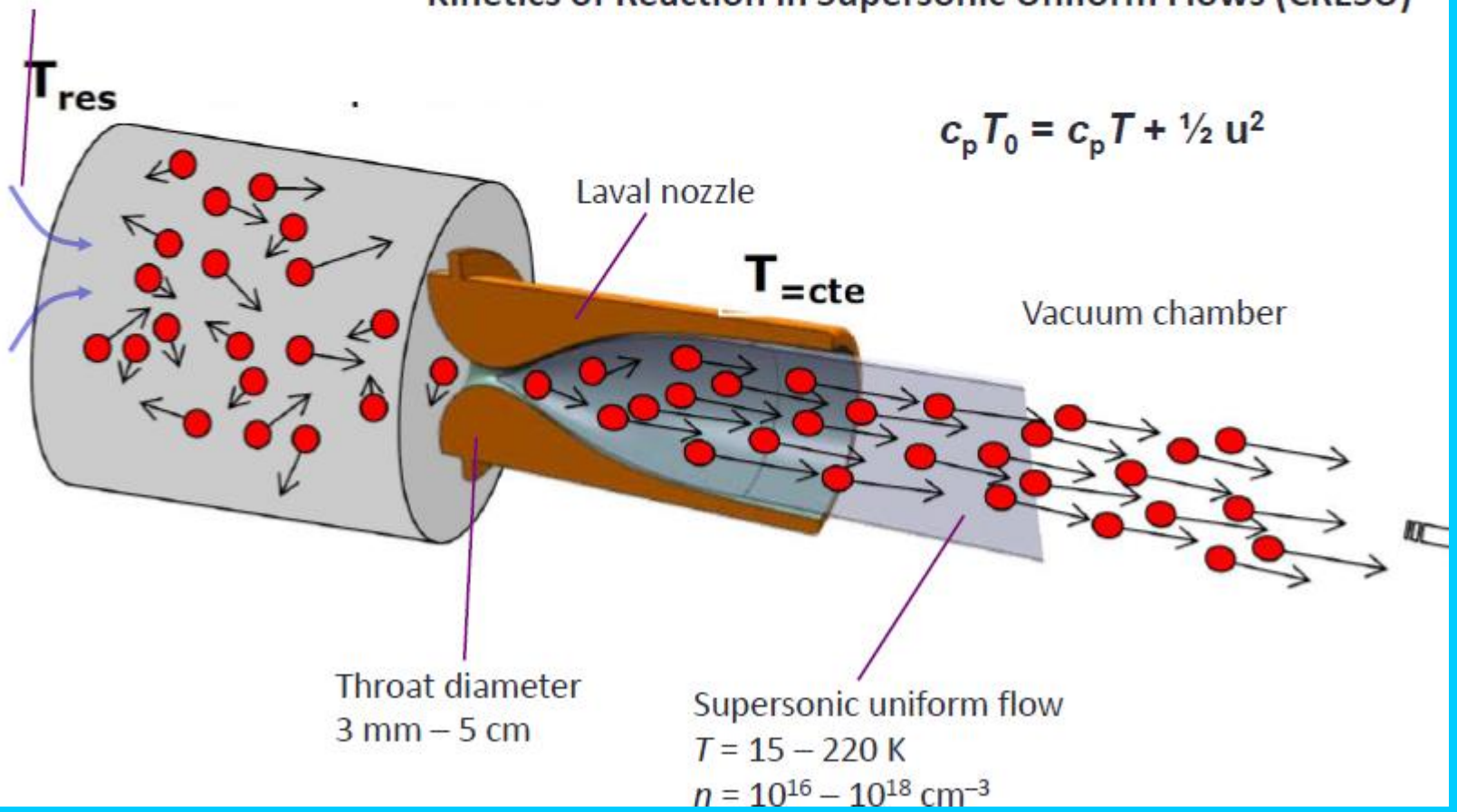

Kinetics of anion-molecule reactions at low temperature

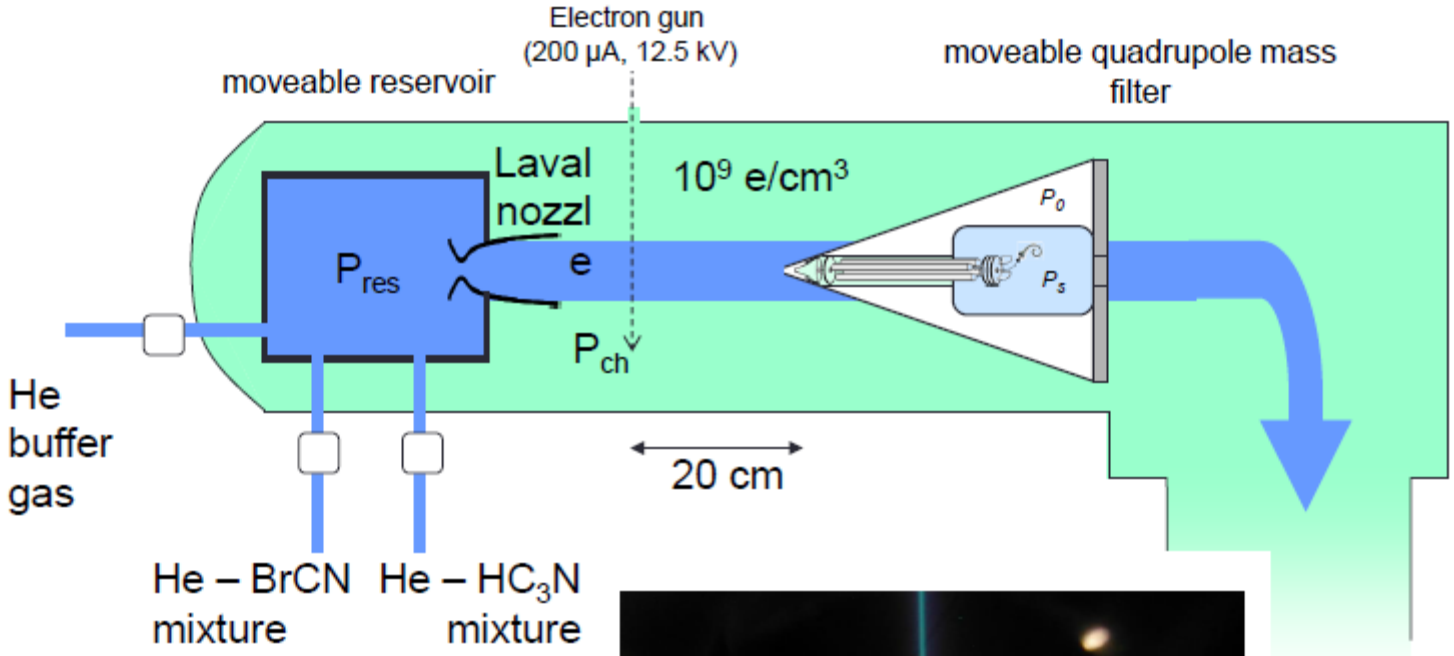

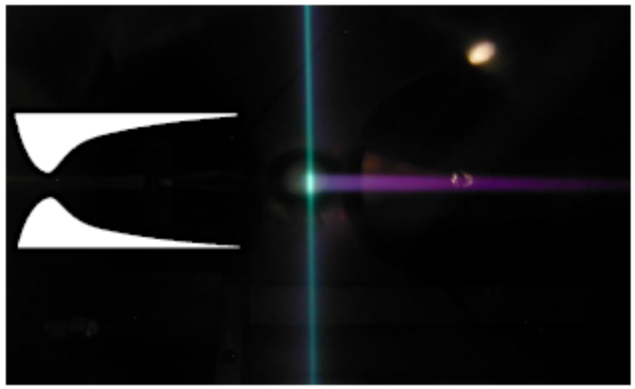

- CN^- + HC_3N (L. Biennier, S. Carles, J-C Guillemin et al. Icarus, 227, 123, 2014)
- C_3N^- + HC_3N (in progress)
- Collaboration with C. Alcaraz and co-workers (Orsay and Prague)

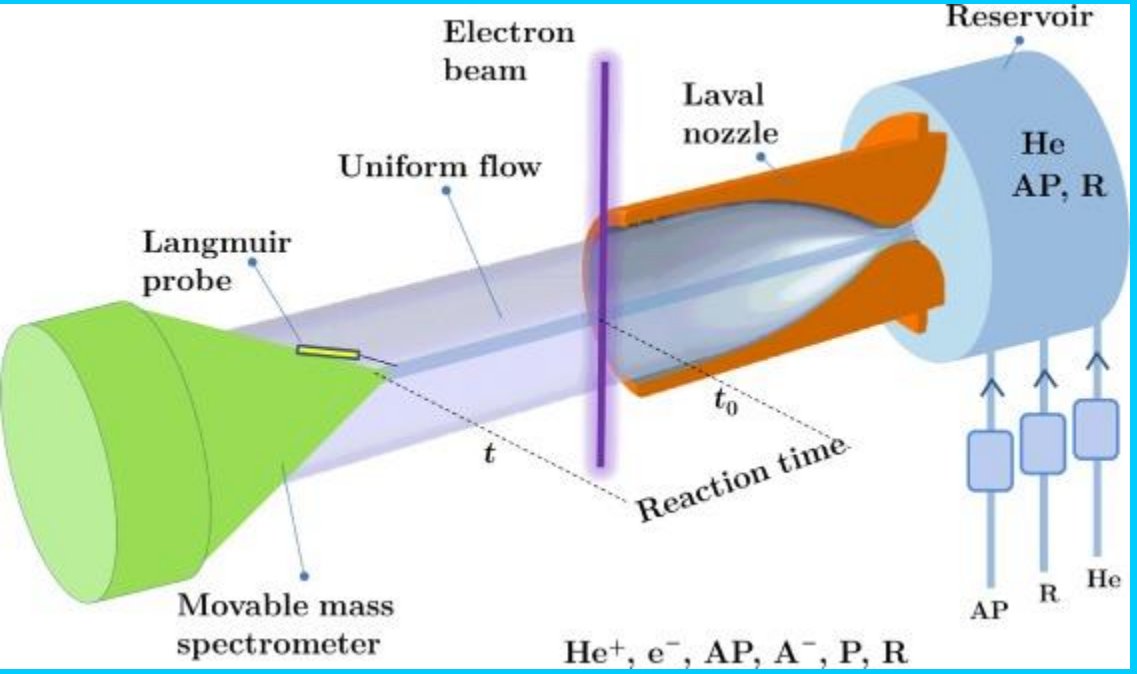
Electron beam
Reservoir
Laval nozzle
He
AP, R
Uniform flow
Langmuir probe
t_0
t
Reaction time
Movable mass spectrometer
AP
R
He
He⁺, e⁻, AP, A⁻, P, R

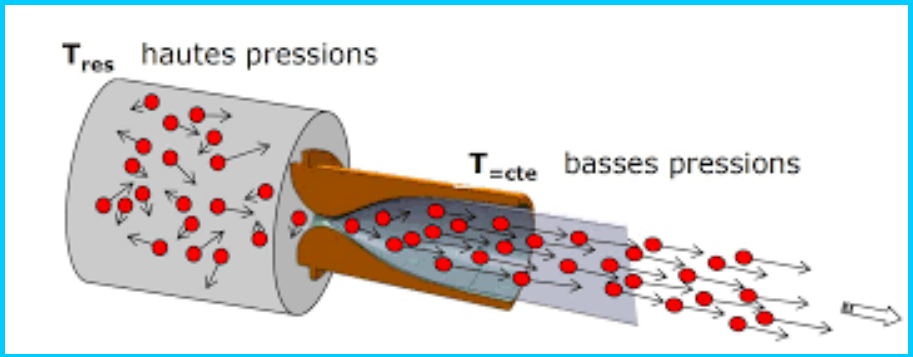
T_{res} hautes pressions
$T_{=cte}$ basses pressions

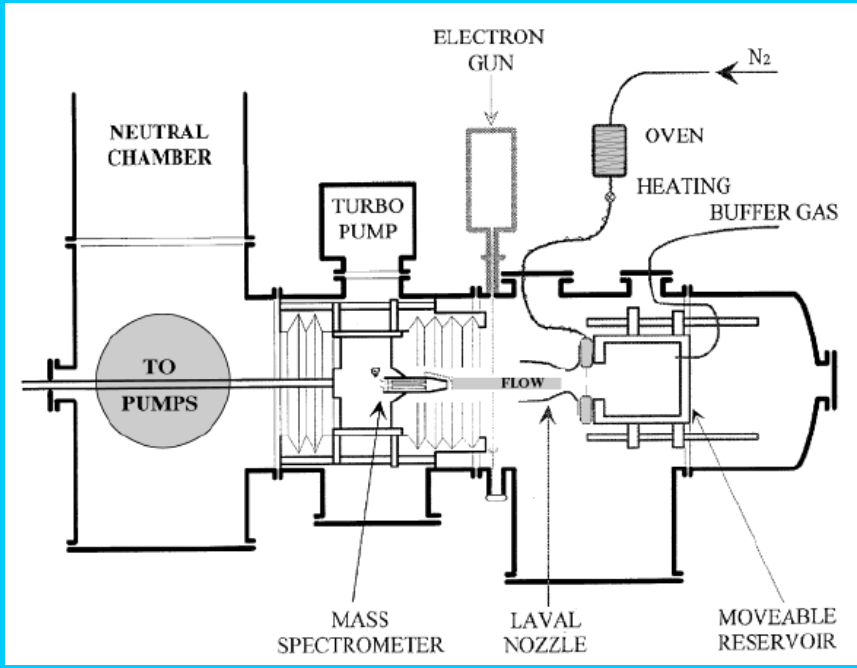
ELECTRON GUN
N_2
NEUTRAL CHAMBER
OVEN
HEATING
BUFFER GAS
TURBO PUMP
TO PUMPS
FLOW
MASS SPECTROMETER
LAVAL NOZZLE
MOVEABLE RESERVOIR

TSR

Outlook: Electron-beam collision studies

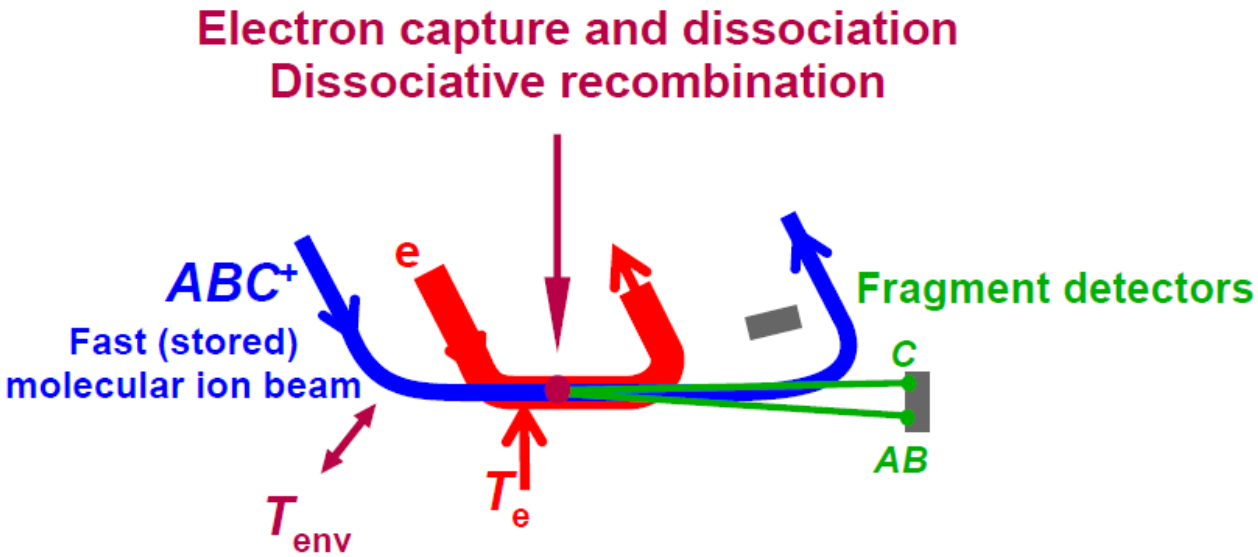

$$E_{coll} = \frac{1}{2} m_e (v_e - v_i)^2$$

can be scanned from ~ 1 meV ... 50 eV

Experiments

PLASMA experiments SA and FA	- multi collisions	$\{\alpha(T)\}$
Crossed beam experiments	- single collisions	$\{\sigma(v_r)\}$
Marched beam, Storage rings - TSR, Cryring, Astrid	- single collisions	$\{\sigma(v_r)\}$

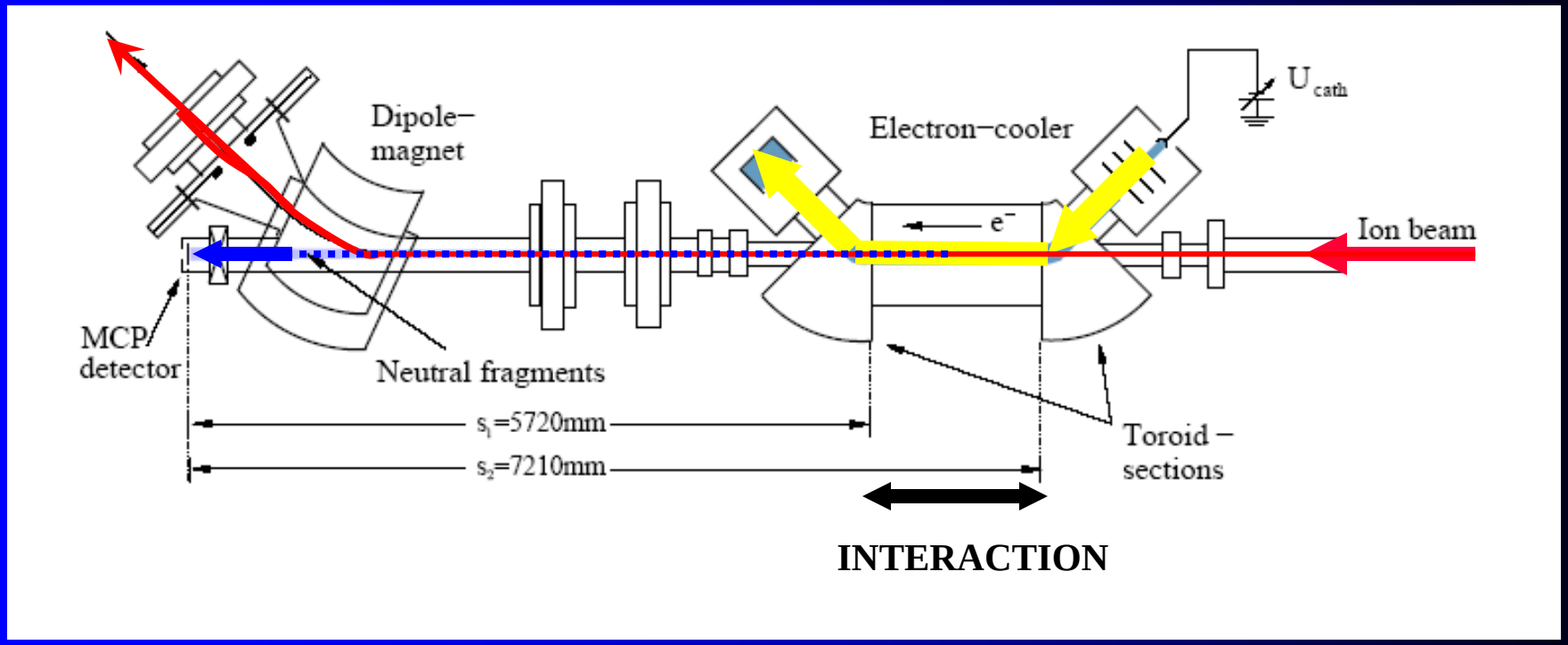

$$H_3^+ + e^- \rightarrow H, H_2$$

Electron-cold molecular ion reaction: Dissociative Recombination → Merged Beam Kinematics

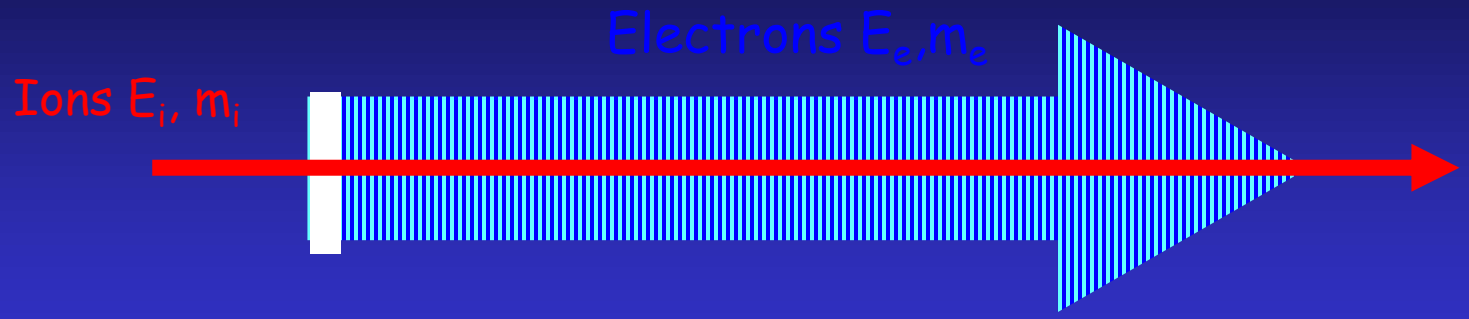

$$E_{cm} = \frac{1}{2} m_e v_{cm}^2 \approx \left[\sqrt{\frac{m_e}{m_i} E_i} - \sqrt{E_e} \right]^2$$

Center of mass resolution:

$$\Delta E_{cm} = \left\{ \left[\left(1 - \frac{v_e}{v_i} \right) \frac{m_e}{m_i} \Delta E_i \right]^2 + \left[\left(1 - \frac{v_i}{v_e} \right) \Delta E_e \right]^2 \right\}^{1/2}$$

~ meV resolution for zero relative kinetic energy!

TSR electron target

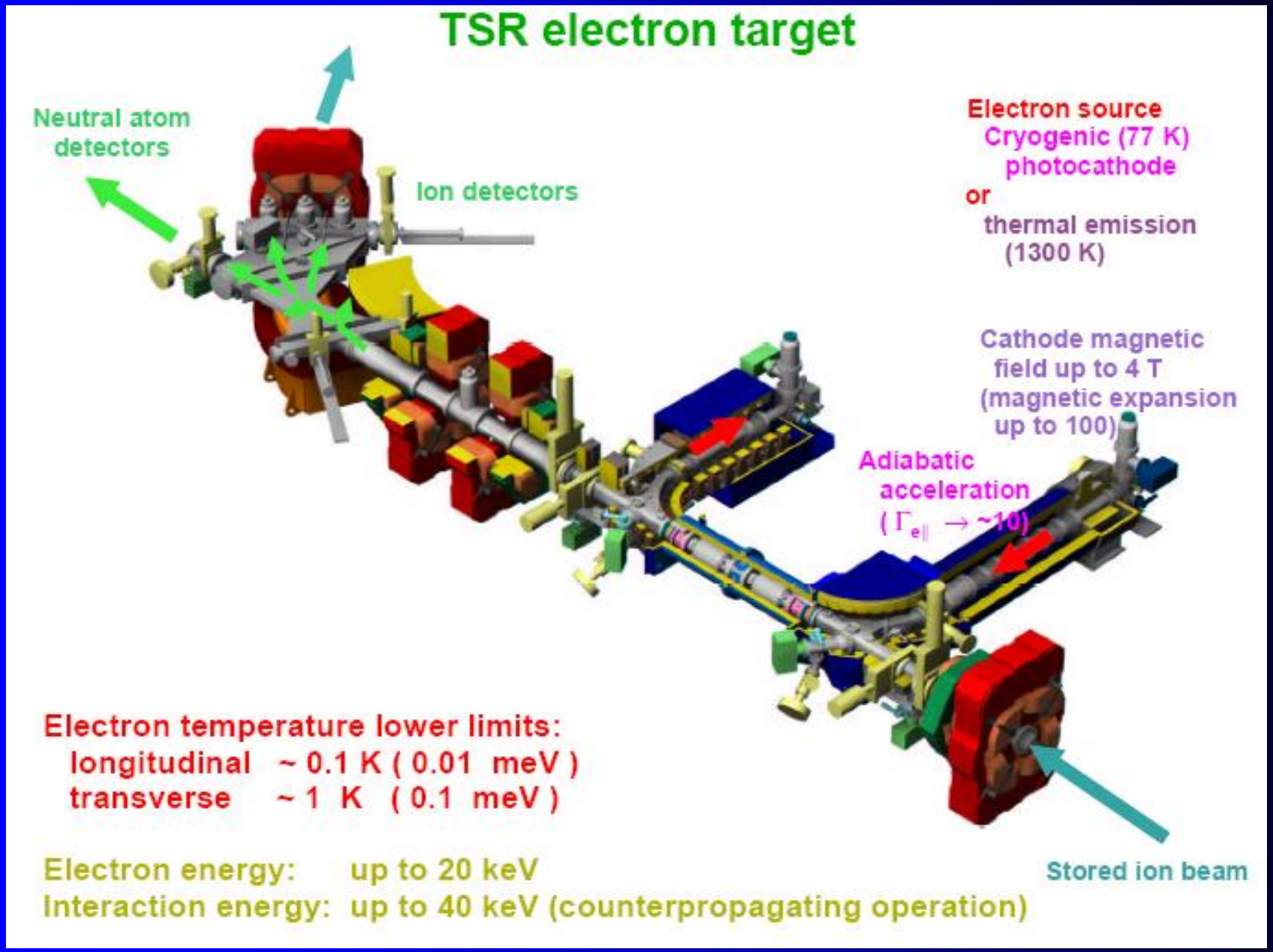

Reality - TSR (MPIK Heidelberg)

Injection of INTERNALY COLD H_3^+ IONS(12-50K) with kinetic energy 1-2 MeV

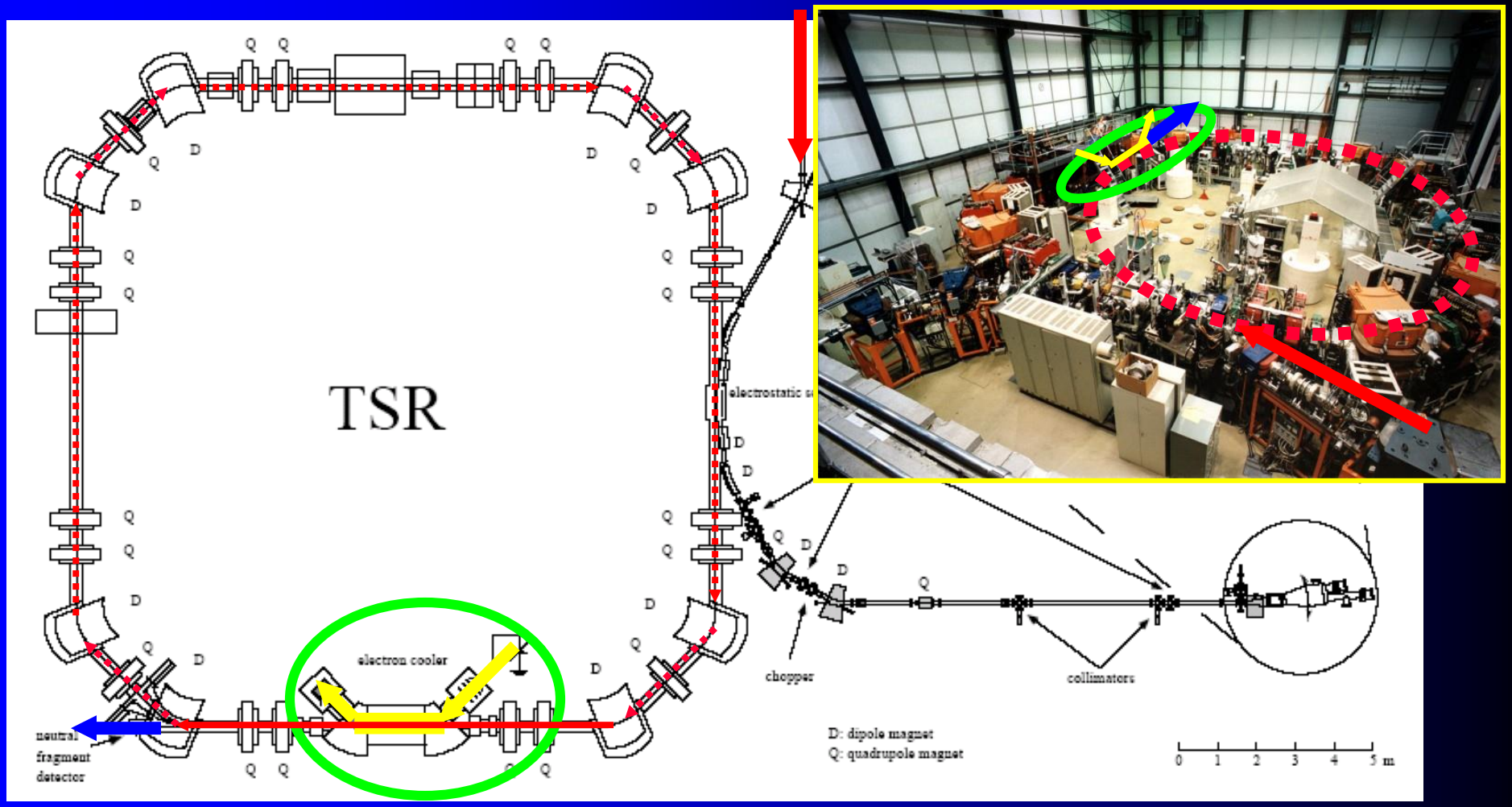

Detection of neutrals

INTERACTION at meV collision energies

Detection of $H_3^+(v,j)$

PLASMA PHYSICS I/7

Recombination

TSR (MPIK Heidelberg)

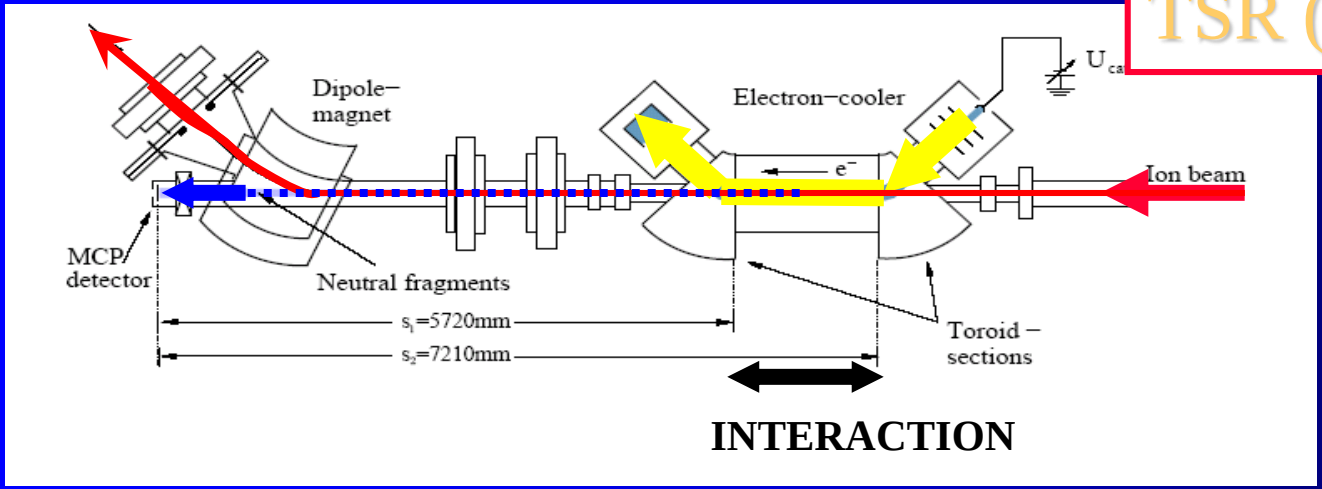

Kumulativní prstenec

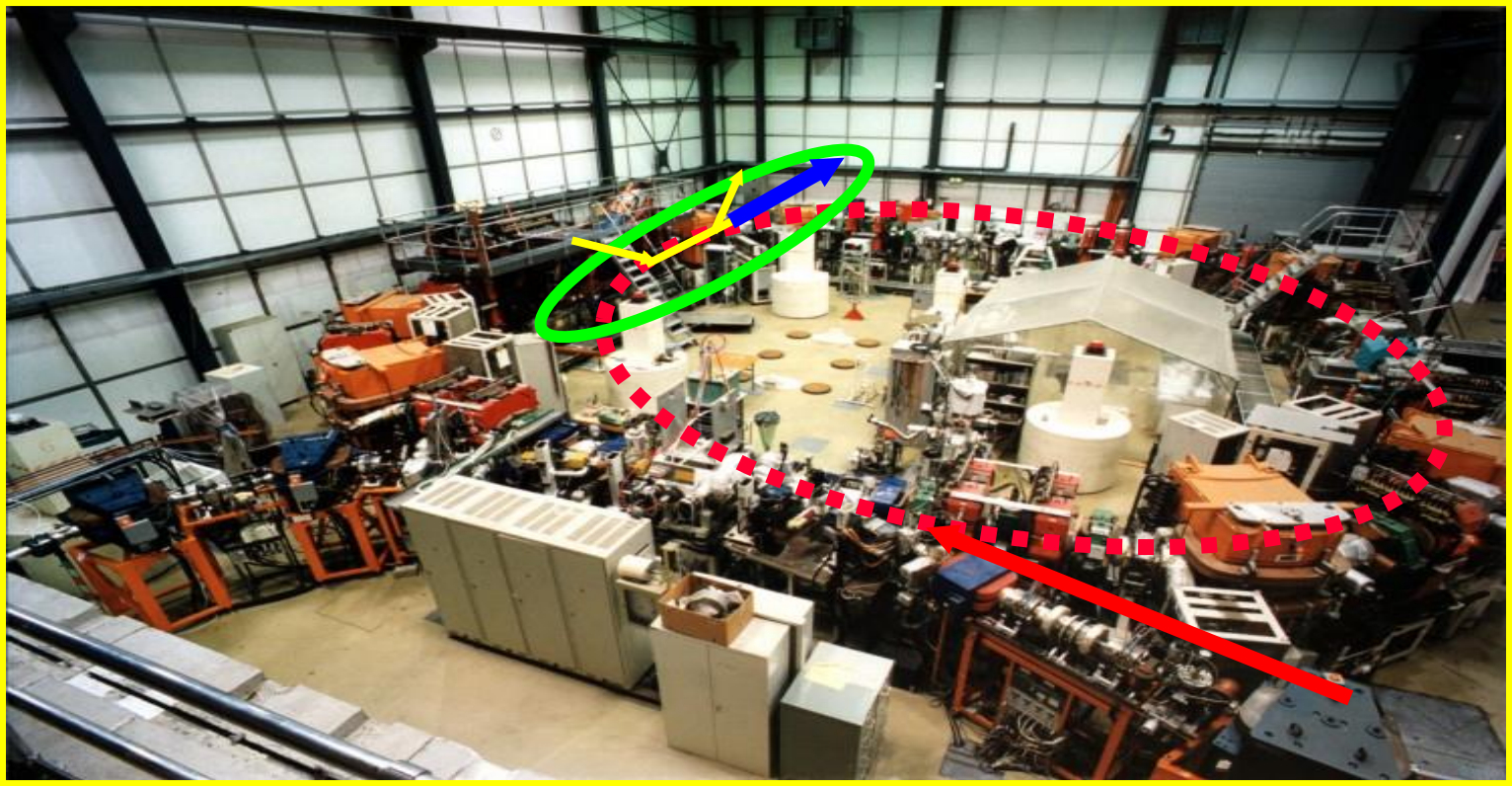

TSR Heidelberg, ion injection and ion source

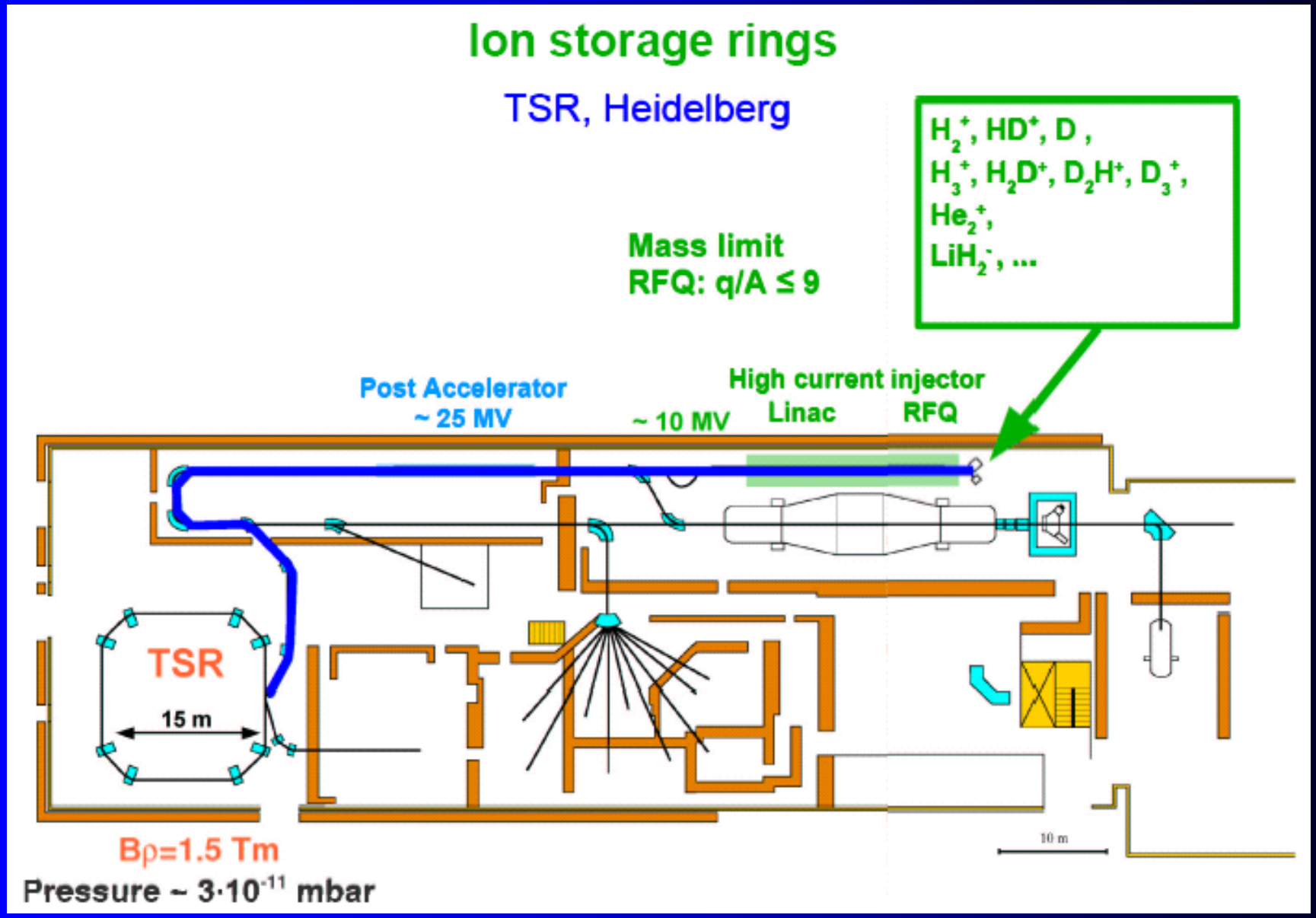

State diagnostics

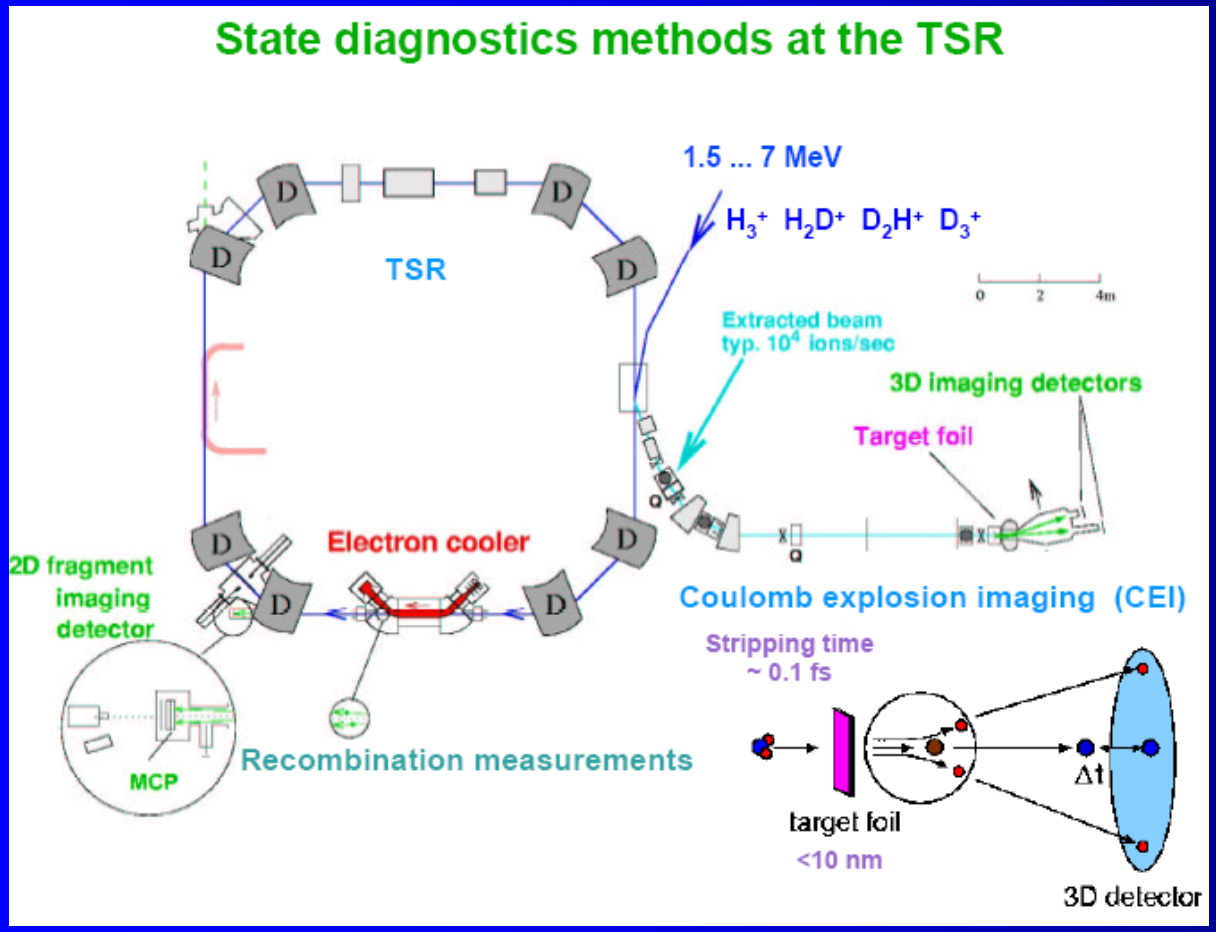

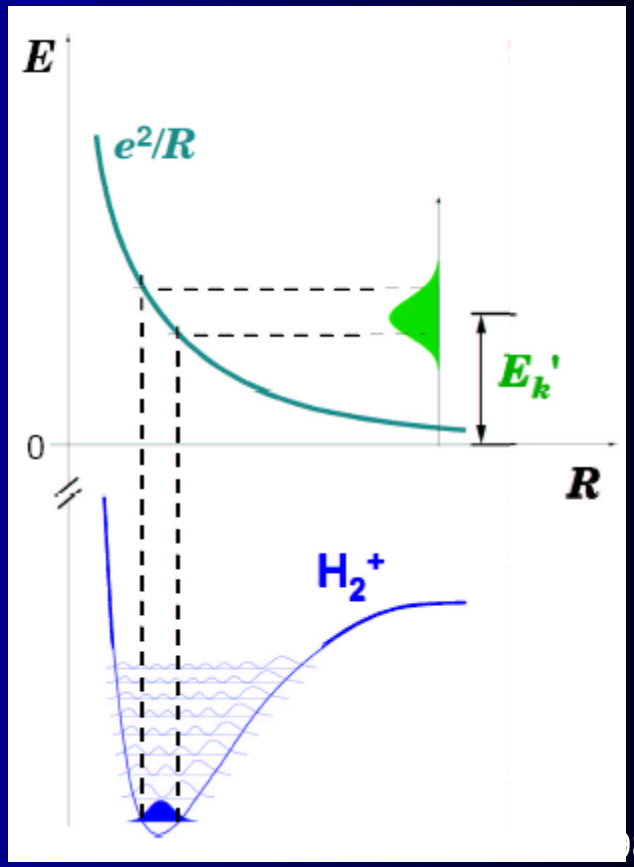

Thanks for your attention!

CSR team

A. Becker
K. Blaum
C. Breitenfeldt
F. Fellenberger
S. George
J. Göck
M. Grieser
F. Grussie
R. von Hahn
P. Herwig
J. Karthein
C. Krantz
H. Kreckel
S. Kumar S.
M. Lange
J. Lion
S. Lohmann
C. Meyer
P. M. Mishra
O. Novotný
P. O'Connor
R. Repnow
S. Saurabh
S. Schippers
C. D. Schröter
D. Schwalm
L. Schweikhard
K. Spruck
X. Urbain
S. Vogel
A. Wolf
D. Zajfman

JUSTUS-LIEBIG-UNIVERSITÄT GIESSEN

CSR

The CSR – overview

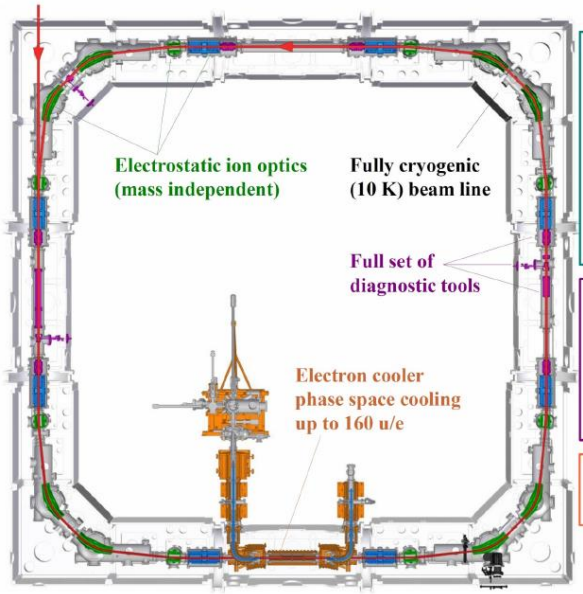

circumference:	35 m
beam energy:	20 keV × q ... 300 keV × q
temperature:	10 . . 300 K
res. gas press. (@ < 10 K):	10^{-14} mbar (~ 100 cm^{-3})

- Beam profile monitors (3x)
- Current pickup
- Schottky pickup
- Position pickups (6x)

... with electron cooling

m/q range:	1 ... 160 u/e (@ 300 kV)

R. v. Hahn
M. Grieser

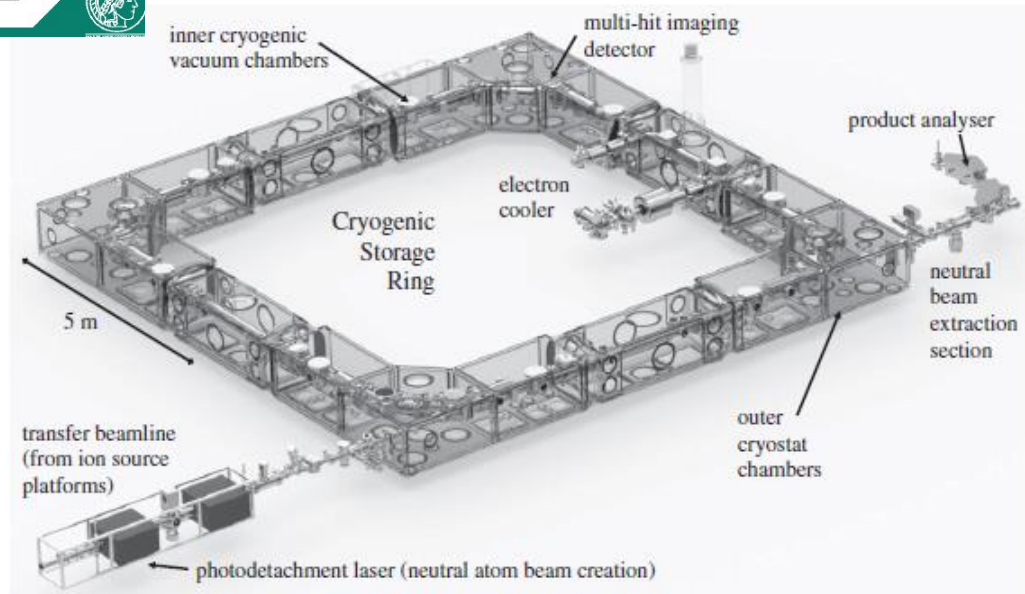

Figure 1. Overview of the CSR. The experimental set-ups relevant for astrochemical studies are labelled in the insets. The image includes the new low-energy electron cooler as well as the photodetachment section for the neutral beam creation in the injection beamline, the neutral beam extraction and some of the corresponding detector units.

PHILOSOPHICAL TRANSACTIONS A
royalsocietypublishing.org/journal/rsta

Astrochemical studies at the Cryogenic Storage Ring

H. Kreckel, O. Novotný and A. Wolf
Max Planck Institut für Kernphysik, 69117 Heidelberg, Germany

The CSR – overview

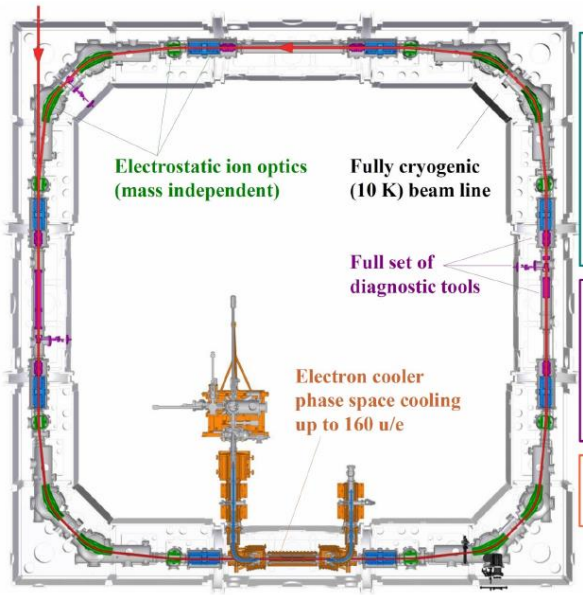

circumference:	35 m
beam energy:	20 keV × q ... 300 keV × q
temperature:	10 . . 300 K
res. gas press. (@ < 10 K):	10^{-14} mbar (~ 100 cm^{-3})

- Beam profile monitors (3x)
- Current pickup
- Schottky pickup
- Position pickups (6x)

... with electron cooling

m/q range:	1 ... 160 u/e (@ 300 kV)

1 m

R. v. Hahn
M. Grieser

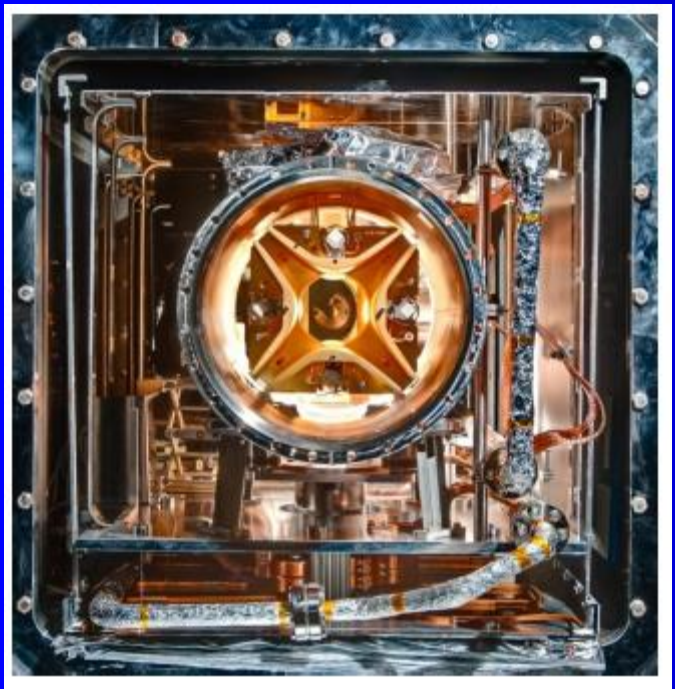

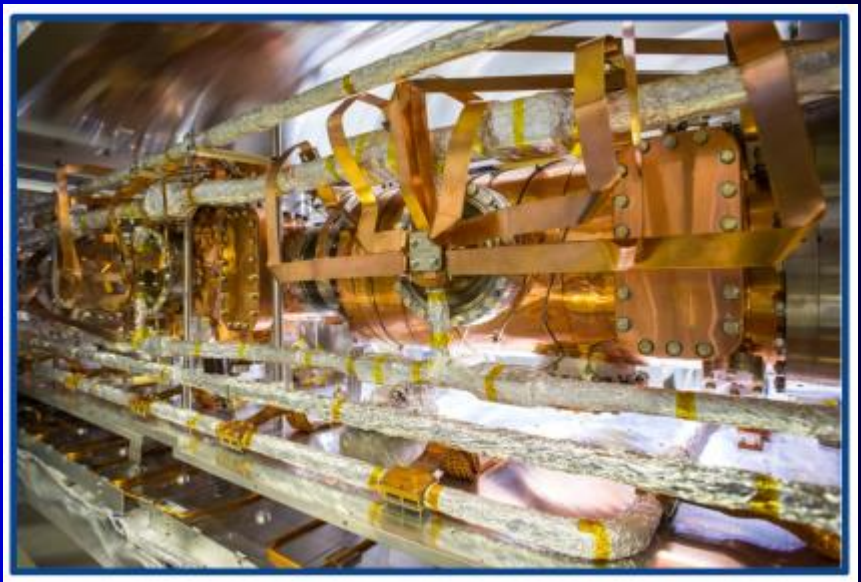

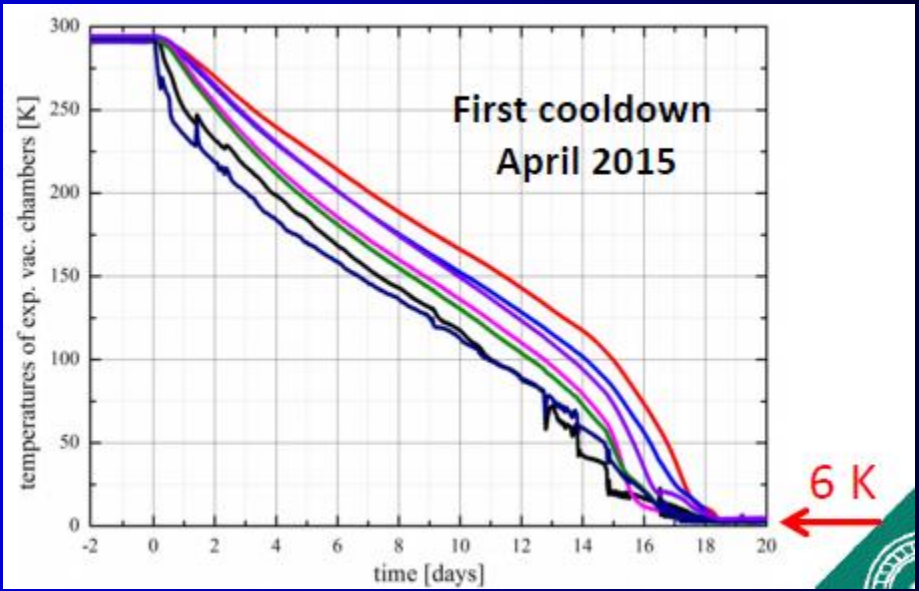
First cooldown
April 2015
temperatures of exp. vac. chambers [K]
time [days]
300
250
200
150
100
50
0
-2
0
2
4
6
8
10
12
14
16
18
20
6 K